RNA structures within Venezuelan equine encephalitis virus E1 alter macrophage replication fitness and contribute to viral emergence

Sarah Hickson

A dissertation
submitted in partial fulfillment of the
requirements for the degree of

Doctor of Philosophy

University of Washington
2024

Reading committee
Jennifer Hyde, Chair
Adam Geballe
Naeha Subramanian

Program authorized to offer degree:
Microbiology

University of Washington

Abstract

RNA structures within Venezuelan equine encephalitis virus E1 alter macrophage replication fitness and contribute to viral emergence

Sarah Hickson

Chair of Supervisory Committee:
Jennifer Hyde
Department of Microbiology

Venezuelan equine encephalitis virus (VEEV) is a mosquito-borne positive-sense single-stranded RNA genome virus belonging to the *Togaviridae*. Present throughout Central and South America, VEEV is responsible for significant outbreaks of epidemic/epizootic VEEV causing febrile disease and encephalitis in both equids and humans. While endemic/enzootic VEEV persists in nature and circulates between reservoir host rodents and mosquitoes, periodic mutation of enzootic VEEV gives rise to the emergence of epizootic VEEV. Using equines as amplification hosts, epizootic VEEV can have devastating outcomes for equine populations as well as cause large spill over events and disease in humans. The main mutations linked to epizootic VEEV emergence involve amino acid mutations within the E2 glycoprotein, which enhance viral entry and equine amplification. Interestingly, the majority of mutations found within epizootic strains are synonymous, indicating that other viral factors, such as RNA secondary structure, may play a critical role in their emergence. Understanding these mechanisms is crucial for predicting and mitigating future outbreaks.

In this study, we discovered novel RNA structures within the E1 coding sequence that specifically affect VEEV replication in macrophages, which are critical early targets during infection. Using mass spectrometry and targeted gene knockdown, we identified several RNA-

binding proteins essential for the altered macrophage phenotype, none of which had previously been associated with VEEV replication. Our findings also revealed the conservation of single-nucleotide polymorphisms (SNPs) within epizootic VEEV lineages, as well as the preservation of RNA structures across all lineages. Taken together, these findings suggest a previously unrecognized role for RNA secondary structure in the emergence of epizootic VEEV.

Table of Contents

List of Figures and Tables

Acknowledgements

As I come to the end of this journey, there are some people that I would like to thank and acknowledge as their support of me over the years has been instrumental to me successfully completely my PhD. First, I would like to thank Jenny for taking me on as her graduate student and bearing with me despite my changing priorities over the years. Your passion, drive and enthusiasm for science have been an example to me. Adam, I count myself lucky for the time I spent in your lab. You have been a true inspiration and your continued support and mentorship over the years has been invaluable to me. I would also like to thank my committee for all their scientific input and guidance over the last 7 years.

Neel, who would have guessed all those years ago that you would become such an important friend to me. Even though you left me to fend for myself for the last year, you have been such a source of encouragement for me. You made lab fun, helped me google all my stupid questions and most importantly kept me from having to autoclave stuff for myself. I don't think I would have made it through without you.

Thank you to my Mum. Your support of me has always been unconditional and unwavering. You have always believed I could do this even when I thought it was all a lost cause. Thank you for giving me the courage and motivation to persevere.

To my husband, Maddison, you have been such a pillar of strength for me over the years. Thank you for supporting my decision to pursue a PhD and continuing to support me throughout. It has not been an easy journey but having you by my side has made easier. Thank you for all the sacrifices you have made, so that I could complete it. I would not have graduated without your help. I love you.

Lastly, thank you to my kids, Emilia and Luca, for constantly making life fun. You both mean the world to me.

Chapter I: Introduction

Alphaviruses

Alphaviruses (family *Togaviridae*) represent a diverse group of arthropod-borne RNA viruses that are known to infect a wide range of hosts, including mammals, birds and mosquitoes (reviewed in[1]). The alphavirus genus is subdivided into Old-World Alphaviruses and New-World Alphaviruses, depending on the geographical location where they were initially isolated and their disease characteristics. New-World alphaviruses include Eastern, Western and Venezuelan Equine Encephalitis Virus (EEEV, WEEV and VEEV), all of which were first isolated within North and South America. These viruses tend to cause febrile disease in humans, with more severe cases leading to encephalitis and in some instances death. Old-World alphaviruses, such as Sindbis virus (SINV), Chikungunya virus (CHIKV), Semliki Forest virus (SFV), Ross River virus (RRV), and O'Nyong Nyong virus (ONNV), were primarily isolated throughout the "Old World" including Europe, Asia, Africa, and Australia. These viruses are typically characterized by symptoms such as rash, fever, and arthralgia, with fatalities remaining rare.

Characterization and early detection of New-World alphaviruses

The first known instance of a New-World alphavirus was recorded in 1930 when Meyer, Haring and Howitt isolated the causative agent of epizootic encephalomyelitis from the brain of a horse in San Joaquin Valley, California [2]. Termed Western Equine Encephalitis virus (WEEV), outbreaks are believed to have occurred periodically in the western United States and Canada dating as far back as 1847. Though human infections were suspected earlier, it was not until 1938 that the first case was confirmed after Howitt[3] recovered the virus from the brain of a child. The discovery of WEEV was quickly followed by the isolation of another equine encephalomyelitis. In 1933, Ten Broeck and Merril[4] and Giltner and Shahan[5] isolated the etiological agent of an outbreak of epizootic encephalomyelitis that occurred in Delaware, Maryland and Virginia. This eastern outbreak exhibited similar disease characteristics as previously reported for WEEV, though appeared to be more acute in nature and caused greater morbidity. Immunological studies confirmed that these two outbreaks were caused by different viruses[5]. Similar to WEEV, reports of Eastern Equine Encephalitis virus (EEEV) were later discovered to have been reported as early as 1831 in Massachusetts[6].

It was not until 1938 that Venezuelan Equine Encephalitis Virus (VEEV) was identified in northern South America. The virus was first recognized by Beck and Wyckoff [7], and later by Kubes and Rios[8], who investigated a severe epidemic of equine encephalomyelitis in Venezuela. This epidemic was comparable to previous outbreaks reported in Canada and the

United States. Immunological studies in animals again distinguished this infectious equine encephalitis from earlier outbreaks of EEEV and WEEV. Infections in humans were not described until the 1950s, when an outbreak of human disease causing mild febrile disease was documented in Columbia[9], and later in 1967 in northern Venezuela[10].

Since its discovery in 1938, VEEV has become an important human and equid pathogen amongst the New-World Alphaviruses. Alone, VEEV has been responsible for several substantial epizootic outbreaks involving hundreds-of-thousands of humans and equines[11], with major VEEV outbreaks occurring approximately every 10 years up until 1973. Following an almost 20-year period with no recorded VEEV, a cluster of outbreaks occurred in the 1990s. This included several smaller outbreaks, such as the 1992-93 outbreak in western Venezuela[12], the 1993 outbreak in the Chiapas State in southern Mexico[13], and the 1996 outbreak in the Oaxaca State in southern Mexico. All these epidemics involved less than 150 reported equine infections and even fewer reported human infections, although the actual numbers were likely much higher. To date, the largest known human outbreak of epizootic VEEV occurred in 1995 in Colombia and Venezuela, with an estimated 50,000 equine and 75,000-100,000 human infections reported[12, 14]. While there have not been any reports of major epizootic VEEV outbreaks in recent years, the maintenance of enzootic VEEV in nature and the sporadic emergence of VEEV epizootic suggests future outbreaks are unavoidable.

VEEV disease and pathogenesis

As discussed above, epizootic VEEV strains are responsible for major outbreaks of equine infections. Equine mortality rates during epizootic outbreaks have been estimated between 32-86% [15]. In equines, symptoms of fever and malaise appear 2-5 days post infection. Encephalitis does not appear until 5-10 post infection with more serious symptoms of ataxia, hyperexcitability and circling, most often followed by death. While under normal circumstances enzootic strains are not capable of causing severe disease and death in equines, when inoculated intracerebrally enzootic strains have been shown to induce encephalitis and death[16]. These findings suggest that the virulence of epizootic strains in equines is related to their ability to travel to the brain, rather than any innate neurovirulence compared to enzootic strains.

In humans, VEEV causes biphasic disease, first causing replication in the periphery, followed by spread to the central nervous system (CNS). Common symptoms of febrile disease such as fever, malaise, headache, nausea and vomiting appear 2-5 days post infection with VEEV. This acute febrile VEEV typically lasts 3-4 days and in most cases resolves without intervention. However, approximately 4-14% of human cases develop into encephalitis,

characterized by convulsions, disorientation, drowsiness and in ~1% of cases, death[14, 17]. While VEEV has no sex bias in humans, children are more likely to develop severe disease and encephalitis compared to adults[18]. VEEV has also been shown to cross the placenta and infect the fetus, causing birth defects, spontaneous abortions and still birth[19]. Contrary to equine infections, enzootic strains of VEEV can be pathogenic in humans and result in human fatalities. Furthermore, no differences in disease presentation or progression have been observed in humans[18]. Due to the overlapping symptoms characteristic of many arboviruses, the true burden of endemic VEEV is likely underestimated. Surveillance studies in South America suggest that VEEV in humans may often be clinically misdiagnosed and the true burden of endemic VEEV may be as high as 10% of reported Dengue-like illnesses [20, 21].

Mouse models are often used to study routes of viral dissemination and pathogenesis *in vivo.* Laboratory mice mimic the biphasic disease pattern seen in epizootic equine and severe human infections, thus making them a good model for recapitulating disease progression. During infection of mice, VEEV initially targets host Langerhans cells, a tissue-resident macrophage cell-type, and dendritic cells (DCs) in the skin[22]. The migratory nature of these immune cells allows the virus to effectively spread from the site of inoculation through the regional draining lymph nodes (dLN), thereby infecting peripheral tissues such as the spleen, thymus and pancreas[23, 24]. VEEV infection is characterized by system wide induction of type-I IFNs and upregulation of proinflammatory cytokines in the spleen and dLN early during infection[23]. Invasion of the central nervous system occurs by 48-72hpi, followed by fatal encephalitis at 7 to 10 days post infection[25, 26].

The VEEV transmission cycle

The VEE complex consists of 9 species that are divided into seven antigenic complexes[27, 28], amongst which VEE-I is most well studied due to its relevant animal and human disease profile. VEEV falls within subtype I and is further subdivided into IAB, IC, ID and IE strains. The VEEV transmission cycle is broken up into either endemic/enzootic or epidemic/epizootic cycles (**Figure 1.1**). Enzootic VEEV strains, ID and IE, continuously circulate in swamps and forested areas in South America, Central America and Mexico. These endemic strains are equine-avirulent due to their inability to induce virulence or viremia in equids [29], though some IE subtypes have been linked to epizootic phenotypes and epidemic outbreaks[30]. Despite their inability to cause disease in equines, enzootic spillover into humans has been identified as a significant contributor to dengue-like disease in neotropical regions within the Americas[21]. Enzootic VEEV is transmitted between reservoir hosts and mosquito vectors.

Sylvatic rodents of the subfamily *Sigmodontinae* are believed to be the primary reservoir hosts for enzootic strains of VEEV[31, 32]. These rodents have been shown to be frequently infected in nature, have high rates of observed immunity and have the ability to develop moderate to high levels of viremia [18]. In particular, several species of spiny rats and cotton rats have been demonstrated as important reservoir hosts for ID strains in South America [33, 34]. The main vectors for enzootic VEEV are various species of forest-dwelling mosquitoes of the genus *Culex*, subgenus *Melanoconion*[35]. Although our knowledge of the ecology of most *Melanoconion* species is limited, a seeming preference for small animals as well as the maintenance of population sizes and their habitat being primarily restricted to forested areas, likely contributes to their role as enzootic VEEV vectors [36].

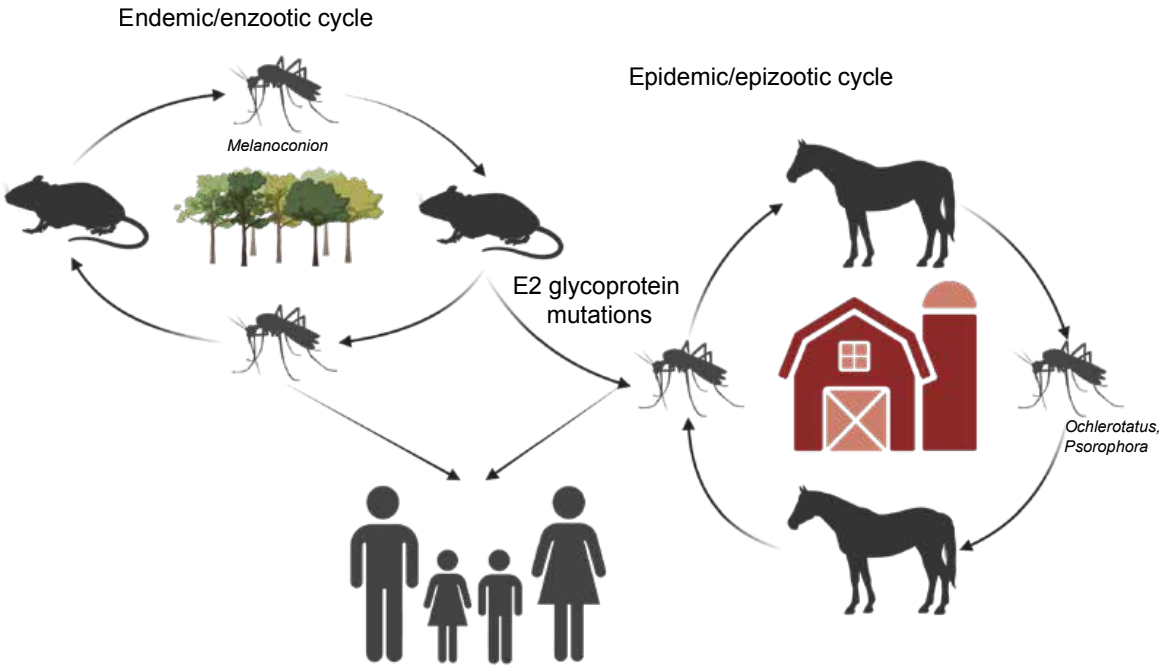

Figure 1.1 The VEEV transmission cycle. Endemic/enzootic VEEV circulates between enzootic mosquito vectors and rodent reservoir hosts in forested and swamp-like regions. While enzootic VEEV is not capable of establishing viremia and virulence in equines, spillover enzootic VEEV into humans has been identified as a significant contributor to dengue-like disease in neotropical regions within the Americas. Sporadic emergence of epidemic/epizootic VEEV occurs through mutation of enzootic strains. Epizootic VEEV is characterized by mutations within the E2 glycoprotein, which allow for adaptation to new mosquito vectors and highly efficient replication in equines as amplification hosts. Epizootic outbreaks not only cause significant disease and pathogenesis in equines, but major spillover events and disease in humans. This image was created using BioRender.

Contrary to enzootic VEEV, epizootic outbreaks are sporadic and characterized by highly efficient replication in equines, which serve as amplification hosts [29, 37, 38]. Traditionally, only the IAB and IC subtypes are considered epizootic and are linked to heightened virulence and viremia in equines[16, 18, 39-44], and furthermore cause major spillover events and disease in humans[21, 45]. Epizootic VEEV has repeatedly emerged through mutation of enzootic VEEV strains, a phenomenon supported by phylogenetic studies[12, 38, 46-48].

The dominant characteristic that has been attributed to the emergence of epizootic VEEV from enzootic strains is amino acid substitutions within the E2 glycoprotein[37, 49]. The importance of the E2 glycoprotein was first identified when comparing the attenuation of the vaccine strain TC83 to its parent strain Trinidad Donkey (TRD). TC83 was developed as a vaccine strain through serial passaging of TRD, which lead to the accumulation of 12 SNPs[50, 51]. Further investigation revealed that the attenuation of TC83 could be attributed to two specific SNPs—one located in the 5'UTR and the other in the E2 glycoprotein[50]. While the 5'UTR mutation was determined to enhance virulence of TRD, the E2 glycoprotein was identified as the main determinant of virulence. When examined, amino acid changes were found to be present within the E2 glycoprotein of all epizootic strains investigated, resulting in an increase in the amino acid charge of the E2 glycoprotein[37]. Conversely, a decrease in charge was observed in the attenuated vaccine strain TC83 compared to its epizootic parent strain TRD [51]. Initial horse studies showed that a single point mutation within the E2 glycoprotein is sufficient to convey an epizootic virulence and viremia phenotype in horses when introduced into enzootic ID strains[47, 48]. Furthermore, these same E2 glycoprotein mutations have also been shown to regulate adaptation to epizootic mosquitos[52], indicating the importance of the E2 glycoprotein in the emergence of epizootic VEEV. While these mutations alone have been demonstrated to be sufficient for imparting epizootic phenotypes, it is worth noting that epizootic subtypes also undergo mutations beyond this specific region[53]. Additional mutations occurring in non-envelope genes and cis-acting elements within the VEEV genome have been shown to also influence the development of viremia and the depletion of lymphoid cells from lymphoid organs, as previously demonstrated in guinea pig models[53]. Early research into the role of interferon during VEEV infection revealed a correlation between increased IFN-α/β resistance and epizootic strains, leading to the hypothesis that epizootic IFN resistance may lead to increased viremia in horses [54, 55]. While further research failed to validate this hypothesis for all epizootic and enzootic strains, the relationship between IFN signaling and epizootic phenotypes has remained of interest [56].

Another consideration in the outbreak of epizootic VEEV is the difference in mosquito vectors used. Two genera of mosquito have been identified as the main vectors in epizootic outbreaks: *Ochlerotatus* and *Psorophora*[57, 58]. Both mosquito genera are considered floodwater mosquitoes and are subject to huge fluctuations in population density during heavy rainfall. This likely contributes to their role as epizootic vectors as epizootic VEEV outbreaks occur more frequently during periods of increase rainfall. Increased oral susceptibility of *Ochlerotatus taeniorhynchus* mosquitos to epizootic IAB viruses compared to enzootic ID and IE strains demonstrates that viral adaption to epizootic vectors may also be an important factor in epizootic emergence[30, 52, 59].

Geographical distribution of VEEV subtypes

Phylogenetic analysis of IAB, IC, ID and IE subtypes divide these into four distinct lineages previously identified by Forrester *et al*. [28], with IE subtype strains being vastly different from IAB, IC and ID subtypes. Independent evolution of the IE subtype strains has resulted in a significant divergence from other VEEV complex viruses, with unique glycoprotein substitutions, likely in part due to their adaptation to their unique mosquito vector *Culex (Melanoconion) taeniopus*[60]. The geographical isolation of the IE subtype, possibly caused by the landscape limiting the mobility of the reservoir host rodents and mosquito vector, has likely contributed to the separate maintenance of this subtype. IE subtype strains are endemic in Mexico and Central America, whereas ID strains are endemic in northern South America, with the driving line between subtypes loosely corresponding with the Panamanian/Costa Rican boarder (**Figure 1.2**). While historically IE subtypes have only been considered as enzootic strains, two small outbreaks in 1993 and 1996 in Mexico contradicted this, as these epizootic strains were found to be closely related to enzootic IE strains previously isolated in Guatemala[13, 61]. While only ID strains have been associated with the emergence of IAB/IC epidemics[12, 38, 46-48], two IAB outbreaks were recorded in the late 60s and early 70s in Mexico and southern Texas, dxespite the absence of endemic ID strains in these regions. Phylogenetic analysis supports the hypothesis that these outbreaks were caused by the use of incompletely inactivated IAB derived vaccines, which were widely used in these areas prior to the introduction of the live-attenuated TC83 vaccine in 1971 [62]. In fact, all IAB associated epidemics that occurred after 1943 are suspected to be due to these inactivated vaccines[28, 62].

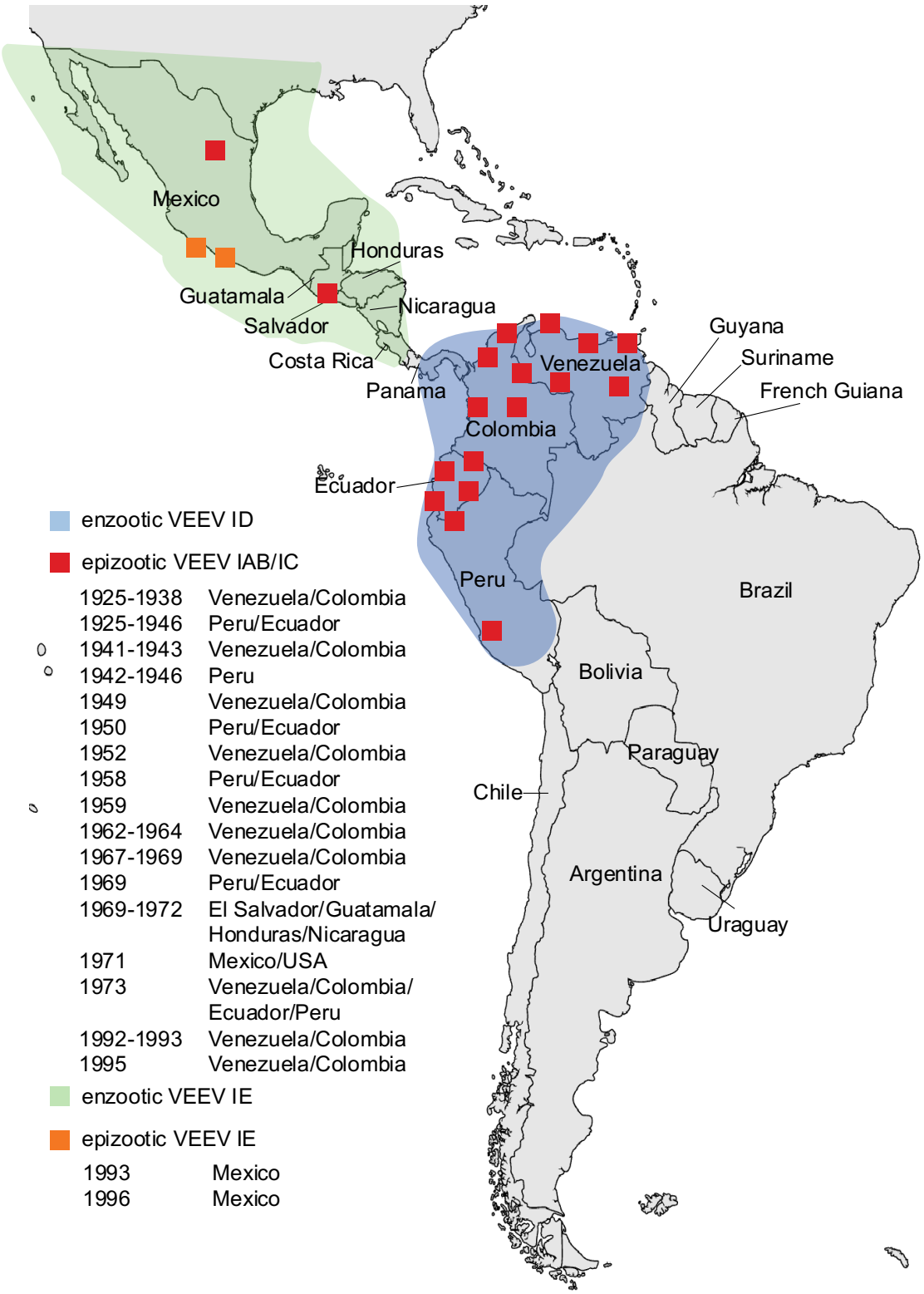

Figure 1.2 Locations of enzootic VEEV and epizootic outbreaks in the Americas. Shaded in blue (ID) and green (IE) are the regions in which enzootic VEEV is considered endemic. The epizootic VEEV outbreaks listed in the legend are indicated with a red (IAB/IC) or orange (IE) box on the map[11].

Alphavirus genome organization and protein functions

The alphavirus virion is roughly 70nm in diameter with the glycoproteins organized in a T = 4 icosahedral symmetry [63, 64]. The virion encapsulates a single-stranded positive-sense RNA genome (~12kb) within a nucleocapsid core, further surrounded by a host-cell derived lipid membrane. The RNA genome contains a 5'UTR cap0 (N7mGppp)[65], a 3' polyA tail and is composed of two open reading frames (ORFs). ORF1 contains four non-structural proteins (nsp1-4) which mediate viral translation, replication, whereas ORF2 contains five structural proteins (capsid, E3, E2, 6K/TF and E1) (**Figure 1.3**).

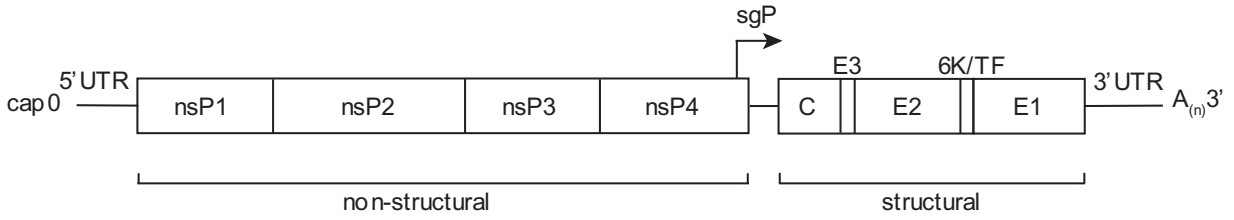

Figure 1.3 Alphavirus genome organization

NON-STRUCTURAL PROTEINS

nsP1, a 60 kDa protein encoded by alphaviruses, performs a diverse array of functions critical for efficient viral replication. The N-terminus of nsP1 encodes methyltransferase and guanylyl transferase motifs [66], which play a pivotal role in the 5' RNA capping of viral genomic and sub genomic RNA during replication. This process ensures the stabilization and protection of viral RNA, facilitating its successful translation and replication within the host cell. Additionally, nsP1's involvement in minus-strand RNA synthesis has been recognized, although the underlying mechanism remains elusive[67-70]. Studies have revealed that mutations within nsP1 can adversely impact minus-strand synthesis without affecting the enzymatic properties of the protein, suggesting a nuanced role in RNA synthesis regulation[68, 70]. Lastly, nsP1 contains a packaging signal located in the VEEV genome between nt positions 856-1150[71]. While there is heterogeneity between both the sequence and location of packaging signals from different alphaviruses, most contain 4-6 stem-loops along with a short GGG motif in the loop. The GGG sequence has been shown to be critical in VEEV packaging, with the presence of at least one stem-loop being required to maintain wild-type packaging efficiency[71].

nsP2 is a 90kDA protein that functions as a helicase, a triphosphatase and a protease during alphavirus replication. The helicase activity is crucial for unwinding the RNA secondary structure during viral replication and is dependent on the nucleoside triphosphatase (NTPase) activity of the N-terminal domain[72, 73]. This domain is also associated with the RNA

5'triphosphatase (RTPase) activity of nsP2. This RTPase activity is responsible for replacing the γ-phosphate at the 5'end of the newly synthesized RNA with a diphosphate, thereby allowing for capping by nsP1[74]. The C-terminal domain of nsP2 contains a cysteine protease, responsible for processing the non-structural polyprotein [69, 75]. This protease activity is absolutely vital for viral replication [76]. Crystallographic analysis of nsP2 has further identified the presence of an methyltransferase-like domain at the C-terminus[77]. Yet due to the lack of the active-site residues required for enzymatic activity, this domain likely does not exhibit any enzymatic activity, though it has been implicated in facilitating substrate binding to the protease [77, 78]. In addition, through mutational analysis of nsP2, two putative N-terminal domains have been described. The first domain has been implicated as a cofactor for the protease, whereas the second putative domain may play a role in promoter selection [79, 80]. Lastly, in Old World alphaviruses such as Sindbis virus (SINV) and Semliki Forest virus (SFV), nsP2 is responsible for the induction of host transcriptional shutoff [81-84]. This differs from New World alphaviruses including VEEV and EEEV, in which the capsid protein has been shown to control transcriptional shutoff[85].

The role of ~60kDA nsP3 during alphavirus replication has long been considered more ambiguous compared to the other non-structural proteins. While mutational studies of nsP3 have clearly demonstrated its importance in RNA synthesis[67, 86-88], particularly in the initiation of minus-strand synthesis and sub-genomic RNA synthesis, the precise role(s) that nsP4 plays during replication remains elusive. Despite this, nsP3 does contains three recognized domains: the N-terminal macrodomain, the alphavirus unique domain (AUD) and the C-terminal hypervariable domain (HVD). The first is an N-terminal macrodomain which is highly conserved amongst alphaviruses. This macrodomain contains both phosphatase capabilities and can bind nucleic acids[89]. In addition, this N-terminal macrodomain has been implicated to be involved in interactions with host proteins[90-92]. The AUD is found within the central region of nsP3 and is mostly conserved amongst alphaviruses. Crystallography of nsP2-nsP3 identified a zinc-binding domain (ZBD) within the AUD of nsP3[93]. Mutational studies of this domain have shown it to be crucial for minus-strand synthesis, sub-genomic RNA synthesis, polyprotein processing and neurovirulence[94-96], though the mechanism through which this happens has yet to be described. Lastly, the hypervariable C-terminal domain of nsP3, is poorly conserved amongst alphaviruses, differing both in length and sequence. While the virus is mostly tolerant to mutation and even deletion of this domain in tissue culture, these mutations frequently lead to attenuation of infection in mouse models[94, 97, 98], emphasizing the importance of this HVD for alphavirus replication. The HVD is phosphorylated at multiple sites during infection, though the extreme diversity of this domain between alphaviruses also results in diversity in the phosphorylation

sites[99, 100]. While mutation of the phosphorylation sites in SFV has little effect on viral replication kinetics in cell cultures, they do result in attenuation in mice[101], highlighting the importance of these sites. In addition, phosphorylation of HVD in VEEV was shown to have no effect on viral replication in vertebrate cells yet was shown to be important in mosquito cells[102]. Foy et al. further demonstrated that while the permissible cell line BHK-21 did not require the HDV for viral replication, it is essential for replication in other cell lines[102]. Together, these data suggest a role for the HVD host-virus interactions and cell-type specificity.

Lastly, nsP4 is a ~70kDa protein which functions as the viral RNA-dependent RNA-polymerase. nsP4 is the most highly conserved protein amongst alphavirus, with upwards of 50% amino acid homology between different viruses [103, 104]. The alphavirus RdRp contains an N-terminal ~100nt alphavirus unique domain, followed by ~500nt of traditional RdRp domains including fingers, palm domain with a GDD active site, and thumb domains[105-107]. Using a recombinant bacterial system, SINV nsP4 was shown to perform terminal adenylyltransferase activity (TATase) independently of other nsPs, an important function in polyadenylation of newly synthesized RNAs[106, 107]. However, de novo RNA synthesis was shown to require all four proteins for efficient replication[106]. The N-terminal region of nsP4 is predicted to be unstructured and the function of this region is less clear. However, deletion studies have shown that this region is essential for both plus and minus strand RNA synthesis and possibly important for protein-protein interactions and template recognition[70, 108].

STRUCTURAL PROTEINS

The main structural proteins are encoded by ORF2 are capsid (Cp), E1, E2 and E3. The Cp protein is responsible recognizing the viral genomic RNA and encapsulating it into a T = 4 icosahedron nucleocapsid [63, 64]. Outside of its structural role, New World Alphavirus Cp has been implicated in shutoff of cell host translation through interactions with importin α/β and nucleoporins[109, 110]. During replication, the E1 and E2 proteins assemble in heterodimers to form the viral spike proteins, which are arranged on the host cell membrane and end up on the envelope of the virions through budding from the host membrane. While E1 and E2 are arranged together in heterodimers on the virions, they both play distinct role in viral entry, with E2 being required for interacting with the host receptor [111-113] and E1 being primarily required for membrane fusion[114, 115]. Prior to E1 and E2 heterodimer formation in the endoplasmic reticulum (ER), E3 is associated with E2 and is required for proper folding of the precursor E2 (pE2) protein as well as formation of the spike protein and transportation of the spike protein to the site of budding[116-118]. It has been proposed that E3 is necessary for stabilizing the spike

protein as it travels through the more acidic environment of the Golgi, though cleavage of E3 from pE2 by furin-like proteases is required to make the virions fusion competent [119]. Despite the cleavage of E3, the presence of E3 on the virions of some alphaviruses (e.g. SFV and VEEV) but not on others (e.g. SINV) suggests some heterogeneity in the function of this protein[120, 121].

The last two structural proteins are the 6K and the trans-frame (TF) proteins. Translation of ORF2 results most often results in the production of 6K and E1. However, during roughly 10-18% of ORF2 translation, ribosomal stalling occurs due to the presence a UUUUUUA motif followed by an RNA stable structure[122, 123]. This causes a -1 frameshift, and the TF protein is translated in place of 6K and E1 occurs. 6K and the TF protein both contain identical N-terminal transmembrane helix, thought to be involved in ion-channel activity[124]. In addition, 6K contains a cytoplasmic loop followed by a second transmembrane helix, which functions as a translocation signal for E1. On the other hand, TF encodes a unique cytoplasmic C-terminal extension domain and precludes the translation of E1. 6K deletion studies have demonstrated the importance of 6K and TF protein in assembly, possibly by stabilizing spike protein and glycoprotein processing [124, 125]. Functional studies investigating the role of TF protein during infection have demonstrated that disruption of TF protein production decreases replication in mammalian and insect cell cultures, and furthermore significantly reduced mouse mortality in SINV infected mice[123], emphasizing the importance of the -1 frameshift and TF protein production during infection.

UNTRANSLATED REGIONS

In alphaviruses, the 5'UTR varies in length between 27nt and 83nt, with VEEV complex 5'UTRs between 42-48nt[126]. The 5'UTR plays several distinct roles during alphavirus replication. The alphavirus 5'UTR and sub-genomic promoter capping is performed by nsP1 (as described below) and results in the addition of a 5' 7-methylguanosine (m7G) to form a cap structure (cap 0)[127, 128]. This cap structure is required for both mRNA stability and translation of the viral mRNA. Contrary to what is seen with Flaviviruses, both the sequence and structure of the 5'UTR do not alter capping efficiency of the 5'UTR of alphaviruses[129].

While all alphavirus RNA requires a cap to be translated, the RNA sequence and structure of the 5'UTR and sub-genomic promotor further regulate translation[130, 131]. This is evidenced by the differences in translation efficiency observed between RNAs containing the genomic or sub-genomic sequences of both SINV and SFV. Differences in the sequence and predicted RNA secondary structures directly adjacent to the 5' cap were shown to alter the affinity of host translation initiation factors eIF4E and eIF4F to the RNA, highlighting an additional role of untranslated regions in translation regulation.

Next to its role in translation, the 5'UTR is critical for alphavirus RNA replication. RNA replication is reliant on the synergistic function of two independent RNA elements contained within the 5'UTR [132-134]. The first is the AU dinucleotide at the 5' terminus of the 5'UTR. This unpaired dinucleotide sequence is highly conserved amongst alphaviruses and plays a crucial role in viral RNA synthesis. Furthermore, this sequence may be required at the 3'end of the negative-sense RNA for initiation of positive-sense genomic RNA synthesis, through binding of the viral RdRp (nsP4)[70]. The second 5'UTR RNA element is a stable G-C rich stem-loop directly adjacent to the AU dinucleotide sequence. While mutational studies altering the loop sequence had no effect on viral replication, changes to the thermostability of the stem had a deleterious effect on viral replication, highlighting the importance of this structure [132].

In addition to its roles in viral translation and RNA replication, the 5'UTR of alphaviruses has been implicated in immune restriction and viral pathogenesis. A single point mutation at the 3rd nucleotide position in the 5'UTR of VEEV TC83 resulted in attenuation both *in vitro* and *in vivo[50, 51].* Further investigation demonstrated that while this strain was attenuated in immunocompetent cells and mice, in the absence of type I IFN signaling there was no effect on replication[54, 135]. Similar analogous point mutations identified in the 5'UTRs of both SINV and SFV were also shown to effect rodent pathogenicity and neuro-invasion[136-139]. The mechanism by which these mutations were affecting viral replication was later identified, as these 5'UTR mutations in SINV and VEEV resulted in enhanced interactions of IFIT1 with viral RNA[140]. Ifit1 is an interferon-stimulated gene (ISG) that is quickly upregulated following viral invasion and suppresses the translation of non-self RNAs (reviewed in[141]). It does this by recognizing Cap 0 RNAs, which lack the 2'O methylation found in Cap 1 structures on host mRNAs. Although alphavirus genomic and sub-genomic RNAs contain Cap 0 structures, they evade IFIT1 recognition due to the thermodynamically stable 5' stem-loop in their 5'UTRs. Reducing the stability of this stem-loop increases the susceptibility of SINV and VEEV to IFIT1 by promoting IFIT1 binding to viral RNA.

Like the 5'UTR, there is considerable variation in the length of the 3'UTR, particularly between different complex alphaviruses. Despite the differences in length, most alphaviruses share common 3'UTR features, including repeated sequence elements (RSE), and a 19-24nt CSE located directly adjacent to the viral poly(A) tail[142-144].

Reflecting the variation in 3'UTR length, the number of RSEs and the length of these regions vary significantly amongst alphaviruses. While the precise function of these RSEs has not been identified for all alphaviruses, deletion studies in both EEEV and CHIKV have resulted

in poor replication in mosquito cells without affecting mammalian cell replication, indicating that retention of these regions is required for mosquito adaptation[145-147].

The 19-nt CSE is located directly adjacent to the viral poly(A) tail and is highly conserved amongst members of the alphavirus genus[142-144]. Mutation studies of this CSE in SINV have shown reduction of plaque size and viral replication as well as a reduction in the efficiency of minus-strand synthesis[142, 148, 149]. Furthermore, the poly(A) tail has been shown to work in conjunction with the 19-nt CSE to maintain the efficient of minus-strand synthesis. In this, the importance of the position of the 19-nt CSE in relation to the poly(A) tail as well as the minimum required length (11-12 residues) of the poly(A) tail has been demonstrated[149, 150].

Lastly, alphavirus 3'UTRs have also been shown to contain important miRNA and protein binding sites, which can regulate translation of viral RNAs during infection[151-153]. For example, the myeloid specific miRNA miR-142-3p can interact with the viral genome of EEEV though binding sites within the 3'UTR and block translation of the viral genome. *In vivo*, this myeloid specific repression of EEEV viral translation and replication has been shown to result in a reduction of type I IFN signaling and limited early signs of disease, yet increased pathogenicity in mice[151]. This is mirrors what is seen in human infections, where short prodrome is associated with poor clinical outcomes in children[154]. Mutation of these miRNA binding sites restores viral replication and translation in myeloid cells *in vivo*, while also enhancing type I IFN signaling, early disease indicators, and viral attenuation[151]. Furthermore, the protein human antigen R (HuR) has been shown to interact with most alphaviruses through a binding site directly upstream of the 3'UTR CSE. HuR is a universally expressed RNA binding protein (RBP), which preferentially binds to AU rich elements (ARE), thereby stabilizing mRNA and enhancing translation. During infection, alphaviruses have been shown to sequester HuR thus preventing viral RNA decay[153, 155]. In addition, this sequestration of HuR away from host mRNAs also results in the destabilization and decay of host mRNAs reliant on HuR, consequently dysregulating the expression of cellular proteins[153].

Alphavirus replication

Like many RNA viruses, alphaviruses replicate in the cell cytoplasm. Alphavirus infection begins when the E2 glycoprotein on the virion interacts with a receptor on the host cell surface, thereby initiating cell entry. The required receptor is not universal amongst alphaviruses. While some receptors such as CD147 protein complex have been shown to facilitate entry of both Old and New World Alphaviruses (eg. CHIKV, RRV, SINV, WEEV and EEEV)[156], other receptors have only been associated with entry of a particular virus. The first and so far, only receptor

described for VEEV entry was recently identified by Ma *et al.*[157]. Ldlrad3, a member of the scavenger receptor family, is conserved between mammals, birds, fish, amphibians and reptiles[157]. Ma *et al.* demonstrated that Ldlrad3 binds directly to the VEEV virion and enhances viral attachment and internalization of viral particles in neuronal cells. Despite being widely conserved amongst many species, mosquitos do not encode Ldlrad3, suggesting that a different entry receptor is required in mosquito infections. Next to receptors, three types of attachment proteins have been described for alphaviruses: C-type lectins, heparin sulfate and phosphatidylserine receptors[158-164]. While these factors play a role in concentrating virus on the surface of a cell, they are not sufficient to mediate cell entry and not always required.

Following receptor binding, the virions are internalized through clathrin-mediated endocytosis [111-113]. Once internalized, the maturation of the endosome results in a progressive decrease in the pH. This low pH environment causes the dissociation of the E1-E2 dimer, thereby allowing the hydrophobic fusion peptide of E1 to insert itself into the endosomal membrane to form a fusion pore. This results in the release of the viral nucleocapsid into the cytoplasm [114, 115]. In contrast to Old World alphaviruses, such as Sindbis virus and Semliki Forest virus, which enter from early endosomes, VEEV entry is dependent on the further acidification of the endosome that occurs with the maturation of early endosomes into late endosomes [165]. Once in the cytoplasm, the nucleocapsid is almost immediately uncoated releasing the viral RNA [166].

Due to the presence of the 5' cap and 3' polyA tail, the viral genomic RNA is treated as an mRNA and directly translated upon entry into the cytoplasm. ORF1 is translated into the polyproteins P123 and P1234. Approximately 90% of translation events result in P123 with P1234 only being translated upon readthrough of the opal stop codon between nsP3 and nsP4[167, 168]. After translation of P1234, nsP4 is released from the polyprotein through to the proteolytic activity of nsp2. Once released, nsP4 can perform its duty as RNA-dependent RNA polymerase and in complex with P123 initiates the synthesis of the minus-strand RNA, which in turn serves as a template for the genomic and sub-genomic RNA [169]. The polyprotein is then further processed into nsP1 and P23 [170, 171]. The replicase complex nsP1-P23-nsP4 is then formed at which point the switch from negative-sense RNA synthesis to positive-sense RNA synthesis happens [169, 172]. While the replication complex nsP1-P23-nsP4 is capable of synthesizing both the sub-genomic and genomic RNAs, P23 is extremely short-lived and quickly cleaved into nsP2 and nsP3 [169, 172]. The majority of sub-genomic and genomic RNAs are therefore synthesized by the complex nsP1-nsP2-nsP3-nsP4, with the sub-genomic RNA being synthesized in excess of the genomic RNA.

The process of alphavirus RNA synthesis occurs in association with host cell membranes. Once translated, nsP1 initiates the formation of membrane invaginations, named spherules, by binding to negatively charged phospholipids on the cytoplasmic side of the plasma membrane [173-175]. Studies using SFV and SINV have shown that these spherules are first initiated at the plasma membrane and later internalized and fused with endosomes and lysosomes, forming type I cytopathic vacuoles (CPVs) [173, 174]. The extent to which spherules are internalized is highly dependent on the alphavirus, with SFV and SINV spherules being mostly internalized and CHIKV spherules remaining associated with the cell membranes. All four non-structural proteins as well as newly synthesized viral RNA and dsRNA have been detected in association with these spherules, supporting their role in alphavirus RNA synthesis[170, 176]. During synthesis, sub-genomic RNA is released from the replication complex into the cytosol, where it is translated.

As with the non-structural proteins, the structural proteins are translated as a polyprotein. Upon translation, Cp is immediately proteolytically cleaved due to its auto-protease activity and released into the cytoplasm[177, 178]. Once in the cytoplasm, Cp recognizes the packaging signal located within nsP1 of the genomic RNA and encapsulates a single copy of the genome into the nucleocapsid[179, 180]. Cleavage of Cp also exposes the localization signal for the remaining polyprotein causing translocation into the ER membrane[181]. Once in the ER, the polyprotein undergoes further processing of the glycoproteins into the spike protein, which is then trafficked through the trans-Golgi network to the plasma membrane. Finally, interactions between the viral glycoproteins on the membrane with the nucleocapsid promote budding of newly formed virions.

Innate immunity during VEEV infection

One of the hallmarks of VEEV infection is the system wide upregulation of type-I IFNs and proinflammatory cytokines early during infection[23]. During infection, viral dsRNA structures and sequences act as pathogen-associated molecular patterns (PAMPs) that are recognized by host RNA-binding proteins (RBPs), particularly pattern recognition receptors (PRRs). These PRRs are crucial for the early detection of viral invasion[182]. In VEEV infections, the primary PRRs involved are RIG-I-like receptors (RLRs), specifically RIG-I and MDA5[183]. RLRs are a family of cytosolic RNA helicases that signal through the mitochondrial-associated protein MAVS, leading to the activation of transcription factors IRF3 and IRF7. Once activated, these transcription factors move to the nucleus, where they promote the expression of type I IFNs. The secretion of type I IFNs triggers autocrine and paracrine signaling, which amplifies the antiviral response by upregulating interferon-stimulated genes (ISGs). While the number of ISGs upregulated after IFN-β treatment

ranges in the hundreds, only a small number of upregulated ISGs have been implicated in restriction of VEEV infection[184].

The most prominent ISG in the context of VEEV infection is IFIT1[140, 184, 185]. IFIT1 belongs to a family of IFN-induced proteins with tetratricopeptide repeats (IFITs), which is highly upregulated during alphavirus infection. As discussed previously, IFIT1 recognizes and inhibits translation of Cap 0 RNAs, which lack the 2'O methylation present on host mRNA Cap 1 structures (reviewed in[141]). While natural VEEV strains utilize Cap 0, they evade IFIT1 recognition due to the presence of a thermodynamically stable 5'UTR stem-loop[140]. A single mutation within this stem-loop, as seen in the vaccine strain TC83, alters the thermodynamic stability of this structure, resulting in increased sensitivity to IFIT1. Next to the importance of IFIT1, knock down of IFIT3 has also been shown to be beneficial for viral replication, implicating it as another anti-viral factor at play during VEEV infection[184, 186]. However, the antiviral function of IFIT3 does not involve direct interaction with the viral genome. Instead, it binds to IFIT1, enhancing its half-life and allosterically regulating its RNA-binding activity, thereby improving IFIT1 recognition of Cap 0 structures[141]. Recent work conducted by our lab also identified IFIT2 as a restriction factor for VEEV[186]. Recombinant VEEV containing the 3'UTR sequences from different epizootic and enzootic isolates were differentially sensitive to inhibition by IFIT2, though contrary to previous studies[187], IFIT2 restriction was not mediated through translation inhibition. This work further suggests that next to mutations in the E2 glycoprotein, changes in RNA structure within the VEEV genome may also contribute to the emergence of epizootic VEEV.

One of the interesting aspects about VEEV is that while it produces a robust IFN response *in vivo*, commonly used cell lines such as fibroblasts and other non-myeloid cells are not capable of producing type-I IFNs during infection[188-190]. While these cells do produce type-I IFN mRNA, nsP2 mediated translation shut-off efficiently restricts secretion of type-I IFN proteins during infection. Contrary to non-myeloid cells, a subset of immortalized and bone marrow derived mouse macrophages have been identified as resistant to macromolecular shut-off by VEEV and allow for IRF7-mediated upregulation and secretion of IFN-α/β during infection[190]. This further emphasizes the importance of myeloid cells as the main contributors of system wide IFN signaling during *in vivo* infections.

Additional roles for RNA structure during infection

Several important viral RNA structures and conserved sequence elements (CSE) have been identified within the Alphavirus genomes. These viral RNA structures and CSE interact with viral and host proteins to facilitate viral replication, transcription, translation and packaging of viral

RNAs. As discussed previously, there are several critical CSE contained within the untranslated regions of the alphavirus genome: a 5' AU dinucleotide and adjacent stable G-C rich stem-loop, and the 19-nt CSE at the 3'end of the 3'UTR. However, there are various additional well described CSE across the coding regions of the viral genome that have also been implicated in viral replication which will be discussed here.

Firstly, the 5'end of nsP1 contains a 51-nt CSE, which is widely conserved amongst alphaviruses and functions as an enhancer of viral replication [133, 191-193]. Both predictive and experimentally informed RNA structure analysis of this region has identified two short stem-loops within both the plus and minus strand viral RNAs[194, 195]. Mutational studies of this element suggest that while this CSE is not strictly required for replication in vertebrate cells, disruption of this element has deleterious effects on replication in mosquito cells[191].

Next, alphaviruses also contain an RNA packaging signal (PS) located within nsP1[71, 179]. Despite divergence of different alphavirus clades, most retain PS with similar structural and functional properties, allowing Cp proteins from different clades to recognize PS from heterologous alphaviruses. Alphavirus PSs contain 4-6 stem-loop structures with conserved GGG motifs within the loop, with one GGG-motif stem-loop being minimally required for efficient packaging. Mutation of either the stem-loops or just the GGG motif result in dysfunctional packaging and lead to mostly non-infectious virions containing sgRNA[71].

While not present in other alphaviruses, SINV and SFV contains a prominent hairpin-loop RNA structure, also referred to as downstream loop or DLP, located 24nt downstream from the ORF2 AUG codon[196, 197]. During most viral infections, protein kinase R (PKR) is activated by dsRNA and phosphorylates eukaryotic initiation factor 2α (eIF2α) effectively halting host translation in an attempt to inhibit viral replication. Most viruses have developed means by which to circumvent PKR activation, such as sequestering dsRNA or degrading PKR (reviewed in[198]). Contrary to most viruses, SINV infection strongly activates PKR, causing the phosphorylation of eIF2α and shutdown of host translation[197, 199]. Despite activation of PKR, SINV is able to efficiently translate its structural proteins as the DLP promotes 40S ribosomal binding to the AUG codon in the absence of eIF2[197, 200]. While this DLP is required for replication in vertebrate cells, it is fully dispensable in insect cells as they do not have PKR.

Lastly, the -1 ribosomal frameshifting required to produce the TF protein is dependent on the presence of a slippery UUUUUUA motif in conjunction with a stable RNA structure[122, 201]. While the heptanucleotide slip site is conserved between all alphaviruses, there is considerable variation in the accompanying predicted RNA secondary structures, varying between stem-loops,

hairpins and pseudoknots[122]. Regardless, the presence of these structures is required to induce backward slipping of the ribosome during translation for the production of the TF protein.

Thesis work

The maintenance of enzootic VEEV in nature and the sporadic emergence of epizootic VEEV makes future epidemics unavoidable. While the significance of E2 amino acid mutations in driving the emergence of epizootic phenotypes is well-documented[12, 38, 46] [48, 52], additional mutations occurring in non-envelope genes and cis-acting elements within the VEEV genome have also been shown to affect IFN sensitivity and pathogenicity[53, 140]. Previous work by our lab and others, have demonstrated the importance of RNA structure not only in alphavirus replication, but also in protection against host innate immune responses. Interestingly, the majority of mutations which arise between enzootic and epizootic isolates are synonymous. In this thesis work, I sought to identify additional RNA elements within the VEEV genome which contribute to emergence of epizootic VEEV. Through RNA structure predictions of enzootic and epizootic VEEV strains and mutational studies (described in detail below) I was able to identify RNA structures which confer enhanced replication in macrophages, which are early targets of VEEV infection. Understanding how enzootic and epizootic RNA structures influence cell-type specificity in macrophages will provide valuable insights into how initial stages of infection affect viral pathogenesis.

Chapter II: RNA structures within Venezuelan equine encephalitis virus E1 alter macrophage replication fitness and contribute to viral emergence

Adapted from accepted manuscript: Hickson SE, Hyde JL (2024). "RNA structures within Venezuelan equine encephalitis virus E1 alter macrophage replication fitness and contribute to viral emergence." PLoS Pathog 20(9): e1012179

Introduction

Alphaviruses are a group of enveloped positive-sense RNA (+ssRNA) viruses belonging to the *Togaviridae* family. These viruses are transmitted by arthropod vectors and are etiological agents of several significant human and veterinary diseases. Alphaviruses are globally distributed and can be broadly classified in two groups based on their associated pathologies, chiefly arthritogenic or encephalitic. Venezuelan equine encephalitis virus (VEEV) causes periodic outbreaks of febrile and encephalitic disease in equids and humans throughout Central and South America [36]. Endemic/enzootic VEEV is predominantly transmitted between *Culex (Melanoconion)* spp. mosquitoes and sylvatic rodents such as cotton rats and spiny rats which are believed to be the major reservoir host for these endemic/enzootic viruses (subtypes ID and IE) [35]. Emergence of epidemic/epizootic VEEV (subtypes IAB and IC) occurs de novo via mutation of enzootic subtypes [37]. In contrast to endemic/enzootic VEEV, epidemic/epizootic subtypes are primarily transmitted between several mammalophilic mosquitoes and equines which are the major amplification hosts during these outbreaks [52, 58]. Spillover infections into humans also occur during epidemic/epizootic episodes and can be associated with severe encephalitic disease and death, as well as long-term debilitating sequelae [45]. Repeated emergence of epidemic/epizootic VEEV has previously been shown to involve mutation of the viral attachment protein (E2) of ID endemic/enzootic subtypes which give rise to epidemic/epizootic VEEV subtypes IAB and IC [12, 38, 46]. E2 mutations were found to facilitate increased replication levels in horses, heightened virulence, and adaptation to epizootic mosquito vectors [48, 52]. While these mutations alone have been demonstrated to be sufficient for imparting epizootic phenotypes in a laboratory setting, epidemic/epizootic subtypes contain numerous additional mutations across the viral genome which studies suggest may contribute to epidemic/epizootic emergence [53, 54].

The VEEV genome is approximately 11.5kb in length and contains a 5'methylguanosine (m7G) cap and a 3' polyA tail [51]. The genome consists of two open reading frames, ORF1 which

encodes four non-structural proteins (nsp1-4) and ORF2 which encodes a subgenomic RNA from which the viral structural proteins are translated. We have previously shown that RNA structures present in the 5'UTR of the VEEV and Sindbis virus (SINV) confer resistance to the interferon stimulated gene (ISG) IFIT1, by preventing IFIT1 recognition of viral m7G capped RNA [140]. Similarly, we have observed that changes in VEEV 3'UTR structure alters IFIT2-mediated restriction of viral replication in a subtype-dependent manner [186]. Notably, most SNPs acquired by epidemic/epizootic strains following VEEV emergence are synonymous, suggesting that in addition to protein coding mutations in E2, changes in viral RNA structure may contribute to emergence of epidemic/epizootic VEEV. In this study we identify novel RNA structures in E1 that alter replication in macrophages which are early targets of VEEV infection in vivo. Conservation of SNPs and RNA secondary structures in this region suggest that these structures may contribute to emergence of epidemic/epizootic VEEV. These findings have significance for our understanding of VEEV evolution and emergence.

Results

To first identify putative RNA structures that differ between endemic/enzootic and epidemic/epizootic strains we used phylogenetic analysis to identify closely related pairs of enzootic and epizootic strains for subsequent RNA structure analysis (**Figure 2.1**). We compared 143 isolates and identified three enzootic (subtype ID) strains (R16905, 307537, and 204381) which exhibited 99.4%, 96.5%, and 96.2% sequence identity to the epizootic (subtype IAB) vaccine strain TC83. For downstream RNA structure analysis, we chose to compare TC83 and 307537. TC83 is a BSL2 attenuated vaccine strain developed by serial passage of strain Trinidad donkey (TRD) which was originally isolated from a sick donkey during an epizootic outbreak in Trinidad [50, 51]. TC83 shows 99.9% sequence identity with TRD but contains attenuating mutations in the 5'UTR and the viral attachment protein E2 [50, 51]. 307537 is a geographically distinct strain first isolated from mosquitoes and shares 96.5% sequence identity with TC83. To determine the predicted secondary structure of each viral genome, we used RNAfold [202, 203] [204] [205] to perform a sliding window analysis of each strain and generate an RNA structure score (RSS) for each window (**Figure 2.2B**). The RSS is generated by dividing the frequency of the minimum free energy structure (MFE) by the ensemble diversity (ED), and thus captures some qualitative data of RNA secondary structures formed by that sequence. In this instance, a higher RSS suggests the presence of RNA structures which are more thermodynamically stable and have a higher probability of forming. By reducing the complexity of RNA secondary structure to a single numerical value, we can compare large groups of sequences (e.g. phylogenetic analysis)

and identify RNA 'signatures' which may be unique or conserved within these groups. Our analysis revealed several regions with highly stable putative RNA structures (z-score >2), including nsp1, nsp2, nsp4, capsid, and E1 (**Figure 2.2B, Figure 2.3**). Previously defined functionally relevant RNA structures were also identified using this analysis, notably the nsp1 packaging signal [71] , and the ribosomal frameshift (RFS) motif in 6K/E1 which is required for production of TF protein [122, 206]. In addition, we identified several regions in which the predicted RNA structure differed between TC83 and 307537, including within E1 (**Figure 2.2C**). As we observed a high proportion of synonymous mutations in this gene (97.6%; **Figure 2.2A**) and have previously shown that RNA structures proximal to this gene (3'UTR) alter replication properties of VEEV [186] , we sought to define the role of E1 RNA structures in viral replication and their potential contribution to emergence of epizootic VEEV.

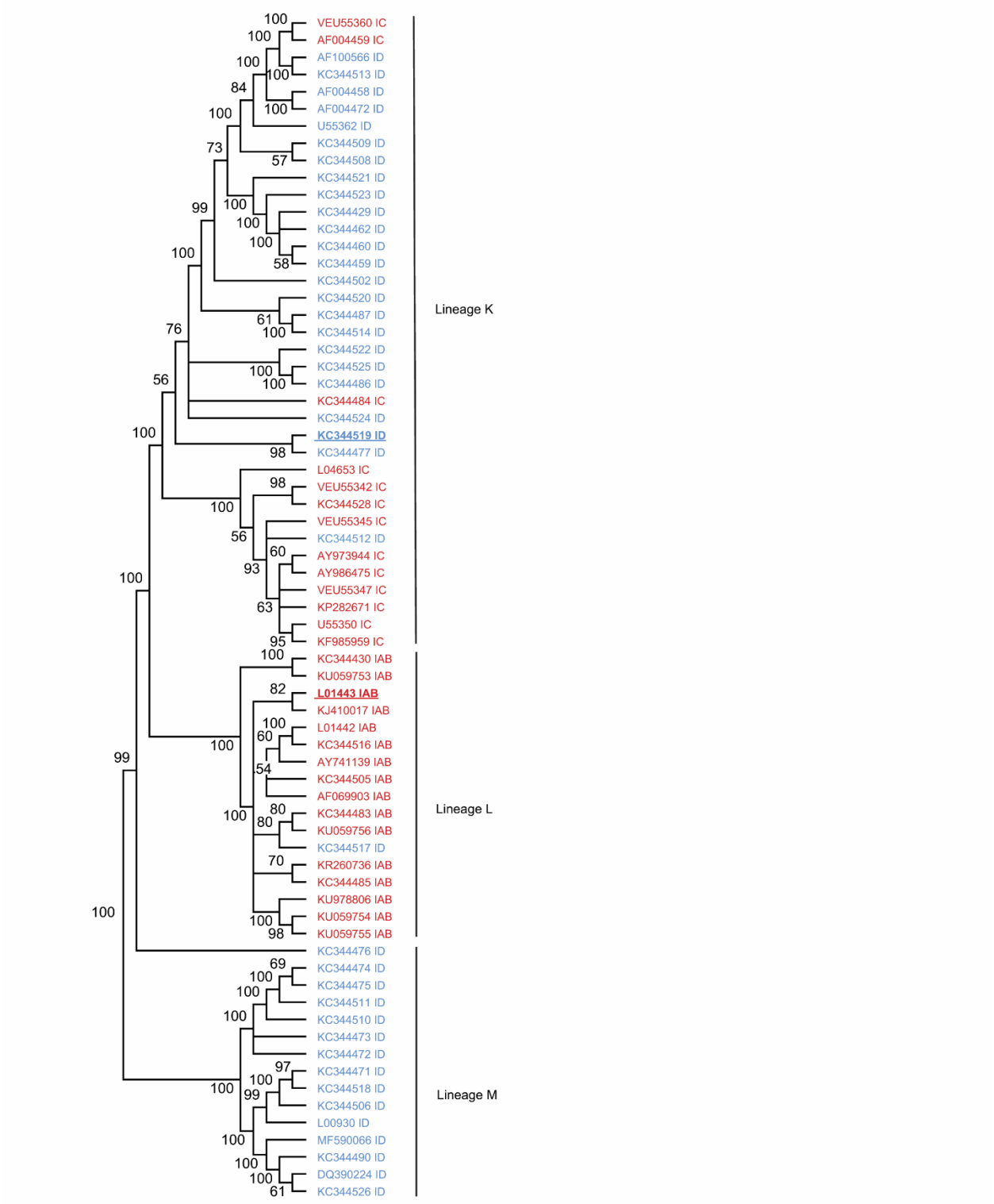

Figure 2.1 Phylogenetic tree of VEEV IAB, IC and ID subtypes. The optimal phylogenetic tree of lineages K, L and M (previously described in [28]) as determined by the neighborhood-joining method [207]. Shown next to each branch is the percentage of replicate trees in which the associated taxa clustered together in the bootstrap test (1000 replicates).

A

Gene	SNPs	Synonymous		Non-synonymous	
		#	%	#	%
5'UTR	2	2	100	-	-
nsp1	35	33	94.3	2	5.7
nsp2	86	76	88.4	10	11.6
nsp3	61	47	77	14	23
nsp4	73	71	97.3	2	2.7
SGP	0	-	-	-	-
capsid	32	27	84.4	5	15.6
E3	3	3	100	-	-
E2	57	41	71.9	16	28.1
6K	7	5	71.4	2	28.6
E1	41	40	97.6	1	2.4
3'UTR	6*	6*	100	-	-
Total	**403**	**351**	**87.1**	**52**	**12.9**

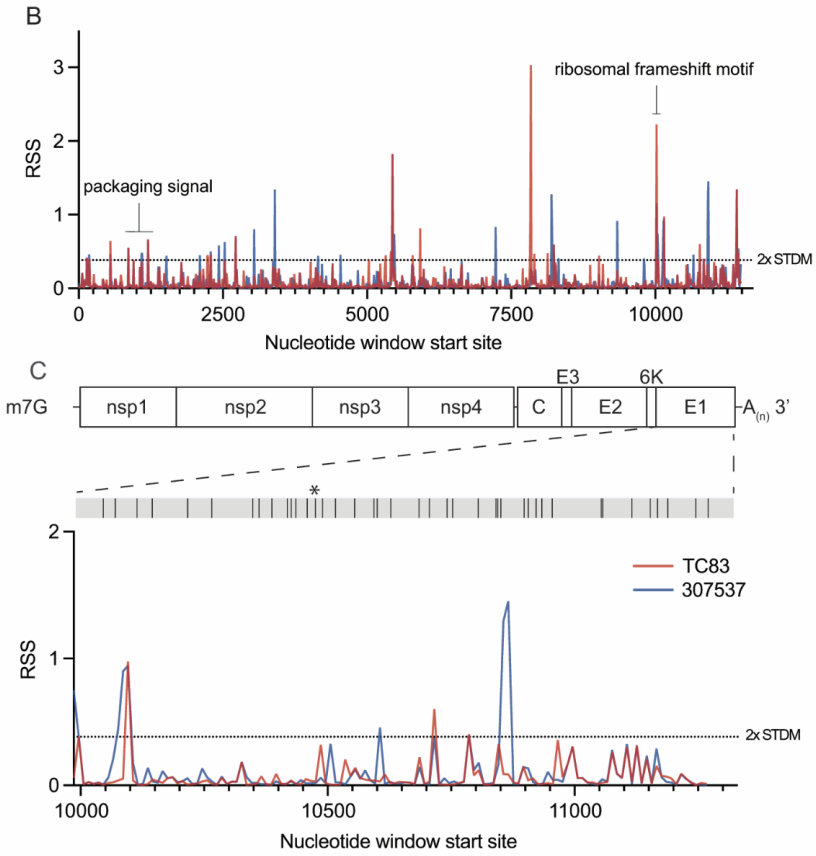

Figure 2.2 Predicted RNA secondary structure of E1 differs between epizootic and enzootic VEEV. (A) Summary of all SNPs identified between TC83 and 307537. (B) RNA structure analysis of subtype IAB and ID VEEV. RNA structure prediction of VEEV strain TC83 (IAB; accession L01443) and strain 307537 (ID; accession KC344519) was performed using RNAfold [17] (window size = 50nt, step size = 10 nt). The RNA structure score (RSS; frequency of MFE/ensemble diversity) is plotted against the nt window start site. Higher RSS indicates greater thermodynamic stability of predicted structures. The 2-fold standard deviation is indicated by a dotted line. (C) RSS analysis of gene E1 from strains TC83 and 307537. Location of all SNPs across E1, including a single coding change (*), are depicted in the grey bar above.

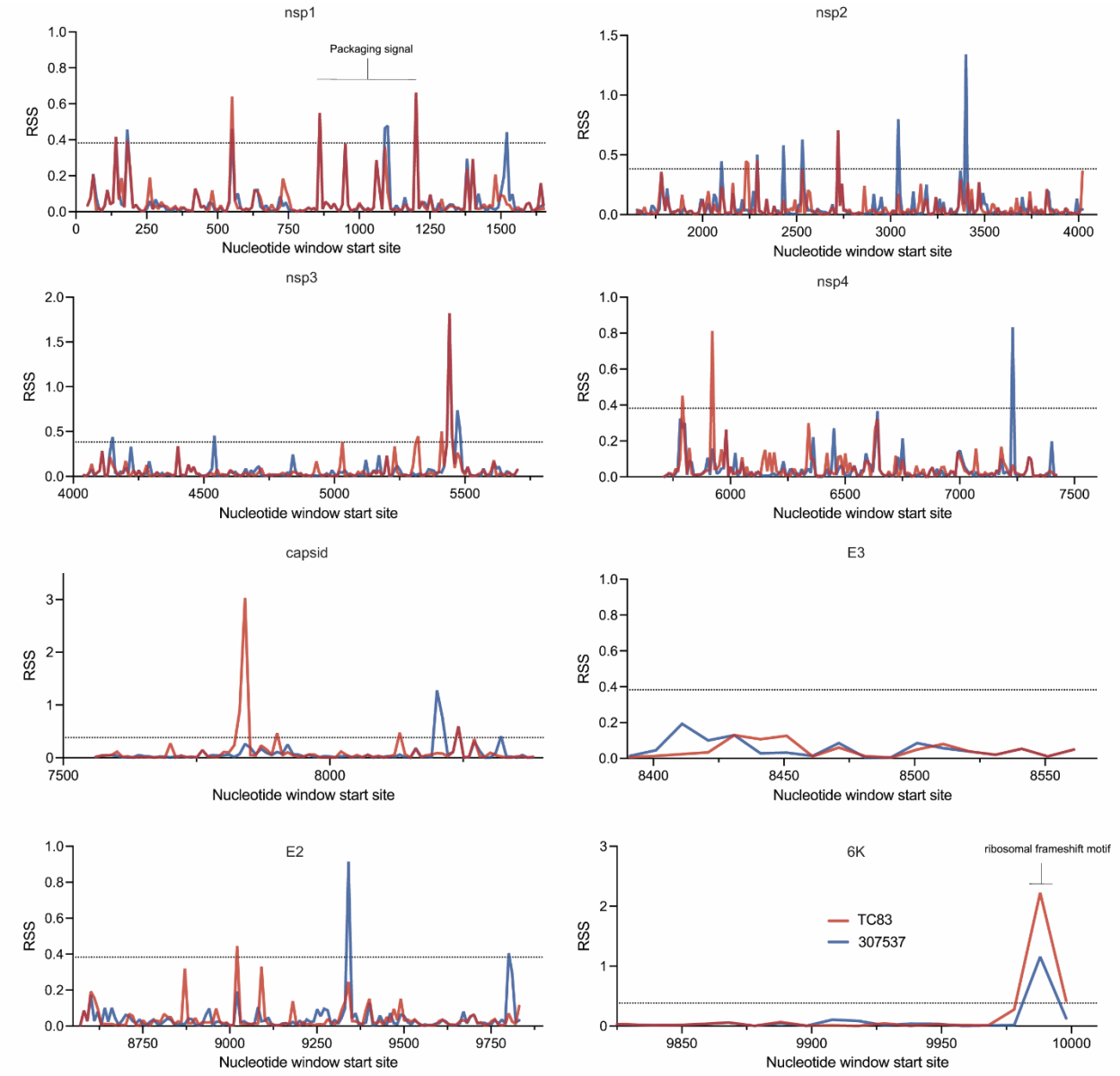

Figure 2.3 Sliding window analysis of the relative structure score (RSS) across the VEEV genome broken up by gene. The RSS was calculated as the minimum free energy (MFE)/ensemble diversity for each window of 50 nucleotides with a step size of 10. TC83 is shown in red and 307537 is shown in blue. Two standard deviations from the mean was calculated across the entire genome and is represented as a dotted line.

To determine whether changes in predicted E1 RNA structures alter VEEV replication properties, we generated a chimeric TC83 virus encoding all synonymous changes from E1 of strain 307537 (TC83/E1$_{IDsyn}$) (**Figure 2.4A**). To disentangle confounding effects of amino acid changes on replication phenotypes, this chimera excluded the single protein coding mutation found within this region (nucleotide (nt) 10,481, **Figure 2.2C**). Notably, inclusion of this mutation in our structure analysis did not significantly alter the RSS in this region, and thus was predicted to have minimal effect on E1 RNA structure (**Figure 2.2C**). We then compared replication kinetics of TC83 and TC83/E1$_{IDsyn}$ in several cell types including the macrophage cell line Raw264.7, primary bone marrow-derived macrophages (BMDM), primary bone marrow derived dendritic cells (BMDC), and mouse embryonic fibroblasts (MEF) **(Figure 2.4B-E**). Here, cells were infected with WT or mutant viruses at an MOI of 0.1 and production of infectious virus measured over time by focus forming assay (FFA). Myeloid cells including macrophages are early targets of encephalitic alphavirus infection in vivo and have been shown to be a source of type I IFN production early during infection [84, 208]. Thus, replication fitness in macrophages would be predicted to have significant impacts on outcomes of VEEV infection *in vivo*. In both Raw264.7 and primary BMDM we observed an increase in TC83/E1$_{IDsyn}$ relative to TC83 (at 12hpi, 8-fold in Raw264.7, P = 0.0035; 10-fold in BMDM, P = 0.0005) (**Figure 2.4B, C**). Remarkably, we observed no significant difference in replication of TC83 and TC83/E1$_{IDsyn}$ in either BMDC or MEF (**Figure 2.4D, E**), indicating that RNA sequences from E1 of enzootic VEEV specifically increases replication fitness in macrophages but not in other cell types.

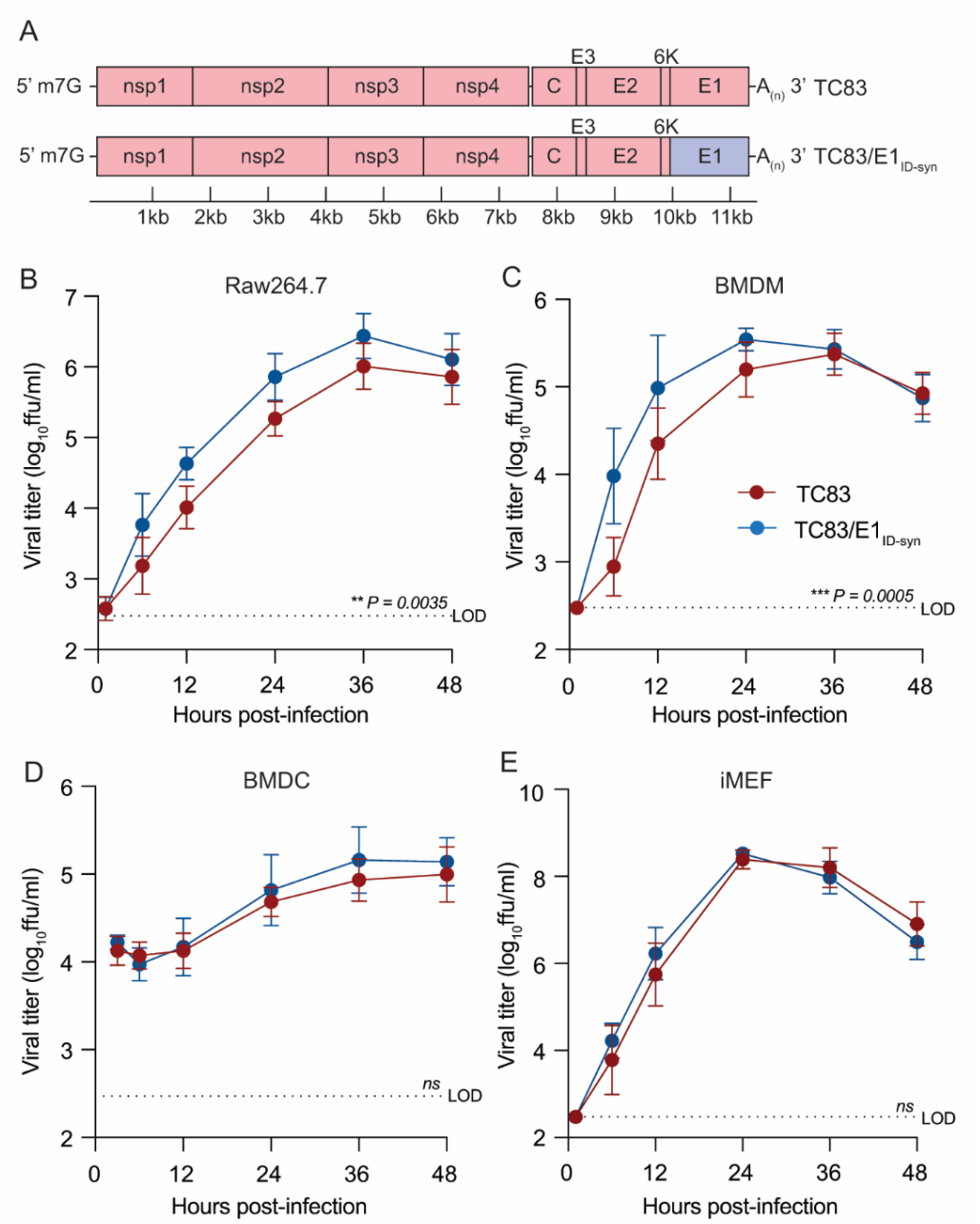

Figure 2.4 Changes in E1 RNA sequence alters viral replication fitness in macrophages, but not other cell types. (A). Schematic representation of the TC83 and TC83 E1 RNA mutant (TC83/E1$_{ID\text{-}syn}$) genomes. Synonymous SNPs from E1 of enzootic VEEV (strain 307537) were introduced into the vaccine epizootic VEEV (strain TC83) to generate an RNA mutant (TC83/E1$_{ID\text{-}syn}$). The single coding change present in E1 (Figure 2.2C, asterisk) was omitted from the mutant. Red denotes sequences from the parent epizootic strain (TC83), and blue denotes sequences from the enzootic strain (307537). **(B-E)**. Replication kinetics of VEEV TC83 and TC83/E1$_{ID\text{-}syn}$ in **(B)** Raw264.7, **(C)** primary bone marrow-derived macrophages (BMDMs), **(D)** primary bone marrow-derived dendritic cells (BMDCs), and **(E)** immortalized mouse embryonic fibroblasts (iMEF). Cells were infected with indicated viruses at a MOI of 0.1 (Raw264.5,

BMDMs, iMEF) or MOI 0.01 (BMDCs). Cell culture supernatant was serially harvested at 1, 6, 12, 24, 36, and 48 hpi and infectious virus was titered using focus forming assay (FFA). Each experiment was performed in triplicate three to four times independently and the mean and SD are graphed. Statistical analysis was performed by calculating the area under the curve (AUC) for each replicate, and the AUC values from WT and mutant viruses were analyzed by unpaired t-test.

Type-I IFN is important in restricting replication and pathogenesis of alphaviruses [209-211], and we have previously shown that VEEV RNA structure facilitates evasion of IFN-stimulated genes (ISGs) [140, 186]. Thus, we hypothesized that putative E1 RNA structures from TC83/E1$_{IDsyn}$ could enhance replication in macrophages by facilitating evasion of host antiviral immunity. Specifically, we predicted that mutant E1 RNAs may evade sensing of VEEV RNA by RLRs RIG-I and MDA-5 which are known to play a role in alphavirus RNA sensing, particularly of 3' RNAs [183, 212]. To test this hypothesis, we used CRISPR to generate *Ddx58* and *Ifih1* knock out (KO) Raw264.7 macrophages and compared replication kinetics of TC83 and TC83/E1$_{ID\text{-}syn}$ in these cells (**Figure 2.5A-C; Figure 2.6**). Contrary to our expectations, TC83 replication was still impaired relative to TC83/E1$_{ID\text{-}syn}$ in both the absence and presence of RIG-I or MDA-5 expression (**Figure 2.5A-C**). To confirm these data, we used transient siRNA knock down of *Ddx58* and *Ifih1*, as well as *Irf3* (**Figure 2.5D; Figure 2.6**) and examined titers of TC83 and TC83/E1$_{ID\text{-}syn}$ compared to cells treated with a non-silencing control (NSC) siRNA. We predicted that if enhanced replication of TC83/E1$_{IDsyn}$ was due to evasion of RLR-dependent sensing and antiviral restriction then knock down of RLR expression or expression of downstream signaling molecules (IRF3) would result in an increase in replication of TC83 but no change in the replication of TC83/E1$_{ID\text{-}syn}$. However, consistent with CRISPR data, we observed no increase in replication of TC83 in the absence of either RLR expression or IRF3. Furthermore, knockdown of *Irf3* did not lead to an increase in TC83 replication relative to TC83/E1$_{ID\text{-}syn}$, suggesting that preferential sensing and/or inhibition of TC83 RNA cannot explain the observed replication differences in macrophages.

While these data did not support a role of RLR-mediated RNA sensing in differential replication of TC83 and TC83/E1$_{ID\text{-}syn}$, we could not rule out a role for other RNA sensing pathways or antiviral effectors which are independent of these pathways. As antiviral signaling pathways converge on expression of type-I IFNs which are critical for restriction of alphaviruses through expression of antiviral effectors, we examined whether differences in type-I IFN signaling and ISG expression accounted for enhanced replication of TC83/E1$_{ID\text{-}syn}$. To determine whether infection with TC83 or TC83/E1$_{ID\text{-}syn}$ led to differential activation of type-I IFN responses, Raw264.7 were

treated with antibodies specific for the IFN-alpha receptor (IFNAR) or an IgG isotype control antibody prior to and during infection (**Figure 2.5E**). We expected that if diminished TC83 replication was due to impaired evasion of RNA sensing and IFN activation then IFNAR blockade would result in an increase in viral replication to levels similar to the mutant. However, while IFNAR blockade led to a significant inhibition of ISG expression as measured by qRT-PCR (**Figure 2.5F-H**), neither infectious viral titers nor viral RNA production were affected when compared to treatment with an isotype control (**Figure 2.5E and I**). Collectively, this data suggests that differential replication of TC83 and TC83/$E1_{ID\text{-}syn}$ cannot be explained by altered evasion or induction of IFN or ISG expression by either virus.

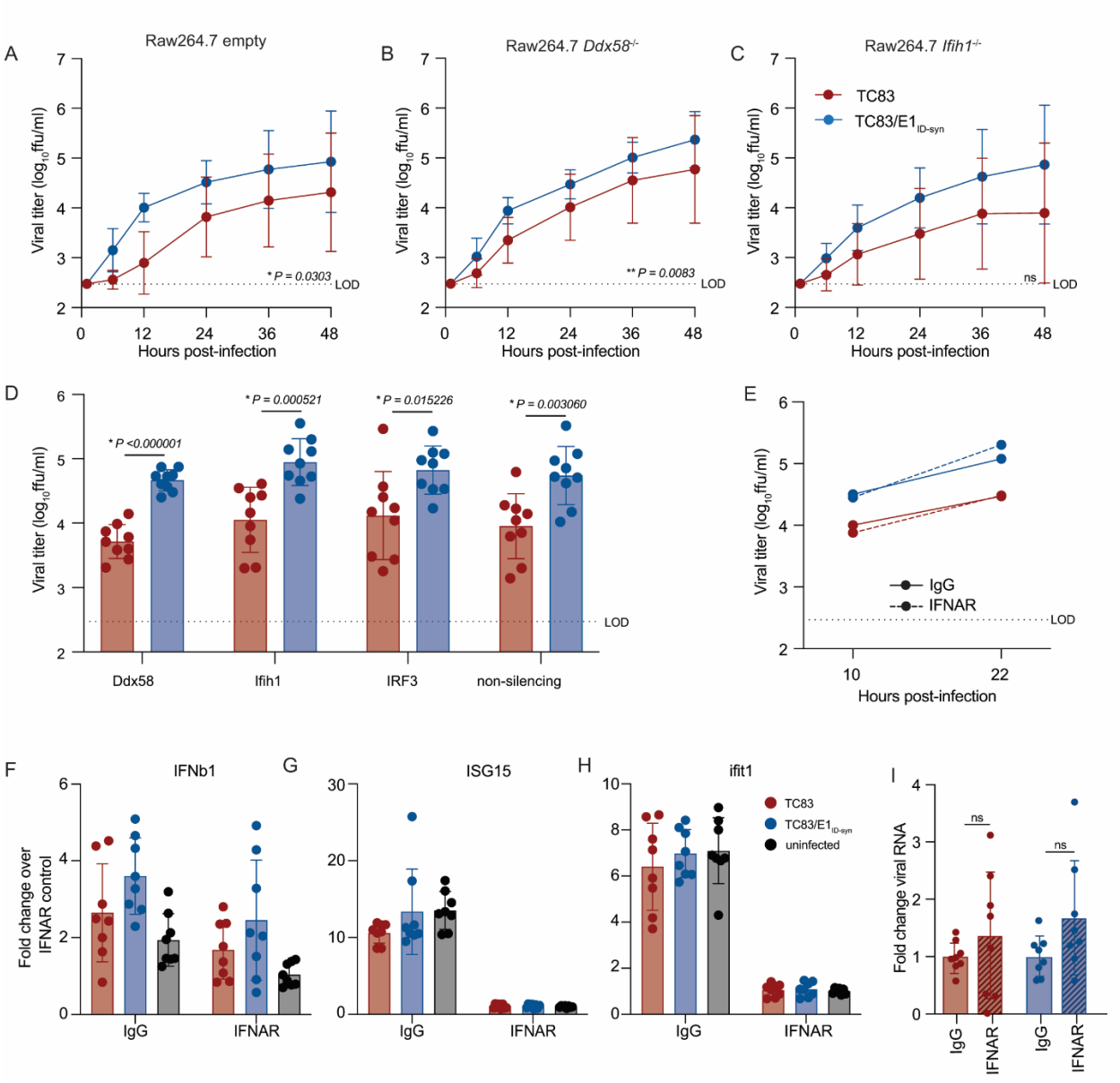

Figure 2.5 Differential macrophage replication of TC83 and TC83/E1$_{ID\text{-}syn}$ viruses is IFN- and RLR-independent. (A-C) Replication kinetics of VEEV TC83 and TC83/E1$_{ID\text{-}syn}$ in **(A)** empty vector, **(B)** *Ddx58*$^{-/-}$, and **(C)** *Ifih1*$^{-/-}$ CRISPR Raw264.7 cells. Cells were infected with indicated viruses at a MOI of 0.1. Cell culture supernatant was serially harvested at 1, 6, 12, 24, 36, and 48 hpi and infectious virus was titered using focus forming assay (FFA). Each experiment was performed in triplicate three times independently and the mean and SD are graphed. Statistical analysis was performed by calculating the area under the curve (AUC) for each replicate and experiment, and the AUC values for each virus analyzed by unpaired t-test. **(D)** Raw264.7 were treated with non-silencing control (NSC) siRNA or siRNA targeting *Mavs*, *Ddx58*, *Ifih1*, or *Irf3*. Cell culture supernatants were harvested at 24 hpi and infectious virus quantified by FFA. **(E)** Raw264.7 were pretreated for 1 hour with 10μg of IgG or IFNAR blocking antibody, then infected with TC83 or TC83/E1$_{ID\text{-}syn}$ at an MOI of 0.1 in the presence of antibody. Infectious virus from cell culture supernatants

harvested at 10 and 22 hpi was titered by FFA. Each experiment was performed three times independently. **(F, G, H, I)** IFNAR blocking antibody assays were performed in WT Raw264.7 as described in E, and cell lysates collected at 22 hpi. IFNb1, ISG15, Ifit1 and VEEV viral RNA transcripts quantified by qRT-PCR. (**F, G, H)** Gene expression within samples was normalized to hprt, and fold change in gene expression relative to IFNAR samples was calculated. **(I)** Viral RNA fold change over IgG control was calculated and displayed per virus. Each experiment was performed three times independently in duplicate or triplicate, and statistical analysis was performed using unpaired t-test.

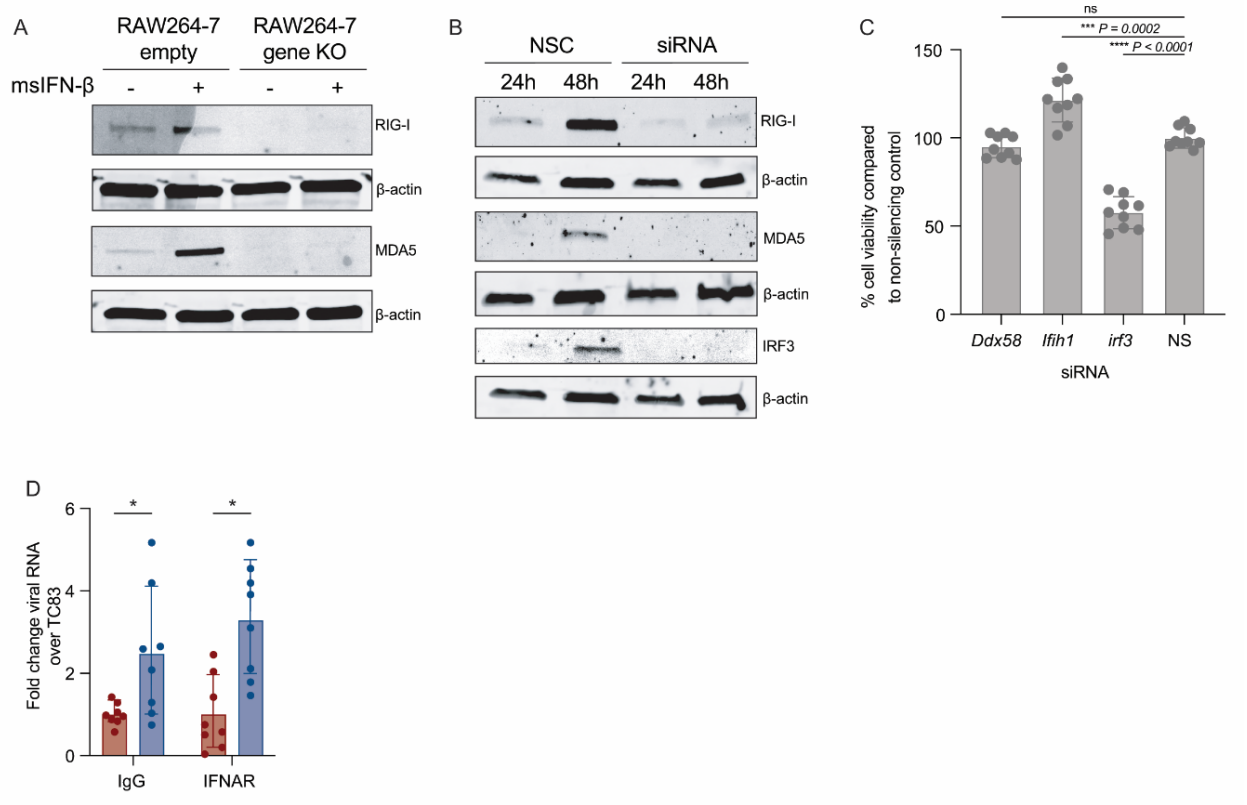

Figure 2.6. Validation of CRISPR KO and siRNA KD in Raw 264.7 macrophages. (A) Western blots from Raw264.7 6hrs after treatment +/- 100U/ml msIFN-β. **(B)** Western blot of Raw264-7 after transfection with NSC or protein of interest siRNA siRNA pool (10μM) pool for 24hrs or 48hrs. **(C)** Cell viability was determined using alamarblue Cell Viability Reagent and calculated as a percentage compared to the NSC. **(D)** qPCR was performed for viral RNA and the fold change in viral RNA over TC83 is expressed. Statistical analysis was performed using GraphPad Prism 9, using an unpaired T-test.

To unveil what IFN-independent mechanisms might underlie the observed differences in TC83 and TC83/E1$_{ID\text{-}syn}$ replication (**Fig. 2.5**), we used a proteomics approach to identify host proteins which interact differently with TC83 and TC83/E1$_{ID\text{-}syn}$ RNA. We hypothesized that changes in primary sequence and/or secondary structure could alter the viral RNA-protein interactome leading to changes in replication. Specifically, we predicted that antiviral RNA-binding proteins (RBPs) would be enriched for TC83 RNA or that proviral RBPs would be enriched for TC83/E1$_{ID\text{-}syn}$ RNA. To define the RNA-protein interactome of TC83 or TC83/E1$_{ID\text{-}syn}$, Raw264.7 were infected at MOI 0.1 and viral RNA immunoprecipitated at 24 hpi using the J2 anti-dsRNA antibody [213]. RNA-bound protein targets were then purified and identified using Liquid chromatography–mass spectrometry (LC-MS). A total of 166 proteins were identified. Differential enrichment of protein targets for each virus was calculated and targets prioritized as follows: (i) targets with spectral counts >10; (ii) targets showing >2-fold enrichment over the paired IgG control in at least one sample; (iii) targets showing >2-fold enrichment in TC83 vs TC83/E1$_{ID\text{-}syn}$ (or vice versa); (iv) targets with known RBP activity (based on RBPbase and GO terms). While MS data was generated from two independent experiments (**Figure 2.7**), we observed much lower spectral counts for targets in the second experiment as well as lower enrichment scores overall. Nonetheless, we identified several targets in both screens that were either differentially enriched for the WT or mutant virus (>1.5-fold; FBL, NOP58, CHTOP) or which were enriched equally for both (DHX9, ADAR, YBX1). Based on the more robust nature of the data set, downstream targets chosen for validation were based on data from experiment 1. Based on the criteria above we identified a total of 24 RBPs which showed differential binding to either the TC83 or TC83/E1$_{ID\text{-}syn}$ genomes (**Figure 2.7A**). In addition, we also identified several highly abundant targets (YBX1, HNRNPC, HNRNPM, and ADAR1) that were equally enriched for both viruses which have also been identified in previous studies as interacting with alphavirus RNA and would not be expected to be differentially enriched [214-216](**Figure 2.7B**). Remarkably, with the exception of UBTF and DHX38, all identified targets were found to be enriched for the mutant, suggesting that enhanced replication of TC83/E1$_{ID\text{-}syn}$ is not due to evasion of antiviral factors that restrict TC83, but recruitment of proviral RBPs to TC83/E1$_{ID\text{-}syn}$. Pathway analysis of these top hits showed enrichment for RBPs associated with snoRNAs and more broadly RNA metabolism (**Figure 2.7C**). To validate IP-MS findings and determine which RBPs were necessary for enhanced viral replication of TC83/E1$_{ID\text{-}syn}$ in macrophages, we used siRNA to inhibit expression of 11 of these targets in Raw264.7 and assess replication of WT and mutant viruses in these cells (**Figure 2.7D, Figure 2.8A**). Here, Raw264.7 were transfected with NSC siRNA or a pool of 3 gene-specific siRNAs, infected with TC83 and TC83/E1$_{ID\text{-}syn}$ at MOI 0.1, and infectious virus

quantified from supernatants by FFA. We observed that knock down of four of these targets (*Thrap3*, *Fbl*, *Ubap2l*, and *Dhx38*) led to reduced TC83/E1$_{ID\text{-}syn}$ replication to levels comparable to TC83, as compared to NSC-treated cells. Association of these RBPs with viral RNA was also validated using affinity purification (**Figure 2.9**). To exclude the possibility that increased cell death following gene knock down could account for non-specific changes in viral replication in siRNA versus NSC treated cells we also measured cell viability in siRNA treated cells following infection at 24hpi (**Figure 2.8D**). Here, we observed no change, or only modest changes in cell viability which could not account for the decrease in TC83/E1$_{ID\text{-}syn}$ replication observed. To determine whether the cell type specificity of the TC83/E1$_{ID\text{-}syn}$ replication phenotype was due to cell-type dependent expression of RBPs, we additionally measured expression of TRAP3, DHX38, AND FBL protein in Raw264.7 and MEF (**Figure 2.8E-H**). Interestingly, we observed no difference in the expression of FBL and DHX38 between Raw264.7 and MEF, but contrary to expectations we observed a 4-fold increase in THRAP3 protein levels in MEF as compared to Raw264.7. Notably, expression of all three proteins was significantly reduced in MEF following viral infection but not in Raw264.7, suggesting that VEEV may downregulate expression of these RBPs in MEF but not macrophages, or that macrophages may be resistant to this downregulation [190]. Collectively this data supports the hypothesis that these proteins are important for macrophage specific phenotype observed with TC83/E1$_{ID\text{-}syn.}$

A

Target	Peptide counts TC83 a-IgG	TC83 a-dsRNA	TC83/E1$_{ID-syn}$ a-IgG	TC83/E1$_{ID-syn}$ a-dsRNA	Enrichment TC83/ TC83/E1$_{ID-syn}$	Enrichment TC83/E1$_{ID-syn}$ /TC83
Ehmt2	1	1	1	40	0.03	**40**
Syncrip	1	2	3	32	0.06	**16**
Bclaf1	1	2	1	25	0.08	**12.5**
Zc3h4	1	1	1	22	0.05	**22**
Hnrnpr	1	3	2	49	0.06	**16.33**
Krt76	2	1	1	16	0.06	**16**
Thrap3	2	3	2	48	0.06	**16**
Dsp	1	1	1	15	0.07	**15**
Jup	1	1	1	13	0.08	**13**
Fbl	17	21	11	100	0.21	**4.76**
Chtop	3	8	1	34	0.24	**4.25**
Tra2b	1	3	1	12	0.25	**4**
Gar1	1	4	1	15	0.27	**3.75**
Hnrnpu	18	26	23	74	0.35	**2.85**
Alyref	5	4	2	11	0.36	**2.75**
Nop56	20	23	16	61	0.38	**2.65**
Ubap2l	6	7	6	17	0.41	**2.43**
Hnrnpl	1	6	1	13	0.46	**2.17**
Acin1	1	10	1	20	0.5	**2**
Matr3	1	9	1	18	0.5	**2**
Nop58	11	16	8	32	0.5	**2**
Rpl31	4	6	5	10	0.5	**2**
Ubtf	15	41	9	13	**3.15**	0.32
Dhx38	6	12	1	5	**2.4**	0.42

B

Target	Peptide counts TC83 a-IgG	TC83 a-dsRNA	TC83/E1$_{ID-syn}$ a-IgG	TC83/E1$_{ID-syn}$ a-dsRNA	Enrichment TC83/ TC83/E1$_{ID-syn}$	Enrichment TC83/E1$_{ID-syn}$ /TC83
Adar	1	80	2	77	1.04	0.96
Ybx1	4	27	6	36	0.75	1.33
Hnrnpc	1	30	1	27	1.11	0.9
Hnrnpm	38	87	39	106	0.82	1.22
Dhx9	5	59	3	52	1.13	0.88

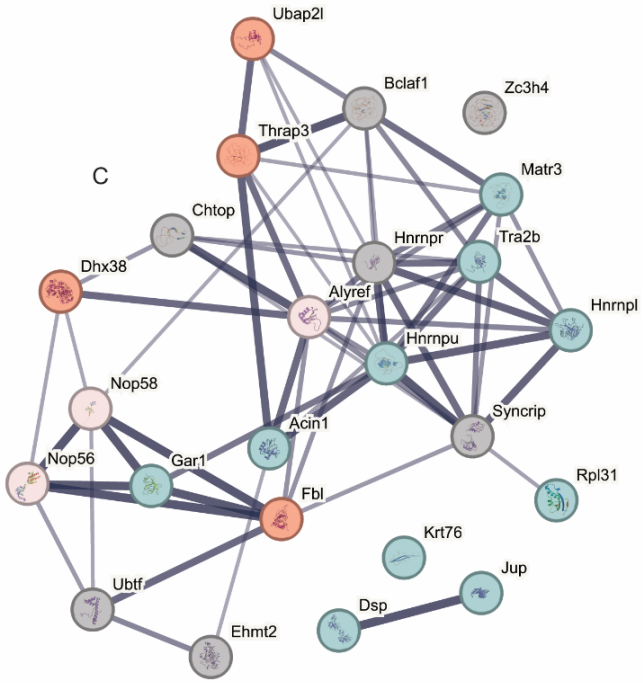

D

Biological process	GO #	Observed gene count	False discovery rate
RNA processing	GO:0006396	13	7.09E-08
Gene expression	GO:0010467	17	1.97E-07
RNA metabolic process	GO:0016070	15	1.97E-07
mRNA processing	GO:0006397	10	3.19E-07
mRNA metabolic process	GO:0016071	11	3.19E-07
Nucleic acid metabolic process	GO:0090304	16	8.08E-07
RNA splicing	GO:0008380	9	8.99E-07
RNA localization	GO:0006403	7	4.55E-06
Cellular nitrogen compound metabolic process	GO:0034641	17	4.22E-05
Regulation of mRNA metabolic process	GO:1903311	7	0.00012
Negative regulation of mRNA metabolic process	GO:1903312	5	0.00017
Regulation of mRNA splicing, via spliceosome	GO:0048024	5	0.00048

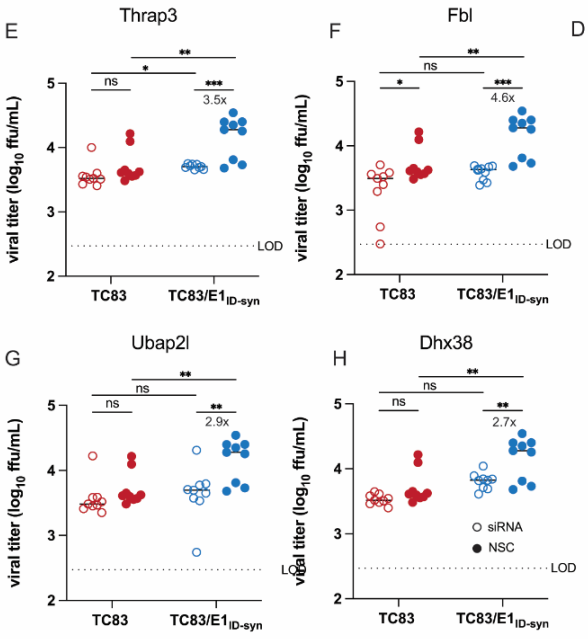

Figure 2.7. Increased macrophage replication fitness of TC83/E1IDsyn is dependent on expression of RNA binding proteins Fbl, Thrap3, Ubap2l, and Dhx38. **(A)** Top hits from dsRNA immunoprecipitation-mass spectrometry (IP-MS) of TC83 and TC83/E1IDsyn in Raw264.7. Raw264.7 cells were infected with TC83 or TC83/E1IDsyn at an MOI of 0.1, and viral dsRNA isolated from lysates at 24 hpi using J2 dsRNA antibody [213] or IgG isotype control. RNA-bound proteins were identified by MS, and

fold-enrichment of spectral counts relative to IgG controls was calculated. Prioritized hits were chosen based on fold enrichment scores, total spectral counts, and whether targets are known RNA binding proteins (RBPbase hits). **(B)** Hits equally enriched in TC83 and TC83/E1IDsyn. **(C)** STRING network analysis of top proteomics hits. Candidates meeting the cutoff criteria (A) were subjected to Protein-Protein Interaction Networks Functional Enrichment Analysis. Candidate proteins identified in the screen are highlighted in red and interacting proteins in blue. **(D)** Enriched biological process GO terms that with a p-value >0.001, along with the observed gene count present in the STRING network **(E-H)** Raw264.7 were transfected with control (NSC) or pooled (3 siRNA) gene specific siRNAs targeting **(E)** Thrap3, **(F)** Fbl, **(G)** Ubap2l, or **(H)** Dhx38 for 24 hours. Cells were infected TC83 or TC83/E1ID-syn at an MOI of 0.1, cell culture supernatants collected at 24hpi, and infectious virus titered by FFA. All siRNAs were assayed simultaneously but for visual clarity, data for each gene is shown separately along with the shared control siRNA samples. Each experiment was performed in triplicate three times independently and the mean and SD are graphed. Statistical analysis was performed using unpaired t-test. ** >0.001, ***>0.0001. Fold change and p-values are indicated on each graph.

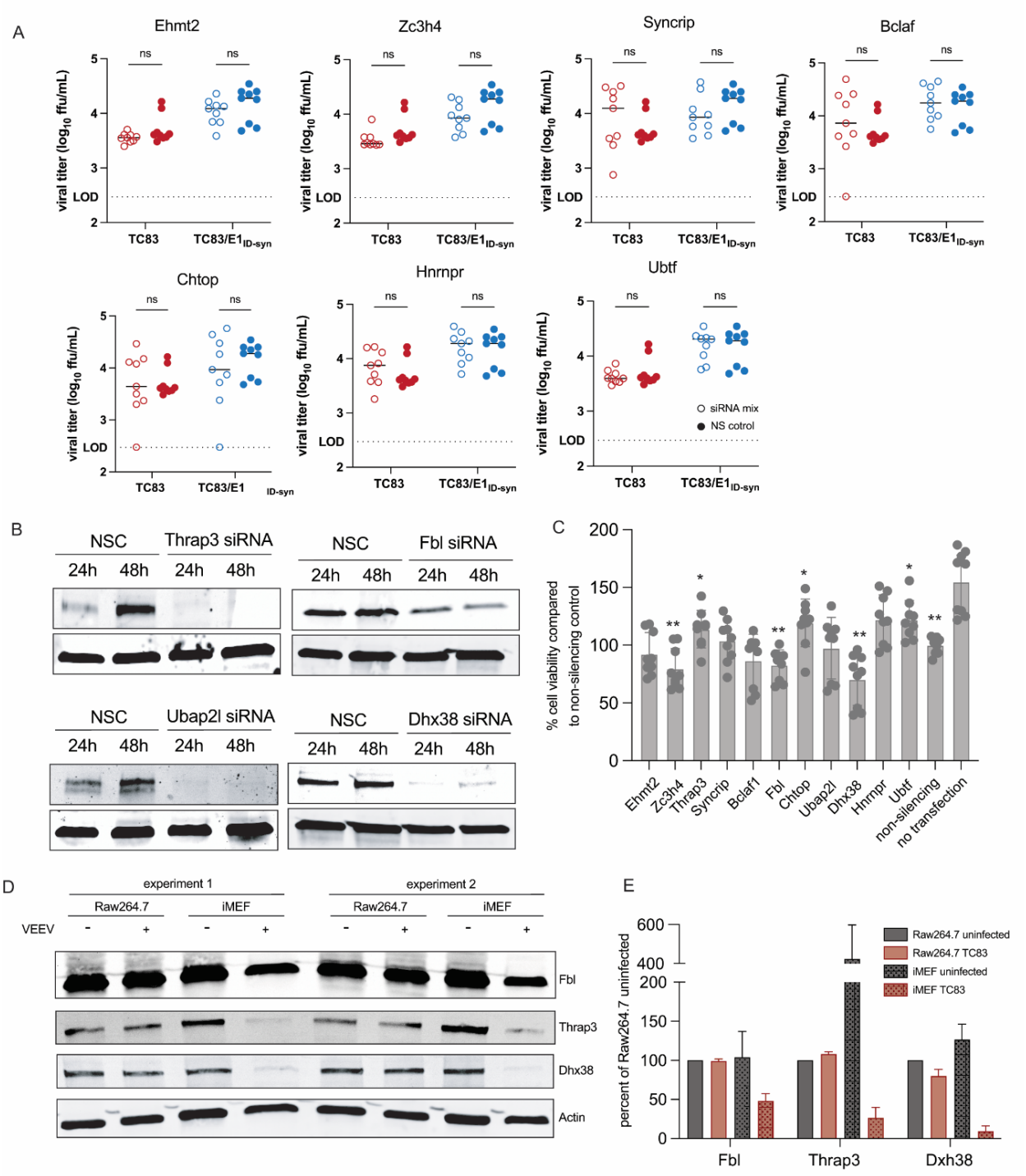

Figure 2.8. Validation of additional mass spectrometry hits. To evaluate the effect of these genes on viral replication **(A)** Raw264-7 cells were transfected with 10mM of a pool of 3 siRNA targeting proteins of interest for 24hrs, after which they were infected with TC83 or TC83/E1$_{ID\text{-}syn}$. Supernatants were collected at 24hpi and infectious virus was titered using FFA. For visual clarity, the individual siRNAs along with the non-silencing control (NSC) are graphed individually, however the NSC is the same in all graphs. Each experiment was performed in triplicate three times independently and the mean and SD are graphed. **(B)**

Western blot of Raw264-7 transfected for 24h or 48h with NSC or protein of interest siRNA pool (10μM). **(C)** Cell viability was determined using alamarblue Cell Viability Reagent and calculated as a percentage compared to the NSC. **(D)** Western blot analysis of Raw264.7 or iMEF +/- TC83 (MOI 0.1) lysates at 24hpi. **(E)** Densitometry was performed using Adobe Photoshop and expression of proteins were normalized to the actin control. The percentage expression was then calculated in relation to the uninfected Raw264.7 control. This is representative of two independent repeats. Statistical analysis was performed using GraphPad Prism 9, using an unpaired T-test. * >0.05, **>0.001.

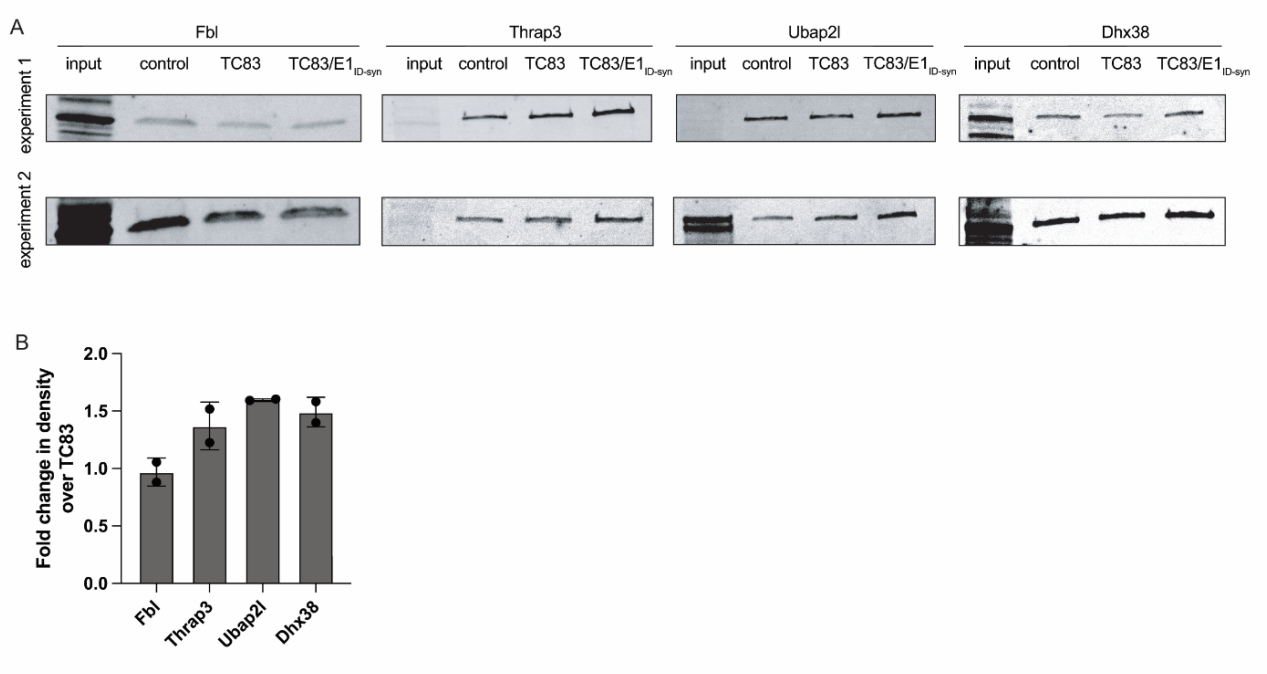

Figure 2.9. RNA aptamer immunoprecipitation of Fbl, Thrap3, Ubap2l and Dhx38. *In vitro* RNAs encoding 4x repeats of the S1m-aptamer followed by the core region of E1 (10,516-10,808) from TC83 or TC83/E1$_{ID\text{-}syn}$ were generated along with a 4x S1m-aptamer only control RNA. RNA was bound to streptavidin beads then incubated with cellular lysates from Raw264.7, and bound proteins eluted and analyzed. **(A)** Western blot analysis of Fbl, Thrap3, Ubap2l and Dhx38 is displayed for the input lysate control, RNA aptamer control, TC83 or TC83/E1$_{ID\text{-}syn}$ aptamer RNAs. **(B)** Densitometry was performed on the bands using Adobe Photoshop and the fold change in density of the TC83/E1$_{ID\text{-}syn}$ over the TC83 RNA aptamer is displayed. This is representative of two independent repeats.

We next sought to determine the possible mechanism by which these RBPs may alter viral replication in macrophages. RNA structures within the 3' end of viral genomes and host mRNAs, are known to be important for translation efficiency [217-219]. Interestingly, all four of the RBPs identified as being required for enhanced TC83/E1$_{ID\text{-}syn}$ replication in macrophages (FBL, THRAP3, UBAP2L, AND DHX38) have been previously linked to regulation of mRNA stability and translation [220-222]. Thus, we hypothesized that FBL, THRAP3, UBAP2L, AND DHX38 increase TC83/E1$_{ID\text{-}syn}$ replication by increasing translation of viral RNA. To test this hypothesis we modified a previously described VEEV luciferase translation reporter to include the E1 sequence from either TC83 or TC83/E1$_{ID\text{-}syn}$ and compared translation of reporter RNAs in Raw264.7 (**Figure 2.10A)** [140, 223]. Raw264.7 cells were nucleofected with *in vitro* transcribed capped reporter RNA and luciferase activity measured at the indicated timepoints. We observed a significant increase in translation of TC83/E1$_{ID\text{-}syn}$ reporter RNA compared to TC83 starting as early as 30 minutes post-nucleofection (~1.3-fold) and increasing over time (2-fold at 240 min) (**Figure 2.10A-B).** To evaluate whether RNA synthesis was also impacted by changes in E1 RNA, we generated a nsp3-tagged nano-luciferase (nLuc) VEEV replicon containing firefly luciferase under control of the subgenomic promoter and compared replication of TC83 and TC83/E1$_{ID\text{-}syn}$ replicons in Raw264.7(**Figure 2.10C-D)**. Similar to the translation reporter assays described above, Raw264.7 cells were nucleofected with in vitro transcribed and capped replicon RNA and nLuc expression measured using Nano-Glo Dual-luciferase reporter assay system (Promega). Consistent with our translation reporter assay data (**Figure 2.10A-B**), we observed a significant increase in nLuc activity of TC83/E1$_{ID\text{-}syn}$ replicon RNA as compared to TC83 at 3 (3.5-fold) and 6 (4.5-fold) hours post-nucleofection, indicating that genomic RNA (gRNA) synthesis is increased in TC83/E1$_{ID\text{-}syn}$ relative to TC83, likely due to the increased translation of this RNA. As firefly luciferase was undetectable in these assays, likely due to the absence of capsid [109], we used RT-qPCR to measure the ratio of gRNA to subgenomic (sg) RNA in Raw264.7 following infection (MOI 5) with TC83 or TC83/E1$_{ID\text{-}syn}$ virus. We reasoned that if changes in E1 RNA sequence or structure specifically affected gRNA but not sgRNA synthesis this would lead to differences in the ratio of sgRNA-to-gRNA between TC83 and TC83/E1$_{ID\text{-}syn}$. Consistent with translation and replicon data, we observed no significant difference in the sgRNA-to-gRNA ratio between TC83 and mutant virus (**Figure 2.10E)**., suggesting that changes in E1 sequence are not only impacting gRNA translation and RNA synthesis but that sgRNA production is also likely impacted.

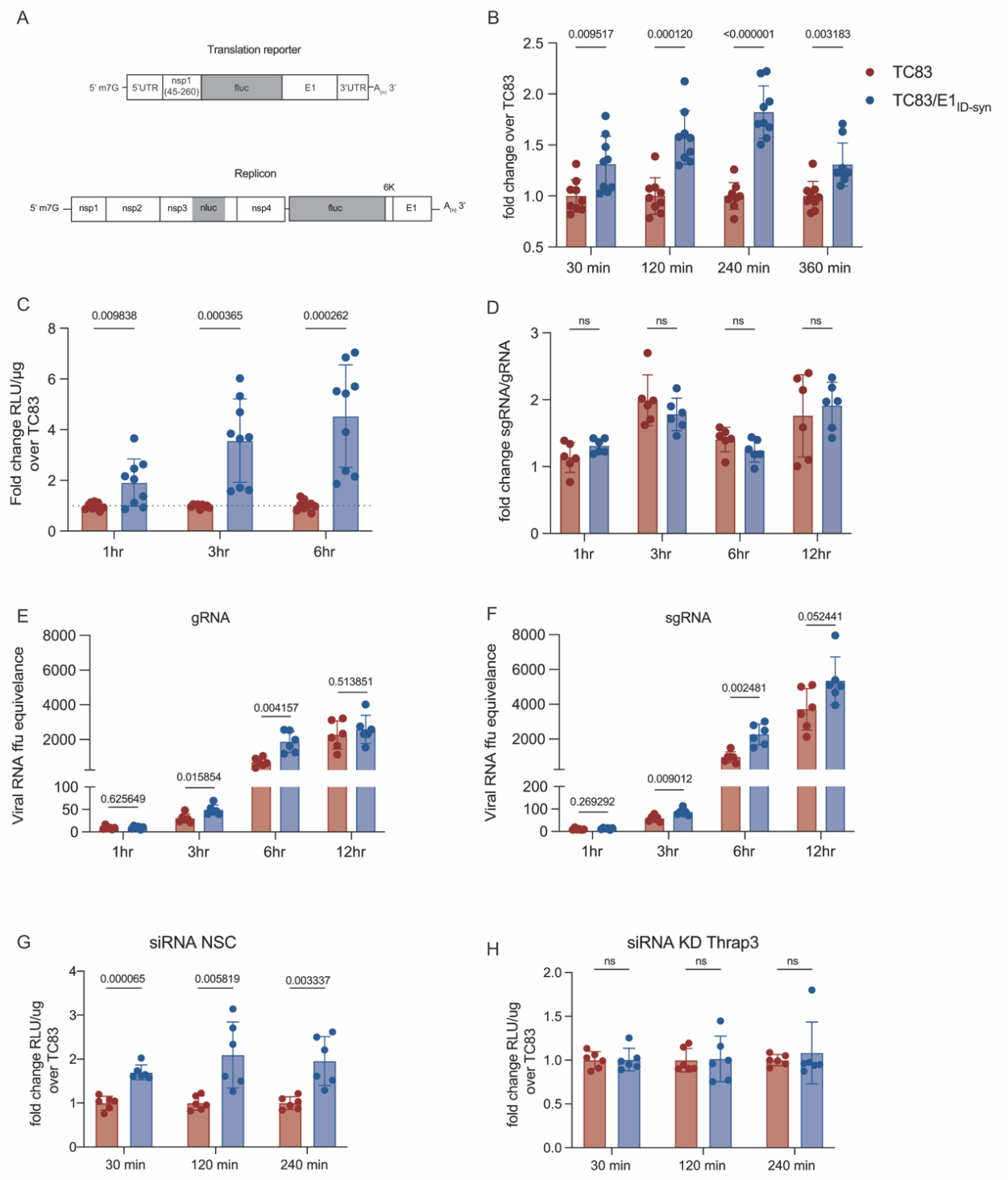

Figure 2.10 E1 RNA mutations alter translation and RNA transcription. (A) Visual representation of translation reporter and replicon. **(B)** 4µg of translation reporter RNA containing the E1 sequence from either TC83 or TC83/E1$_{ID\text{-}syn}$ were nucleofected into Raw264.7 macrophages. Cell lysates were collected at indicated times post nucleofection and luciferase activity measured. Data depicted as fold change over the TC83 samples for all time points. **(C)** 4µg nano/firefly replicon reporter RNAs was nucleofected into

Raw264.7 macrophages and cell lysates were harvested and dual-luciferase activity measured for indicated time-points. Nano-luciferase activity is displayed as fold change RLU/µg over TC83. **(D-F)** Raw264.7 were infected (MOI 1) with TC83 or TC83/E1$_{ID\text{-}syn}$ and lysates were harvested at 1, 3, 6 and 12hpi. RT-qPCR was performed using probes specific for genomic and sub-genomic RNA species. **(D)** the fold change between genomic and sub-genomic RNA per time point is displayed, **(E-F)** viral RNA ffu equivalence was calculated using a standard from RNA derived from a known concentration virus stock. **(G-H)** Raw264.7 were transfected with a non-silencing control (NSC) or Thrap3 siRNA and after 24hs cells were nucleofected with 4µg of translation reporter RNA constructs. Cell lysates were collected at indicated times post nucleofection and luciferase activity measured. The fold-change in RLU/µg is displayed for each time point. Each experiment was performed in duplicate or triplicate, three times independently and the mean and SD graphed. Statistical analysis was performed using an unpaired T-test.

To further evaluate whether the RBPs identified specifically alter translation of TC83 and TC83/E1$_{ID\text{-}syn}$ RNA, Raw264.7 cells were transfected with gene-specific siRNAs then nucleofected with TC83 or mutant reporter RNA 24 hours later, and translation assays performed on cellular lysates at the indicated time points (**Figure 2.10G-H**). We chose to focus on THRAP3 and UBAP2L due to their proposed interactions (**Figure 2.7E, G)** and their shared role in translational control and stress granule assembly[224, 225]. We observed significant translational repression of both TC83 and TC83/E1$_{ID\text{-}syn}$ following treatment of cells with Ubap2l siRNA which led to inconsistencies in translation reporter data, thus we chose to omit this data from our study. Notably, UBAP2L is a ribosome-associate RBP that has been implicated in modulating global regulators of translation [222], thus it is not surprising that we consistently observed poor or no translation of reporter RNA in Ubap2l siRNA-treated cells. Consistent with our initial translation reporter assay data (**Figure 2.10A**) we observed a significant increase (~2-fold) in translation of TC83/E1$_{ID\text{-}syn}$ RNA compared to TC83 in cells treated with NSC siRNA, but notably, KD of THRAP3 resulted in similar levels of luciferase activity for both reporters (**Figure 2.10G, H**). In fact, even partial KD of THRAP3 was sufficient to reduce translation of the TC83/E1$_{ID\text{-}syn}$ reporter RNA **(Figure 2.11)**. Collectively, our data shows that changes in E1 RNA sequence alter translation of viral RNA, and that enhanced translation of TC83/E1$_{ID\text{-}syn}$ is at least in part dependent on THRAP3.

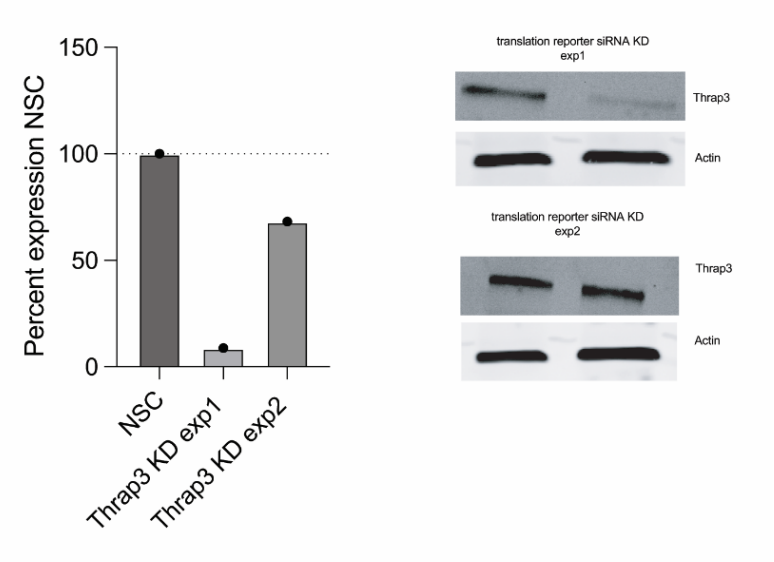

Figure 2.11 Western blot analysis of NSC and Thrap3 siRNA KD in Raw264.7 macrophage used in translation reporter assay. The integrated density of each of the western blot bands was determined using Adobe Photoshop and normalized to the actin control. The expression of each protein is displayed as a percentage of the Raw264.7 uninfected control.

Analysis of primary E1 sequences from TC83 and TC83/E1$_{ID\text{-}syn}$ failed to reveal obvious recognition motifs for any of the targets identified in our proteomics study. Thus, we generated additional E1 mutants to map regions within E1 necessary for differential macrophage replication and RBP recruitment (**Figure 2.12 A**). Here, Raw264.7 cells were infected with parent or mutant viruses at MOI of 0.1 and infectious titers at 12 and 24hpi assessed by FFA (**Figure 2.12 B, C**). We initially compared replication of two mutants in which the 5' or 3' half of E1 was exchanged between TC83 and TC83/E1$_{ID\text{-}syn}$ (mutant 1 and 2). Surprisingly, both mutant 1 and 2 replicated identically to the parent TC83 virus, suggesting that the element responsible for differential replication is located in the middle of E1 and was disrupted in these two mutants. To test this, we generated another mutant (mutant 3) which contained only SNPs from the central region of TC83/E1$_{ID\text{-}syn}$ E1 (nts 10,466-10,843) and compared replication of all viruses in Raw264.7 (**Figure 2.12 B, C**). In contrast to mutant 1 and 2, mutant 3 replicated to similar levels as that of TC83/E1$_{ID\text{-}syn}$, confirming that the elements responsible for enhanced macrophage replication are located in the central region of E1.

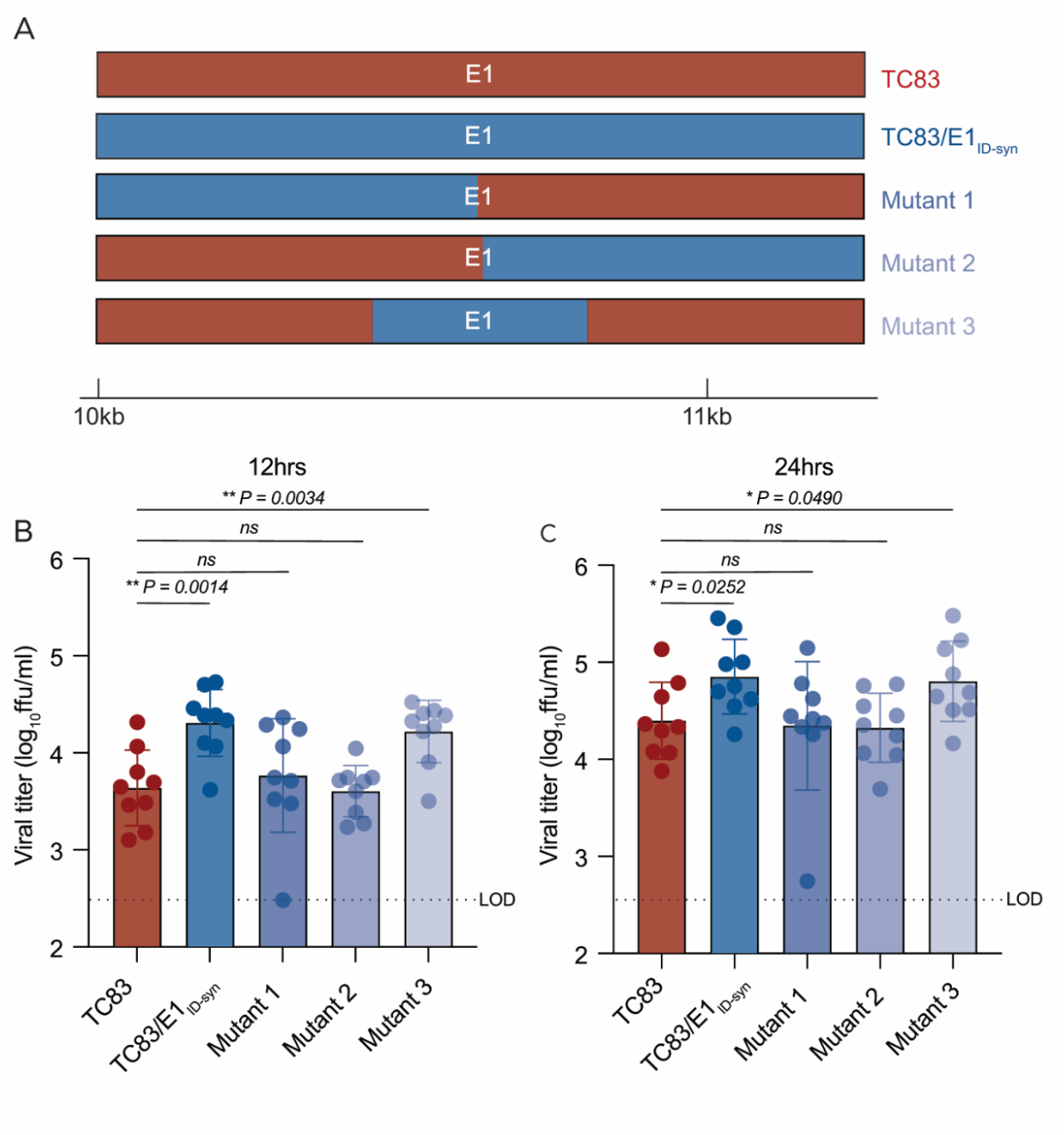

Figure 2.12 RNA sequences in the central domain of E1 enhance macrophage replication of TC83/E1$_{IDsyn}$. (A) Schematic representation of mutant viruses constructed. RNA chimeras containing 5' or 3' half or the central region of E1 synonymous mutations from TC83/E1$_{ID-syn}$ **(B, C)** Viral replication of chimeric viruses from Raw264.7 infected at MOI 0.1. Supernatants were harvested at 12 **(B)** or 24 **(C)** hpi and infectious virus titered by focus forming assay (FFA). Each experiment was performed in triplicate three times independently and the mean and SD graphed. Statistical analysis was performed using an unpaired T-test. * >0.05, ** >0.001.

We hypothesized that altered macrophage replication fitness was driven by changes in RNA structure, which alter binding of RBPs to viral RNA. Therefore, to determine whether SNPs in the central region of E1 altered the underlying structure of E1, we performed in-cell SHAPE-MaP [216, 226] of cells infected with TC83 and TC83/E1$_{ID\text{-}syn}$. Here, VERO cells were infected with TC83 or TC83/E1$_{ID\text{-}syn}$ at an MOI of 0.1, treated with either DMSO (unreacted control) or the SHAPE chemical 1-methyl-7-nitroisatoic anhydride (1m7), and RNA lysates collected at 24hpi. SHAPE-MaP library preparation, sequencing, and analysis was performed as previously described [227], and SHAPE reactivity profiles generated for each viral genome (**Figure 2.13 A, Figure 2.14**). The SHAPE reactivity is indicative of the flexibility of each individual nucleotide, with low SHAPE reactivity correlating to paired nucleotides and high SHAPE reactivity correlating to unpaired nucleotides. Using these reactivity profiles as constraints for RNA folding, the secondary structure of TC83 and TC83/E1$_{ID\text{-}syn}$ E1 was determined using RNAfold (**Figure 2.13 B, Figure 2.15).** Within the central region of E1, we observed conservation of several secondary structural elements (in grey) between TC83 and TC83/E1$_{ID\text{-}syn}$. We also observed conservation of secondary structures in other regions of the viral genome, including the ribosomal frameshift motif in 6K/E1 (**Figure 2.15**). Notably, our data was found to be consistent with previously published SHAPE-MaP analysis of VEEV strain ZPC738 [194] (**Figure 2.15**) and we identified conserved secondary structures across all three viruses, lending further support to our findings. The central region of E1 responsible for the macrophage replication phenotype contains 11 SNPs (in blue, **Figure 2.13**). Three of these reside within the invariant RNA secondary structures identified (grey), and two SNPs (nts 10,481 and 10,633) were found to be unique to strain TC83 and another closely related IAB strain (AB66640; **Figure 2.17**). Of the remaining six SNPs, three were found within regions that displayed the most variable RNA secondary structure (nts 10,522, 10,606, 10,810; **Figure 2.13 A-C**, boxed base pairs). To further define the SNPs responsible for enhanced TC83/E1$_{ID\text{-}syn}$ replication, we made an additional 5 TC83 mutants containing single point mutations at positions 10,495, 10,606, 10,747, 10,759, and 10,810 and compared replication of these viruses to TC83 and TC83/E1$_{ID\text{-}syn}$ in Raw264.7 (**Figure 2.16**). Mutant 10,606 showed no increase in viral replication compared to TC83 at 12h or 24h. Of the remaining mutants tested, only 10,495 consistently showed an increase in replication at 12 and 24 hpi compared to TC83, whereas the other mutants (10,747, 10,759, and 10,810) replicated to levels similar to TC83 at 12hpi but showed increased replication similar to TC83/E1$_{ID\text{-}syn}$ at later times (24hpi). While the role of these three mutants in replication of TC83/E1$_{ID\text{-}syn}$ remains ambiguous, we can conclude from this data that at minimum SNPs that alter the 5'sequence of this E1 core region contribute to the enhanced replication of TC83/E1$_{ID\text{-}syn.}$

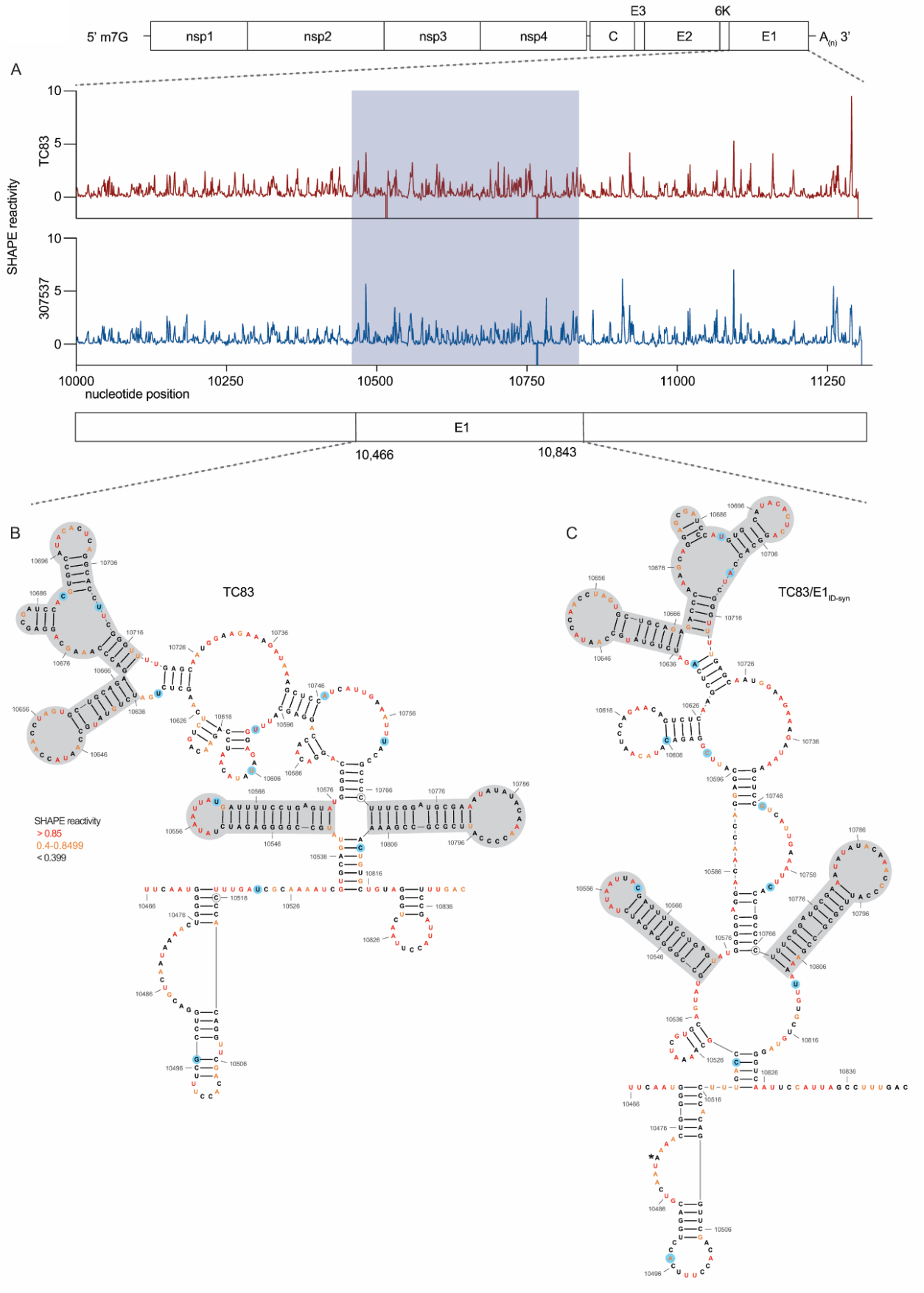
5' m7G
nsp1
nsp2
nsp3
nsp4
C
E3
6K
E2
E1
A(n) 3'
A
SHAPE reactivity
TC83
307537
nucleotide position
10000
10250
10500
10750
11000
11250
E1
10,466
10,843
B
TC83
C
TC83/E1ID-syn
SHAPE reactivity
> 0.85
0.4-0.8499
< 0.399

Figure 2.13 SHAPE-MaP analysis of TC83 and TC83/E1$_{IDsyn}$ infected cells. RNA from VERO cells infected with TC83 or TC83/E1$_{IDsyn}$ (MOI of 0.1) was analyzed by SHAPE-MaP. **(A)** Differential SHAPE reactivities of nucleotides in E1. The central region responsible for enhanced macrophage replication of TC83/E1$_{IDsyn}$ is highlighted in blue. Secondary structures and SHAPE reactivities of nucleotides in the central domain of **(B)** TC83 and **(C)** TC83/E1$_{IDsyn}$. Low reactive nucleotides (black) correspond to base-paired nucleotides and highly reactive nucleotides (orange, red) correspond to exposed bases. Structural elements conserved between both viruses are highlighted in grey, and SNPs are highlighted in blue.

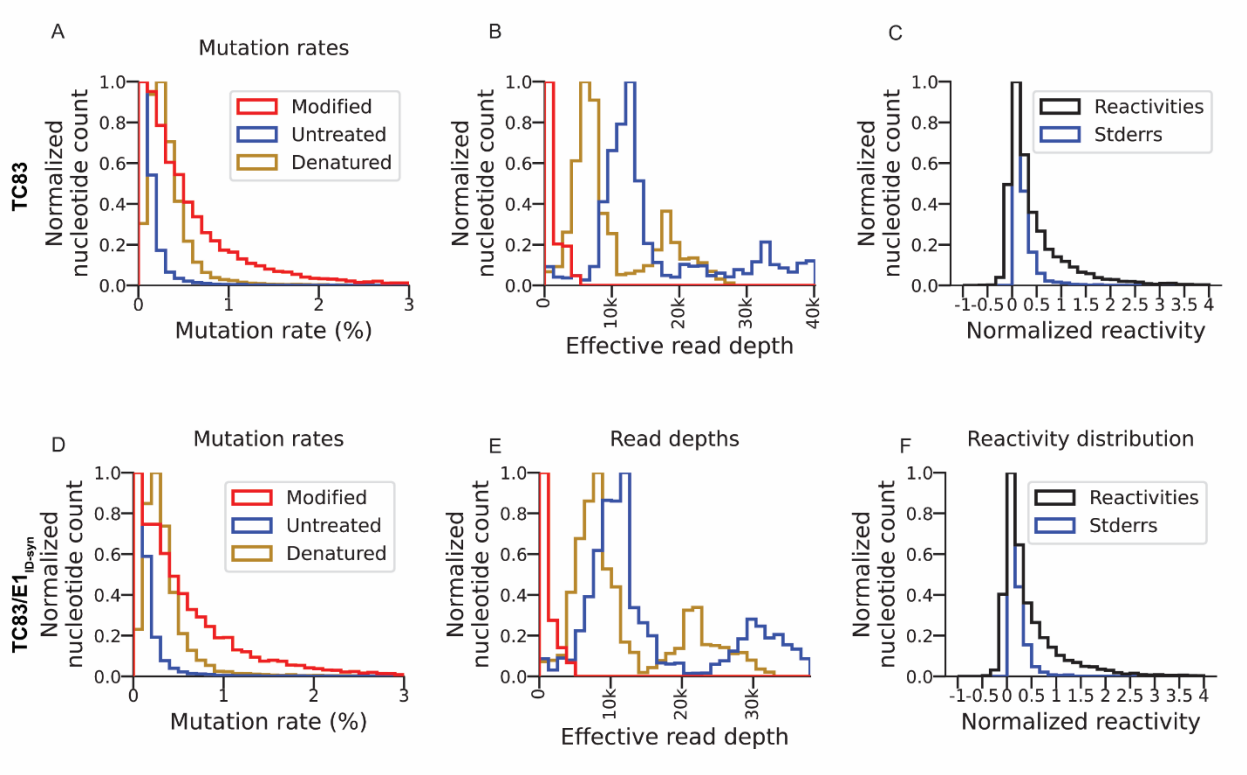

Figure 2.14 Quality matrixes for SHAPE-MaP for TC83 and TC83/E1$_{IDsyn}$. Mutation rates for modified, untreated and denatured control **(A)** TC83 and D. TC83/E1$_{ID\text{-}syn}$. Read depths for modified, untreated and denatured control **(B)** TC83 and E. TC83/E1$_{ID\text{-}syn}$. The distribution of the SHAPE-MaP reactivities and the standard error of the reads for C. TC83 and F. TC83/E1$_{ID\text{-}syn}$.

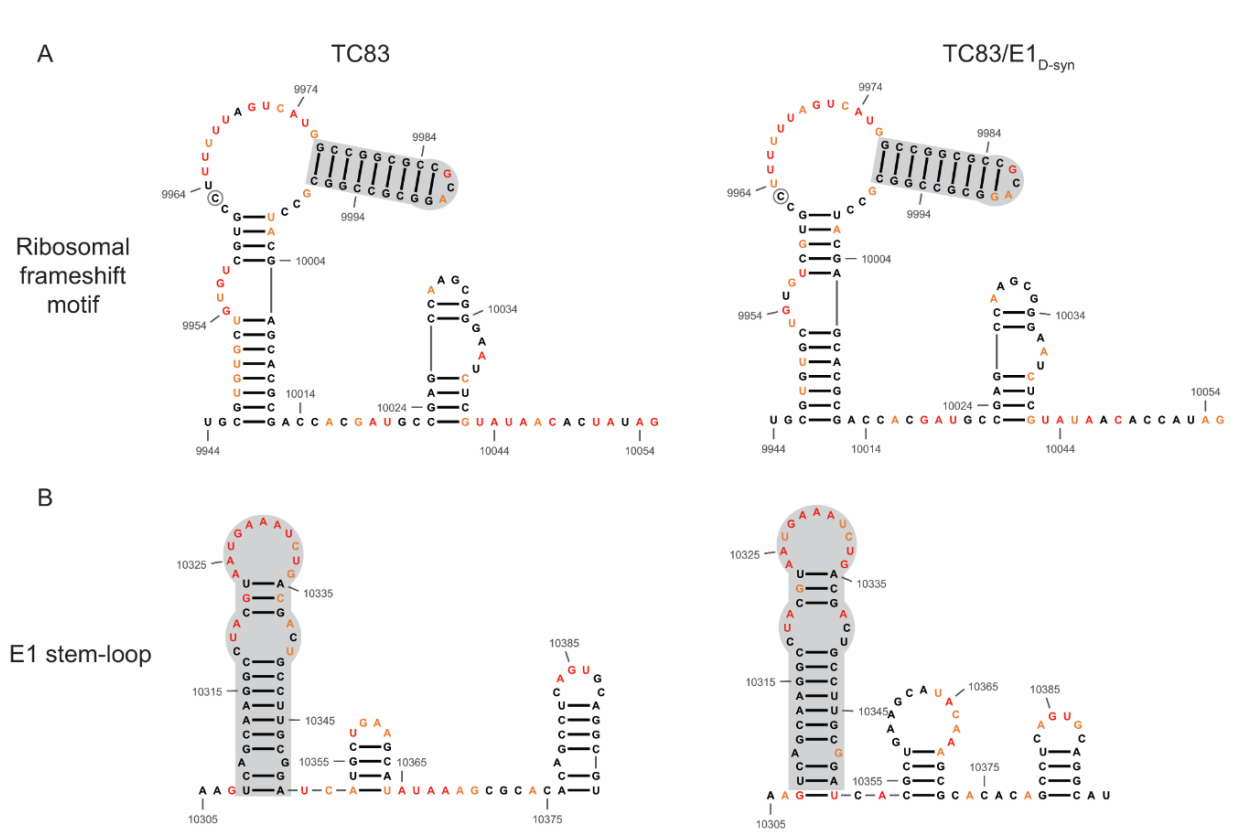

Figure 2.15 Previously described stable RNA structures conserved in SHAPE-MaP informed RNA secondary structure. Previous work by Kutchko *et al.* [194] performed *in vitro* SHAPE-MaP of the enzootic ID VEEV strain, ZPC738, and identified stable RNA structures across the VEEV genome. Displayed here are the SHAPE-MaP informed secondary structure predictions of **(A)** the ribosomal frameshift motif and **(B)** an E1 stem-loop for TC83 and TC83/E1$_{ID\text{-}syn}$. Shaded in grey are the conserved regions identified between the previously described stable structures in ZPC738 and the *in vivo* SHAPE-MaP data generated for TC83 and TC83/E1$_{ID\text{-}syn}$.

Extended data figure 9
Lineage K
Lineage L
Lineage M

Lineage K
Lineage L
Lineage M

Figure 2.16 Sequence alignment of the core E1 region. Alignment contains VEEV sequences from lineage K, L and M shown in the phylogenetic order determined in supp figure 1. Lineage K sequences are shaded in purple, lineage L sequences are shaded in blue and lineage M sequences are shaded in green. The alignment was made using TC83 (L01443 IAB) as the reference sequence. Varying nucleotides between TC83 and 307537 (KC344519 ID) are highlighted in red in the reference sequence. Identical nucleotides are represented as periods (.).

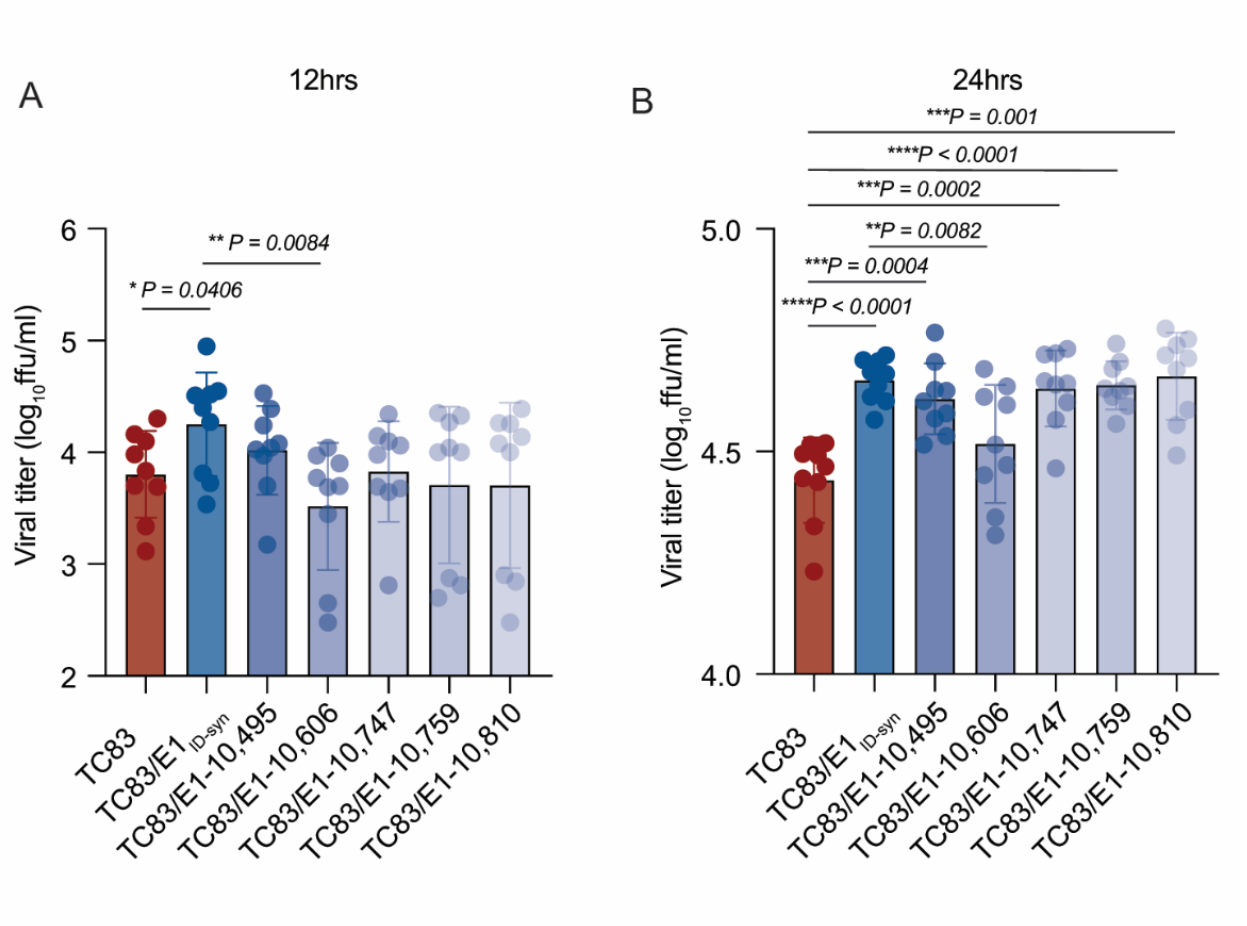

Figure 2.17 Replication of single point mutants in Raw264.7 macrophages. Mutant viruses were made containing a single point mutation from 307537 in the TC83 backbone. Raw264.7 were infected with single point mutants (MOI 0.1) and supernatants were harvested at 12 **(A)** or 24 **(B)** hpi and infectious virus titered by focus forming assay (FFA). Each experiment was performed in triplicate three times independently and the mean and SD graphed. Statistical analysis was performed using an unpaired T-test.

It is possible that complex interactions between RNA sequences is required for enhanced translation and replication, and that a combination of mutations is required to confer this phenotype. Since we hypothesized that changes in viral RNA structure contribute to emergence

of epizootic VEEV in nature, we sought to determine whether SNPs were conserved across other epizootic or enzootic strains. We reasoned that RNA structures associated with epizootic emergence would not be unique to TC83 but would also be present in other epizootic isolates. To this end, we compared sequences across 29 epizootic strains (subtype IAB and IC) and 40 enzootic strains (subtype ID) (**Figure 2.16**). Indeed, with two exceptions, TC83 SNPs in the E1 central region were conserved across all IAB isolates. Phylogenetic analysis shows the presence of distinct lineages which largely correspond to distinct geographic distribution of these viruses[28, 228, 229]. Due to spatial evolution of these lineages, we speculated that epizootic-associated SNPs and RNA structures may also be lineage-specific, and not necessarily globally conserved across different lineages (compare epizootic sequences (red) within lineage K and Lineage L). Indeed, when we compared epizootic IAB (TC83; lineage L) and epizootic IC sequences (lineage K), we observed SNPs distinct to epizootic viruses versus enzootic within the one lineage, but which were different between epizootic viruses across distinct lineages. While almost all TC83-associated SNPs in this region were conserved across other IAB isolates, we observed that in IC isolates only SNPs at position 10,495 and adjacent to 10,522 (yellow highlight; **Figure 2.16**) differed between ID enzootic and IC epizootic isolates in this lineage (lineage K). This suggests that the evolutionary path to epizootic emergence is likely distinct to each outbreak and virus lineage. To determine whether epizootic sequences from different lineages adopt conserved RNA secondary structure despite the presence of distinct SNPs, consensus RNA structure predictions were generated for each epizootic and enzootic group from lineage M, L, and K using RNAalifold [202, 230] (**Figure 2.18**). While overall the predicted secondary structure differed between all lineages, we observed that the 5' structural element and first conserved structural element (**Figure 2.13**; highlighted in blue and grey in **Figure 2.18**) were predicted to be conserved in both IAB and IC epizootic strains. This region encompasses four of the SNPs within the central E1 region responsible for differential macrophage replication, including nt 10,495 which we found was sufficient to increase replication of TC83 to levels similar to TC83/E1$_{ID\text{-}syn}$ (**Figure 2.17**). Collectively, this data shows that SNPs associated with macrophage replication fitness are conserved within lineages. Importantly, RNA structures are predicted to be conserved across epizootic viruses from distinct lineages despite variations in SNPs, suggesting that epizootic VEEV may evolve conserved RNA secondary structures that are functionally relevant for VEEV emergence.

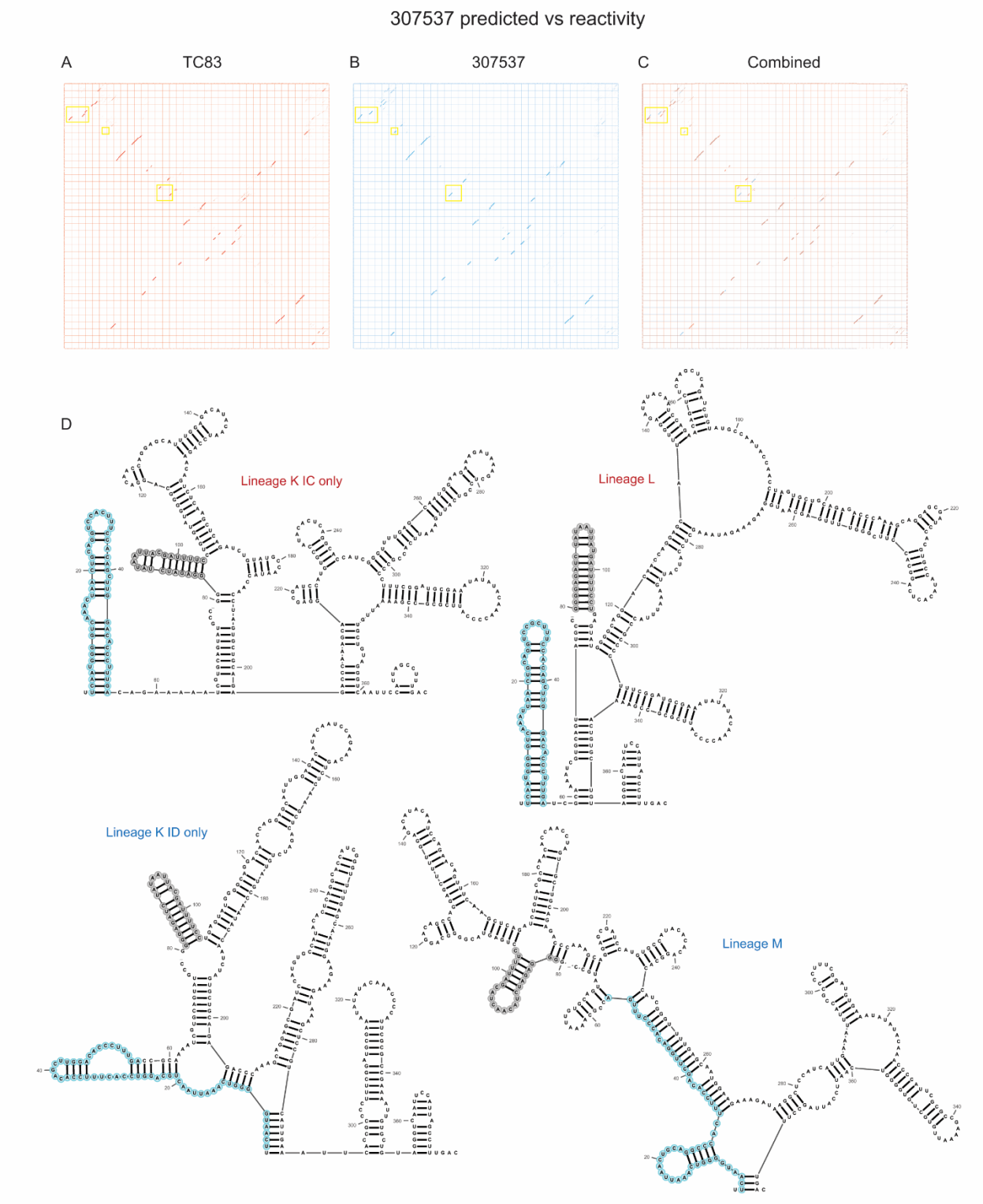

Figure 2.18 TC83 E1 SNPs are conserved in other epizootic strains and are lineage specific. Dot plots from RNAfold [202] predictions of individual SNPs within the E1 core region (10,466-10,843) for **(A)** TC83, **(B)** TC83/E1$_{ID\text{-}syn}$ and **(C)** overlayed dotblots. Yellow boxes highlight regions with differences in RNA structure predictions. **(D)** Predicted RNA secondary structures from RNA alignfold [230]of sequences from

lineages K (divided into epizootic IC and enzootic ID), L and M. Stem-loop conserved in epizootic lineages is highlighted in blue, and stem-loop conserved in all lineage K and L highlighted in grey.

Discussion

Repeated emergence of epidemic/epizootic VEEV as well as the emergence and re-emergence of other viral pathogens in recent times, has highlighted the need to better understand viral and host determinants that drive these processes. For VEEV, widespread vaccination of equines has been essential in the control of epidemic/epizootic outbreaks, though lack of vaccines and therapeutics for use in humans remains a significant gap [231]. Moreover, the ability to produce high levels of viremia in humans, and the presence of susceptible urban mosquito vectors in VEEV endemic regions suggests significant potential for VEEV to evolve the ability to transmit in urban settings without the need for an equine amplification host. Thus, understanding how host and viral factors drive the evolution and emergence of VEEV and other viral pathogens in nature is paramount. While previous phylogenetic studies have emphasized the importance of amino acid mutations within E2 in the emergence of epizootic VEEV [38, 48, 232], our data supports an additional role for RNA structure in viral replication and cellular tropism, which has implications for immune evasion, dissemination, and transmission.

In this study we identified novel RNA structures that alter VEEV replication fitness specifically in macrophages, but not in other cell types. To our knowledge, this is the first time that VEEV RNA structure has been demonstrated to alter cellular tropism. In addition, we identified several RBPs which enhance replication of E1 enzootic mutants, namely THRAP3, UBAP2L, FBL, and DHX38.

As far as we know, none of these RBPs have previously been shown to play a role in facilitating alphavirus replication, or for the most part, other RNA viruses. While these RBPs have been implicated in a wide variety of cellular functions, they have all been shown play a role in mRNA stability and translation [220-222]. Consistent with these reports, we have demonstrated that changes in E1 sequence and structure increases translation of TC83/E1$_{ID\text{-}syn}$ RNA, which is dependent in part on THRAP3. THRAP3 (thyroid hormone receptor-associated protein 3) is most notably described as an RNA splicing factor [233-236] and has also been implicated in transcriptional regulation [237, 238] and RNA stability [239]. However, the mechanisms by which THRAP3 regulate RNA metabolism is poorly described. Interestingly, recent studies have demonstrated a central role for THRAP3 in stress granule assembly [224, 225] along with UBAP2L and other notable stress granule-associated proteins (G3BP1/2)[240-244]. While we were unable to conclusively demonstrate a role for UBAP2L in increasing translation of TC83/E1$_{ID\text{-}}$

$_{syn}$ reporter RNA due to significant translational repression following KD in these assays, we clearly observed interaction of this RBP with viral RNA and demonstrated its role in enhanced replication of TC83/E1$_{ID\text{-}syn}$ (**Figure 2.10G-H**). Stress granule assembly dependent on G3BP1/2 and UBAP2L has been suggested to prevent excessive innate immune activation [242], thus in addition to regulation of viral RNA translation, we speculate that recruitment of UBAP2L to the VEEV genome could potentially regulated inflammatory responses, though in a manner that is independent of IFN and ISG expression (**Figure 2.5**).

At present the exact RNA structures necessary for recruitment of THRAP3 to TC83/E1$_{ID\text{-}syn}$ RNA is unclear and future efforts will focus on defining the precise structural and biochemical determinants of this interaction. Notably, we identified several hairpins in the core region of E1 that are conserved between TC83 and TC83/E1$_{ID\text{-}syn}$ and other strains (**Figure 2.13B-C**, grey boxes; **Figure 2.18B**) which contain AU-rich and AC-rich loop sequences. Many factors which regulate translation are known to bind to AU-rich and AC-rich sequences [153, 245-248], thus we speculate that conservation of these hairpins may suggest a role for these structures in translation of viral RNA. Whether THRAP3 interacts with these AU/AC-rich elements or functions by altering association of other translation factors with these elements remains to be determined. Defining RNA motifs and the structural basis of THRAP3-RNA recognition during VEEV infection will provide important insight into novel mechanisms of VEEV translational control.

Given the cell type specific nature of the replication phenotype observed, we speculated that the RBPs identified may be expressed preferentially in macrophages compared to other cell types in which TC83 and TC83/E1$_{ID\text{-}syn}$ replicated to similar levels. In contrast to our expectations, we observed that THRAP3, FBL, UBAP2L, and DHX38 were all expressed in both MEF and Raw264.7, but unexpectedly, expression of these RBPs was significantly repressed in MEF, but not macrophages following infection **(Figure 2.8D).** Previous studies have shown that a subpopulation of macrophages is resistant to macromolecular synthesis shutoff following VEEV infection [190]. Given that fibroblasts are sensitive to macromolecular synthesis shutoff, it is logical that these RBPs implicated in translational control (THRAP3, FBL, UBAP2L, and DHX38) would be downregulated in MEF. Thus, while these RBPs are not macrophage-specific per se, they may play a more prominent role in macrophages since these cells are resistant to translational repression following infection. It is tempting to speculate that VEEV may have evolved to exploit RBPs that regulate translation (such as THRAP3) that are more abundant in macrophages but downregulated in other cell types. Future studies will focus on broadly defining replication phenotypes of epizootic and enzootic VEEV in macrophages and the role of THRAP3 and other RBPs in translation. Whether enhanced replication of other alphaviruses in myeloid

cells is also specifically dependent on these RBPs or is more generally regulated by RBPs that control translation remains to be determined.

The observation that macrophage replication is specifically impacted by changes in E1 RNA is highly relevant, as myeloid cells are important targets early during in vivo infection and macrophages are important producers of IFN in this system [84, 208]. Notably, we observed that VEEV encoding E1 RNA sequences and RNA structures from an epizootic strain (TC83; IAB) replicated less efficiently in macrophages in relation to enzootic mutants. This is consistent with our prior studies, which similarly demonstrated that VEEV encoding either epizootic or enzootic 3'UTR sequences replicate differentially in an IFIT2-dependent manner [186] and to differences in replication that we have observed between the epizootic derived TC83 and the enzootic strain ZPC738 (**Figure 2.19**). While seemingly counterintuitive, we predict that diminished myeloid cell replication is associated with enhanced dissemination and viremia *in vivo*. In our proposed model, enhanced replication of enzootic mutants in myeloid cells in the lymph node leads to enhanced immune activation in neighboring cells which restricts viral replication in the periphery, leading to poor dissemination and viremia, reduced transmission, and possibly reduced pathogenesis. In contrast, epizootic mutants which replicate more poorly in these cells do not induce robust immune responses leading to more efficient dissemination and transmission. This model is also supported by studies with eastern equine encephalitis virus (EEEV), in which increased macrophage replication fitness leads to potent attenuation *in vivo* [208]. While increased macrophage replication with EEEV correlated with enhanced IFN production, we did not observe any significant difference in IFN expression or signaling between WT and E1 mutant VEEV. Nonetheless, we predict that multiple mechanisms (IFN-dependent and -independent) may possibly play a role in VEEV emergence, given the demonstrated role for this cytokine [54, 55].

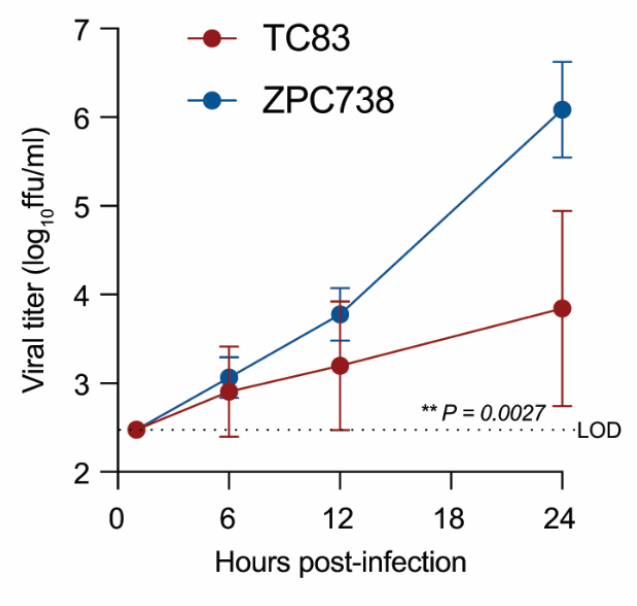

Figure 2.19 Enzootic ID strain ZPC738 replicates more efficiently than TC83 in macrophages. Replication kinetics of VEEV TC83 and ZPC738 in Raw264.7. Cells were infected with indicated viruses at a MOI of 0.1. Cell culture supernatant was serially harvested at 1, 6, 12, and 24 hpi and infectious virus was titered using focus forming assay (FFA). The experiment was performed in triplicate, three independently and the mean and SD are graphed. Statistical analysis was performed by calculating the area under the curve (AUC) for each replicate, and the AUC values from TC83 and ZPC738 were analyzed by unpaired t-test.

In addition to the 3'UTR and E1, we are also examining how other VEEV RNA sequences and structures may contribute to myeloid cell replication fitness, and how this impacts dissemination, pathogenesis, and transmission. Based on our observations we propose a more complex mechanism of VEEV emergence which entails acquisition of multiple mutations across the genome that collectively facilitate viral entry, replication fitness, and immune evasion in amplification hosts and vector species that facilitate transmission during epizootic episodes. We predict that diminished macrophage replication fitness is a hallmark of epizootic VEEV isolates. Furthermore, we suggest that macrophage replication phenotypes may be a more accurate cell culture-based predictor of epizootic potential, instead of determination by E2 sequences alone. These findings highlight the complexity of factors that contribute to viral emergence and highlight the importance of examining multiple cell types and host factors.

Chapter III: Conclusions and Future Directions

Summary

Venezuelan equine encephalitis virus (VEEV) is a zoonotic virus that has been responsible for significant epizootic outbreaks over the last century. The unique lifecycle of VEEV allows it to maintain endemic/enzootic reservoirs in mostly tropical regions of South and Central America, with the ever-present potential to cause major epidemic/epizootic outbreaks in the Americas. Constant further globalization as well as global warming have led to concerns for additional epizootic outbreaks in the future. Changes in the climate can lead to longer transmission seasons, increases in mosquito populations, and further geographical distribution of mosquito vectors, thereby widening areas at risk for epizootic outbreaks [21, 249]. Therefore, furthering our understanding of how host and viral factors contribute to the emergence of epizootic VEEV from enzootic VEEV is crucial. While amino acid mutations in the E2 glycoprotein have long been recognized as key drivers of epizootic VEEV emergence[38, 48, 232], variation in the pathogenicity of epizootic strains suggests that additional factors contribute to epizootic emergence.

The work described in this thesis supports an additional role for RNA structure in VEEV viral replication and cellular tropism. Using predictive RNA structure software, we were able to identify regions of predicted structural diversity between the epizootic vaccine strain TC83 and a closely related enzootic strain 307537. Based on this analysis, we generated a chimeric TC83 virus that contained the synonymous mutations from the E1 gene of 307537, termed TC83/E1$_{ID\text{-}syn}$. Incorporation of these synonymous E1 mutations resulted in an increase in viral replication, specifically in macrophages, highlighting the importance of changes in RNA sequence and/or structure within the E1 gene of VEEV for viral replication and cellular tropism.

We then sought to understand the mechanism through which this increase in viral replication was occurring. While we initially hypothesized that changes in E1 RNA structure could be enhancing VEEV viral replication in macrophages by evading recognition by PRRs, our findings did not support this as knock out and knock down of known alphavirus pattern recognition receptors (PRRs) RIG-I and MDA5 had no effect on the observed enhanced replication of the E1 mutant compared to TC83. Furthermore, similar results were obtained in experiments inhibiting all type-I IFN signaling through the IFNAR receptor, suggesting that the differences in macrophage viral replication could not be attributed to altered IFN induction or ISG expression.

To further uncover the IFN-independent mechanism by which TC83/E1$_{ID\text{-}syn}$ is able to increase replication, we used a proteomics approach to identify differences in the viral RNA-protein interactome of TC83 and TC83/E1$_{ID\text{-}syn}$. Using this approach, we were able to identify four

RNA binding proteins (RBPs) (FBL, THRAP3, UBAP2L, and DHX38) that were required for enhanced replication of TC83/E1$_{ID\text{-}syn}$ in macrophages. Interestingly, all four of these proteins have been previously associated with regulation of mRNA stability and translation[220-222]. This, in conjunction with the known importance of RNA structures within the 3'end of viral genomes and host mRNAs for translation efficiency [217-219], led us to hypothesize that the increased viral replication of TC83/E1$_{ID\text{-}syn}$ may be attributed to altered translation efficiency. To test this, we used a previously described translation reporter assay [140, 223] into which the E1 gene from either TC83 or TC83/E1$_{ID\text{-}syn}$ had been cloned to assess the effect of the E1 gene sequence on translation. In this assay, the translation reporter RNA containing the TC83/E1$_{ID\text{-}syn}$ E1 gene sequence showed a significant increase in translation compared to the TC83 reporter, supporting our hypothesis that changes in E1 RNA structure or sequence effect translation efficiency. Furthermore, we were able to show that knock down of THRAP3 removed any difference in translation of the two reporters, suggesting a specific role for THRAP3 in VEEV translation.

Through the generation of additional E1 gene mutants, we were able to establish that the central region of the E1 gene is essential for the enhanced macrophage phenotype. Using SHAPE-MaP analysis, we were then able to generate experimentally informed RNA secondary structure predictions and identify structures which may be involved in translation efficiency of VEEV.

Future directions

Our work here has demonstrated a novel role for RNA structure during VEEV replication, specifically in macrophages. Incorporation of enzootic E1 sequence into the epizootic derived TC83 strain was sufficient to alter viral replication, specifically in macrophages. At first glance, these results may seem counterintuitive, as it would be reasonable to expect that introduction of an enzootic sequence would have an attenuating effect on viral replication of a more pathogenic epizootic strain. Yet these findings were consistent with differences we observed in the macrophage viral replication of another enzootic strain ZPC738 and the epizootic derived TC83, in which ZPC738 achieved ~2log increase in viral replication at 24h. While these results suggest that enzootic strains and/or sequences confer a replication advantage in cell culture macrophages, the question remains how this phenotype might contribute to viral replication and pathogenesis *in vivo*.

In mouse VEEV infections, skin myeloid cells such as macrophages and dendritic cells (DCs) have been identified as the initial targets of infection, as the migratory nature of these cells allows for efficient system wide spread of the virus through the draining lymph nodes (dLNs) [22,

208]. Furthermore, VEEV infection is characterized by a system wide induction of type-I IFNs and upregulation of proinflammatory cytokines in the spleen and dLN early during infection. Based on our findings that epizootic sequences reduce macrophage replication in cell culture, we hypothesize that diminished epizootic replication in macrophages early during infection may lead to increased dissemination and pathogenesis *in vivo*. In this proposed model outlined in **Figure 3.1**, we would expect that enhanced replication of enzootic strains in macrophages early during infection leads to increased immune activation, effectively limiting viral replication in the periphery and possibly leading to reduced pathogenesis. Restricted macrophage replication of epizootic strains would conversely result in poor immune activation, eventually leading to more efficient dissemination and increased pathogenesis. The research presented here has primarily focused on the effects of enzootic versus epizootic sequences on viral replication in cell culture. However, future experiments investigating early myeloid infection, viral dissemination, and immune activation in mice would provide valuable insights into how this macrophage-specific phenotype influences *in vivo* pathogenesis. Additionally, expanding future studies to include replication kinetics in horse macrophages would further enhance our understanding of viral behavior in a more relevant host, providing critical insights into the natural infection dynamics of enzootic and epizootic VEEV.

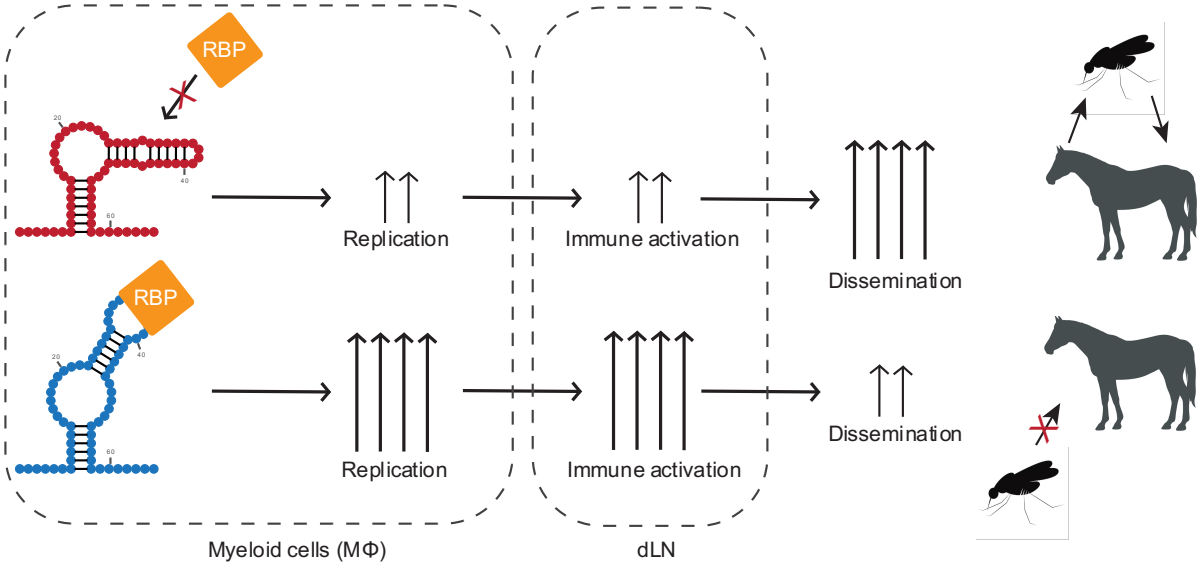

Figure 3.1 Model of RNA structure contributions to emergence and pathogenesis of VEEV. Following infection and trafficking to the proximal draining lymph node of an infected host, enzootic E1 RNA structures lead to recruitment of proviral factors (IFN-independent RBPs) which enhance replication specifically in macrophages, and possibly other myeloid cell types. Enhanced viral replication in the lymph node leads to increased accumulation of dsRNA and stimulates antiviral responses in host cells, preventing efficient dissemination and viremia. Reduced viremia leads to reduced transmission and possibly reduced pathogenesis.

Arthropod borne viruses encounter additional challenges, as they are required to maintain fitness in both vertebrate and invertebrate hosts. Furthermore, changes in the main mosquito vectors responsible for viral transmission during epizootic outbreaks suggest that mosquito adaptation of the virus to epizootic mosquito vectors may be important for epizootic emergence [30, 59]. Several regions within the alphavirus genome have been identified as important for maintaining mosquito vector competence, while having minimal effects on replication in mammalian cells. For example, destabilizing mutations in the putative secondary structure of the nsP1 51nt conserved sequence element (CSE) have been shown to have deleterious effects on alphavirus replication in mosquito cells with only minor effects on replication in mammalian cells [191]. Notably, several viral determinants have been shown to be critical for replication in one or either host. For example, the DLP RNA structural motif in SINV, which is encoded in the 5' end of the capsid gene has been shown to be critical for conferring eIF2α-independent translatability of the sub-genomic RNA when PKR is activated, but deletion of this element has minimal impact on viral replication in mosquito cells[197, 199]. In addition, phosphorylation of the hypervariable domain (HDV) of nsP3 is required for viral replication in mosquitoes yet dispensable for mammalian replication[102]. Understanding how variations in RNA sequences or structural elements across the viral genome impact viral replication in mosquitoes and their adaptability to epizootic vectors remains a crucial area of research. Although this study does not address these aspects, future experiments examining the effects of E1 synonymous mutations on replication in mosquito cells would address whether there is a role for these mutations in mosquito vector competence. Moreover, evaluating replication in mosquito cells derived from both enzootic and epizootic vector genera would provide further insights into whether these mutations specifically influence epizootic vector competence.

One of the remaining overarching questions is whether there are epizootic RNA elements or structures that are more widely conserved across epizootic strains that contribute to epizootic emergence. While we were able to identify conservation of SNPs within the epizootic IAB subtypes, these SNPs were not likewise conserved in other epizootic lineages. Geographical distribution of distinct VEEV lineages has likely led to significant differences in the SNPs identified between different epizootic lineages. Despite this, we were able to generate consensus predicted RNA secondary structures for epizootic and enzootic VEEV lineages, which showed conservation of several structures within the central region of the E1 gene, regardless of differences in the SNPs at these locations. Whether we can attribute the conservation of these predicted RNA secondary structures to convergent evolution of epizootic lineages and whether these structures

actually contribute to epizootic emergences remains to be seen. Future RNA structural studies looking at the conservation of experimentally informed E1 RNA structures of an array of enzootic and epizootic strains will help to identify conserved structures.

Concluding remarks

With continued global warming causing spread of viral vectors and increased globalization, understanding the mechanism involved in the emergence of epizootic VEEV remains crucial. The constant development of new techniques and expanded discoveries regarding the role of RNA structure in cellular functions, emphasizes the importance of furthering our knowledge regarding the varies roles that RNA structure may play in viral infections. Understanding the RNA structural landscape of VEEV and how this contributes to pathogenesis is of vital importance. The work in this thesis lays the groundwork for a method to identify diversity in the predicted RNA structures of various strains of VEEV. Continued exploration of the role that RNA structure plays in cell-type specificity and pathogenesis of VEEV is important for furthering our understanding of how to combat these viruses.

Chapter IV: Materials and Methods

Cell lines

Vero C1008 and Raw264.7 cells were obtained from ATCC. All cell lines were maintained in DMEM supplemented with 10% heat-inactivated FBS (HyClone), 1% L-GlutaMAX (Gibco), and 1% nonessential amino acids (NEAA).

Bone marrow derived macrophages (BMDMs) and Bone marrow derived dendritic cells (BMDCs) were generated independently from 10 to 20-week-old C57BL/6 mice. The mice were sacrificed, the femur and tibia were removed and cleaned. The bones were then briefly dipped in 70% EtOH to sterilized, followed by 1x PBS to remove any excess EtOH. The ends of the bones were then cut to expose the bone cavity and the bones were flushed with media using a 26.5G needle. The cells from one mouse were then divided over 3x 10cm non-tissue culture. To generate BMDMs, the dishes were grown in DMEM supplemented with 10% FBS (HyClone), 1% L-GlutaMAX (Gibco), 1% NEAA, 10,000 U/ml penicillin (Sigma), 10 mg/ml streptomycin (Sigma), and 20% L929-conditioned cell supernatant (described below). To generate BMDCs, the dishes were grown in DMEM supplemented 10% FBS (HyClone), 1% L-GlutaMAX (Gibco), 1% NEAA, 10,000 U/ml penicillin (Sigma), 10 mg/ml streptomycin (Sigma), 55mM β-mercaptoethanol and 20ng/ml GM-CSF (). On day 2 post harvesting, BMDMs were supplemented with 7ml BMDM media. On day 3, the cells were harvested by gently washing with PBS, followed by incubation with 10ml of 1mM EDTA in PBS for 5min at 37°C, and seeded for infection. On day 3 post harvesting, BMDCs were supplemented with 7ml BMDC media. On day 6, the non-adherent cells were harvested and seeded for infection.

The L929-conditioned cell supernatant was prepared by culturing L929 cells in a T175 until 90% confluence. This was then split into 6 new T175 flasks containing 45 ml of supplemented DMEM (10% GBS, 1% NEAA, 1% GluMAX) and cultured for 10 days at 37°C. Cell supernatants were then collected and centrifuged at 3000 rpm for 3 mins at 4°C. Lastly, supernatant was filtered using 45μM filter and stored at -20°C.

Generation of Raw264.7 RIG-I$^{-/-}$ and MDA5$^{-/-}$ CRISPR cells

To make a doxycycline-inducible CRISPR/Cas9 expression vector (pSBtet-puro-Cas9-U6), the Cas9-U6 fragment of pX459 (Addgene #62988; [250] was cloned into pSBtet-pur (Addgene #60507; [251]). Cas9 was first cloned into pSBtet-pur using the following primers: Cas9.F: 5'-CATGAGACCGGTGCCACCATG-3', Cas9.R: 5'-CATGAGGCGGCCGCCTACTTTTTCTTTTTTGCCTGGCCG, pSBtet-pur.F: 5'-CATGAG

GCGGCCGCCTTCC-3', pSBtet-pur.R: 5'-CATGAGACCGGTGGTGGCCGATATCTCAGAG. Post cloning, Cas9 was ligated into the pSBtet-pur backbone using the 5' AgeI and 3' NotI restriction sites. Following this, the U6 promoter was cloned into the new plasmid using the following primers: U6.F 5'-ACTACAGGTACC GAGGG-3', U6.R 5'-TCAGTCCTAGGTCTAGAGC-3', pSBtet-pur-Cas9.F 5'-TCAGTCCTAGGTCTAGAGC-3', pSBtet-pur-Cas9.R 5'-ATGAAGGTACCACATTTGTAGAGGTTTTACTTGC-3'. U6 was then ligated into pSBtet-pur-Cas9 using restriction sites 5' KpnI and 3' AvrII. The additional BbsI site in the pSBtet-pur-Cas9 was removed using site directed mutagenesis and the following primers: dBbsI.F 5'-TTGG GAAGAT AATAGCAG-3', dBbsI.R 5'-CTGCTATTATCTTCCCAA-3'.

Sequence-specific gRNA sequences were designed using the Broad Institute Genetic Perturbation Platform gRNA design tool to target mouse Ddx58 and Ifih1. Dhx58 and Ifih1 gRNA oligonucleotides were cloned into pSBtet-puro-Cas9-U6 using the primers in **Table 1,** as described previously [250].

Raw264.7 CRISPR KO cells were made by electroporating low passage Raw264.7 cells with Dhx58 and Ifih1 pSBtet-puro-Cas9-U6 using Amaxa Nucleofector II and Amaxa Cell Line Nucleofector Kit V (Lonza). Cells were selected with puromycin for 3 days post-nucleofection, and Cas9/gRNA expression was induced at 7 days post-nucleofection. Following this, cells were treated for 14 days with doxycycline and the KO efficiency of the cells was validated by western blotting.

Table 1. Primer sequences for generation of RIG-I and MDA5 CRISPR cell lines

Gene	Primer	Sequence
Ddx58	Ddx58.g19.F	5'- CACCGAAGAACAACAAGGGCCCAA-3'
	Ddx58.g19.R	5'- AAACTTGGGCCCTTGTTGTTCTTC-3'
	Ddx58.g28.F	5'- CACCGATATCATTTGGATCAACTG-3'
	Ddx58.g28.R	5'- AAACCAGTTGATCCAAATGATATC-3',
	Ddx58.g36.F	5'- CACCGTGGATTGTTGATAAAGGTG-3'
	Ddx58.g36.R	5'- AAACCACCTTTATCAACAATCCAC-3'
Ifih1	Ifih1.g24.F	5'-CACCGTGTGGGTTTGACATAGCGCG-3'
	Ifih1.g24.R	5'-AAACCGCGCTATGTCAAACCCACAC-3'

	Ifih1.g69.F	5'-CACCGTTGGCGCAGAACATCCAGGA-3'
	Ifih1.g69.R	5-'AAACTCCTGGATGTTCTGCGCCAAC-3'
	Ifih1.g81.F	5'-CACCGCGTAGACGACATATTACCAG-3'
	Ifih1.g81.R	5'-AAACCTGGTAATATGTCGTCTACGC-3'

Generation of full-length and recombinant viruses

Construction of the full length TC83 VEEV infectious clone [50] and ZPC738 [56] have been previously described. To introduce the E1 gene from KC344519 into TC83, a gBlock containing the E1 gene with flanking TC83 regions was generated (**Table 2**). The following primers were used to amplify two TC83 backbone fragments from the VEEV TC83 infectious clone described above: TC83 F1: 5'-GCTTGGTGCTGGCTACTATTG-3', TC83 R1: 5'-CTCTTCGGATGCACCCTCAC -3', TC83 F2: 5'- GATGCAGAGCTGGTGAG -3', TC83 R2: 5'-GTTATACGAGATTCCCGCTTGG -3'. The backbone fragments were generated using Q5 high fidelity polymerase (NEB, M0491), followed by overnight treatment with DpnI. The DNA was then purified using MicroElute Cycle-Pure Kit (Omega Bio-Tek). Fragment assembly was performed using Quantabio RepliQa HiFi assembly mix (#95190-D10) followed by transformation into NEB Stable Competent *E. coli*.

Mutants 1-3 were generated as follows. Fragments for mutant 1 were amplified using the following primers with corresponding plasmid: TC83/E1$_{ID\text{-}syn}$ fw 5'-GCAAGATAGACAACGACG-3' and rv 5' GTCTCTGCAGCACTAGG 3', TC83: fw 5' CTGTATGCCAATACCAACC 3' and rv 5' CTGGCCCTTTCGTCTTC 3'. Mutant 2 fragments were generated using the same primers, but with the opposite plasmids. Fragments for mutant 3 were generated using the following primers: TC83/E1$_{ID\text{-}syn}$ fw 5' TTCAATGGGGTCAAAATAACTG 3' and rv 5' GTCAAAGGCTAATGGAATTGAC 3', TC83 fw 5'GCAAGATAGACAACGACG 3' and rv 5' GGACCTGCAGTTATTTTGAC 3', TC83 fw 5' GTGCTGTAGGGTCAATTCC 3' and rv 5' CTGGCCCTTTCGTCTTC 3'. The fragments were generated and assembled as described above. Mutants 7-12 were generated using the primers **Table 3**. Site-directed mutagenesis was performed using Q5 high fidelity polymerase (NEB, M0491), treated overnight with DpnI and the DNA was purified using Mag-Bind TotalPure NGS beads (Omega Bio-Tek) followed by transformation into NEB Stable Competent *E. coli.*

Plasmids were linearized at MluI restriction sites located downstream of the poly(A) tail and genomic RNA was transcribed from the SP6 promoter in the presence of N7^{m}G cap analog

using the SP6 mMessage mMachine kit (Ambion). $1x10^7$ BHK21 cells were electroporated with approximately 2 µg of *in vitro* transcribed RNA using a GenePulser Xcell electroporator (Bio-Rad) to generate P0 virus stocks.

Table 2. KC344519 E1 gene block

CGACCACGATGCCGAGCCAAGCGGGAATCTCGTATAACACCATAGTCAACAGAGCAGGC
TACGCGCCACTCCCTATCAGCATAACACCAACAAAGATCAAGCTGATACCCACAGTGAACT
TGGAGTACGTCACCTGCCATTACAAAACAGGAATGGATTCACCAGCCATCAAATGCTGCGG
ATCTCAGGAATGCACTCCAACTTACAGGCCCGATGAACAGTGCAAAGTCTTCACAGGGGTT
TACCCGTTCATGTGGGGAGGTGCATATTGCTTTTGCGACACTGAGAACACCCAAGTCAGCA
AGGCCTACGTAATGAAATCTGACGACTGCCTTGCGGATCACGCTGAAGCATACAAAGCGC
ACACAGCCTCAGTGCAGGCATTCCTCAACATCACAGTGGGAGAACACTCCATTGTGACCAC
CGTGTACGTGAATGGAGAAACTCCTGTGAACTTCAATGGGGTCAAAATAACTGCAGGTCCA
CTTTCCACAGCTTGGACACCCTTTGACCGCAAAATCGTGCAGTATGCCGGGGAGATCTATA
ATTACGATTTTCCTGAGTATGGGGCAGGACAACCAGGAGCATTCGGAGACATACAATCCAG
AACAGTCTCAAGCTCAGATCTGTATGCCAATACCAACCTAGTGCTGCAGAGACCCAAAGCA
GGAGCGATCCATGTGCCATACACTCAGGCACCATCGGGTTTTGAGCAATGGAAGAAAGAT
AAAGCTCCGTCATTGAAATTCACCGCCCCTTTCGGATGCGAAATATATACAAACCCCATTC
GCGCCGAAAATTGTGCTGTAGGGTCAATTCCATTAGCCTTTGACATCCCTGACGCCCTGTT
CACCAGGGTGTCAGAAACACCGACACTTTCAGCGGCCGAATGTACTCTTAATGAGTGCGT
GTATTCATCCGACTTTGGCGGGATCGCCACGGTCAAGTATTCGGCCAGCAAGTCAGGCAA
GTGCGCAGTCCATGTGCCATCAGGGACTGCTACCCTAAAAGAAGCAGCAGTCGAGCTAAC
CGAGCAAGGGTCGGCGACCATTCATTTCTCGACCGCAAATATCCACCCGGAGTTCAGGCT
CCAAATATGCACATCATATGTCACGTGCAAAGGTGATTGTCACCCCCCGAAAGACCACATT
GTGACACACCCCCAGTATCACGCCCAAACATTCACAGCCGCGGTGTCAAAAACCGCGTGG
ACGTGGTTAACATCCCTGCTGGGAGGATCG**GCCGTAATTATTATAATTGGCTTGGTGCTG**
GCTACTATTGTGGCCATGTACGTGCTGACC

Table 3. Single point mutant primers

Mutant	Position	Fw primer	Rv primer
Mut7	10,495	CTGCAGGTCCACTTTCCACAGC	GCTGTGGAAAGTGGACCTGCA G

Mut8	10,522	GACACCCTTTGACCGCAAAATCGTG	CACGATTTTGCGGTCAAAGGGTGTC
Mut9	10,606	GCATTTGGAGACATACAATCCAG	CTGGATTGTATGTCTCCAAATGC
Mut10	10,747	GAAAGATAAAGCTCCGTCATTGAAATTTACC	GGTAAATTTCAATGACGGAGCTTTATCTTTC
Mut11	10,759	CATCATTGAAATTCACCGCCCCTTTC	GAAAGGGGCGGTGAATTTCAATGATG
Mut12	10,810	GCGCCGAAAATTGTGCTGTAG	CTACAGCACAATTTTCGGCGC

Focus-forming assays

Vero E6 monolayers were infected with serial 10-fold dilutions of infectious samples for 1 hour at 37^{o}C, then overlaid with 100 µl per well of medium (0.5x DMEM, 5% FBS) containing 1% carboxymethylcellulose, and incubated for 20 to 22 hours at 37^{o}C with 5% CO_2. Cells were then fixed by adding 100 µl per well of 2% paraformaldehyde directly onto the overlay at RT for 2 hours. After removing the overlay media and fix, cells were washed 3x with 1x PBS and incubated with VEEV E2 glycoprotein specific antibodies (gift of Dr. Michael Diamond) for 2 hours at RT in FFA permeabilization buffer (1x PBS, 0.1% saponin, and 0.1% BSA). Mouse anti-VEEV E2 (clone 36.E5) were generated and purified from a clonal hybridoma cell line, a generous gift from Dr. Michael Diamond (Washington University School of Medicine, St Louis). Cells were washed 3x in ELISA wash buffer (1x PBS, 0.05% triton X-100), then incubated with species-specific HRP-conjugated secondary antibodies (Sigma and ThermoFisher) for 1 hour at RT in FFA permeabilization buffer. Monolayers were washed 3x with ELISA buffer and foci were developed by incubating in 50 µl/well of TrueBlue peroxidase substrate (KPL) for 5 to 10 minutes at RT, after which time cells were washed twice in water. Well were imaged using Immuno Capture software (Cell Technology Ltd.), and foci were subsequently counted using BioSpot software (Cell Technology Ltd.). Samples were titered in duplicate and the average titers were calculated.

Viral growth kinetic assays

Multistep viral growth kinetics were performed by infecting Raw264.7 with WT or mutant VEEV TC83 viruses at a MOI of 0.1. Cells were seeded 18-20hrs prior to infection. Viral titers were determined for indicated time points post-infection by removing cell culture supernatant, replacing it with fresh growth media, and subsequently measuring viral titers through FFA. All experiments were performed three or four times independently in triplicate. Statistical analysis

was performed by calculating area under the curve (AUC) and performing unpaired t-test on AUC values calculated for each experiment. P values are reported in each figure.

siRNA knock-down

DsiRNA transfections were done in 96 well format. DsiRNAs used are listed in **Table 4**. Transfection mix was made up of 10nM DsiRNA pool, 0.2µl *Trans*IT-X2 Dynamic Delivery System (Mirus, 6003) and supplement-free DMEM and incubated at RT for 20mins. 2E4 Raw264.7 cells were combined with the transfection complexes and seeded into a 96 well plate. 24 hours post transfection were mock infected or infected with either TC83 or TC83/E1$_{ID\text{-}syn}$ at an MOI of 0.1. 24 hours post infection, supernatant was collected and titered as describe previously. Cell viability was then assess using alamarBlue Cell Viability Reagent (Invitrogen, DAL1025) as described by the manufacturer.

Table 4. DsiRNA sequences

Gene	**duplex name**	**DsiRNA sequence**
Ehmt2	mm.Ri.Ehmt2.13.1	AUCAAUGCAGUAAACCUCGCCAUCCUU
	mm.Ri.Ehmt2.13.2	GGUAAGAAUCAUCCUCUCUCACAUCAG
	mm.Ri.Ehmt2.13.3	UACCAAACCCAACAUUUAUUGAGAACA
Zc3h4	mm.Ri.Zc3h4.13.1	ACAAUUUAUGACUCAAAGAAAGUACUA
	mm.Ri.Zc3h4.13.2	UAUAAUUUACACGGAAAGUCACCAUGC
	mm.Ri.Zc3h4.13.3	UGUCCUUGGACCUGCGGUACUGGUUCA
Thrap3	mm.Ri.Thrap3.13.1	UUUAGUAAAGCGUUCAUGCAAUGUCAU
	mm.Ri.Thrap3.13.2	GUCGUCAUGCAAGUAAUACUUCUUGCU
	mm.Ri.Thrap3.13.3	AAUUCAGAAGUUUCUUAGAAAACCGUC
Syncrip	mm.Ri.Syncrip.13.1	CUGAAGUAGUAUCCAUGGGCUCUUCAG
	mm.Ri.Syncrip.13.2	AGUAGUAAUCAUCAUACAUUUGAUUCU
	mm.Ri.Syncrip.13.3	GAAUGAAAGCAUAAUCUUUUAGCUUCU
Bclaf1	mm.Ri.Bclaf1.13.1	UGACCUUGGACUAUUAUCAUAAGCUGA
	mm.Ri.Bclaf1.13.2	UAUGUAAGCUAUCCAAUCAGGUACUAG
	mm.Ri.Bclaf1.13.3	ACUCUUUAUCACUAAAGUAAUCUAGAA
Fbl	mm.Ri.Fbl.13.1	CAGAUAAAGACACCUUCAUGACGAUGC
	mm.Ri.Fbl.13.2	CAGGAAUAAUGUUAGUCCUCUUCUUGG
	mm.Ri.Fbl.13.3	UCUGCUGACGCAGUGGAGUCAAUGCAG

Chtop	mm.Ri.Chtop.13.1	AACAUUUCCAAUUUACUACCUUCACUA
	mm.Ri.Chtop.13.2	UUUAGUUUUCGACAUGUAUGCAUCCAA
	mm.Ri.Chtop.13.3	CUGCUUAAGUUUUAAUGCUGCCUGGAC
Ubap2l	mm.Ri.Ubap2l.13.1	CCUGUUGUACUGCCACCUUUAGCUUCC
	mm.Ri.Ubap2l.13.2	AAGUGGAAGGUGAUUCAGAUUUCACUG
	mm.Ri.Ubap2l.13.3	CUGUGAUAUCAAUCAAUUGUUUCACCU
Dhx38	mm.Ri.Dhx38.13.1	AUCUUCAUGCAAGUACUGGGUCAGCUG
	mm.Ri.Dhx38.13.2	ACAGGUGUACCUGCAAGGACUGCUUCA
	mm.Ri.Dhx38.13.3	ACAGAUGAACACGCAGGUGAAAGCCUU
Hnrnpr	mm.Ri.Hnrnpr.13.1	GUCAUUGUACUCUAUAUAGGUUUAACC
	mm.Ri.Hnrnpr.13.2	AACCUAGGUAAGGUUUCUUAUUUUGAU
	mm.Ri.Hnrnpr.13.3	AAUUCUUGGUUGUCAUUAUUGUAACCA
Ubtf	mm.Ri.Ubtf.13.1	UACCGUACUCGGAAUUUCGAAAAGAGA
	mm.Ri.Ubtf.13.2	CUCCAUUCCUUCAAGGCAUGUAACUGU
	mm.Ri.Ubtf.13.3	UUUGUAAGGGUUUUUAACAUGUUCCUG
Ddx58	mm.Ri.Ddx58.13.1	CACCUAACAACUAUUUCCAAAGUUUUC
	mm.Ri.Ddx58.13.2	GAUCUUCAAUGAACAUUAAGUAGUCAA
	mm.Ri.Ddx58.13.3	AAGCUCUAAGGUCAGUAUUUUUAACUU
Ifih1	mm.Ri.Ifih1.13.1	ACCUACUCCGUAGAAUAGCUAUUCGUC
	mm.Ri.Ifih1.13.2	AGGCUCUCUUCUACUACAUAUUUCGAU
	mm.Ri.Ifih1.13.3	GUUGUAGUACUCUGCUAUAAACUUCGU
Mavs	mm.Ri.Mavs.13.1	ACGUAUGUAACUACGAUUAUAUAAGAU
	mm.Ri.Mavs.13.2	UCUAACCAGGGUCAUUUUUGGUACAGA
	mm.Ri.Mavs.13.3	UGGACAAAGUCAUGAUGUGAGUGGUUA

IFNAR blocking antibody infections

Raw264.7 cells were seeded 24h prior to infection. One hour prior to infection, the cells were pretreated with 10µg of mouse IgG2a isotype control (InVivoMAb, BE0085) or IFNAR1 Monoclonal Antibody (MAR1-5A3, Invitrogen 16-5945-85), infected with TC83 or TC83/E1$_{ID\text{-}syn}$ at an MOI of 0.1 in the presence of antibody. Infectious virus from cell culture supernatants harvested at 10 and 22 hpi was titered by FFA. Each experiment was performed three times independently. Cell lysates were collected at 22hpi for RT-qPCR analysis.

RT-qPCR

Cell lysates were prepared using Quick-RNA MiniPrep Kit (Zymo Research, Cat# 11-328) according to manufacturer's protocol. Samples were DNase I (NEB, M0303) treated for 20 mins at 37°C, followed by inactivation of DNase I in 0.1M EDTA for 10 mins at 70 °C. cDNA was generated with 100ng/10µl reaction using iScript cDNA synthesis kit (Bio-rad, 1708890). qPCR was then run with 1µl of cDNA using iTaq Universal Probes Supermix (Bio-rad, 1725130) on Bio-Rad CFX96 Real-Time System. The following primer probe assays were used: Ifit1 (IDT, Mm.PT.58.32674307), IFN-beta (IDT, Mm.PT.58.30132453.g), ISG15 (IDT, Mm.PT.58.41476392.g), VEEVset3 (nt9835-9856) (IDT, probe sequence: /56-FAM/TTT GTC TGG /ZEN/CTG TGC TTT GCT GC/3IABkFQ/), TC83.gRNA (IDT, probe sequence: /56-FAM/AGA AAG CAC /ZEN/AGC GTA AGA GCC GAT /3IABkFQ/) and TC83.sgRNA (IDT, probe sequence: /56-FAM/AGC TGT TAA /ZEN/GTG CCC CGG AAG G/3IABkFQ/).

Western blotting

Cell lysates were generated by washing monolayers with PBS followed by incubation with RIPA lysis buffer (Thermofisher, cat# 89901) supplemented with Halt protease inhibitor cocktail (Thermofisher, cat# 78429) on ice for 5 min. Lysates were then scraped, transferred to microcentrifuge tubes, pulse vortexed and further incubated on ice for 15 mins. Hereafter, lysates were centrifuged at 16,000xg for 20 mins at 4°C and supernatants were transferred to a new tube. Proteins were separated by on a 4-20% Mini-PROTEAN TGX precast protein gel (Bio-rad), transferred to a nitrocellulose membrane (Amersham, 10600008), and then labeled for proteins. The following antibodies were used: beta-Actin Mouse mAb (Cell signaling, 8H10D10), beta-Actin Rabbit mAb (Cell signaling, 13E5), Rig-I mAb (Cell signaling, D1466), MDA-5 Rabbit mAb (Cell signaling, D74E4), Fibrillarin/U3 RNP Rabbit pAb (ABclonal, A1136), Dhx38 (ABclonal A4341), Thrap3 Rabbit pAb (ABclonal, A9396), UBAP2L (E5X4E) Rabbit mAb (Cell Signaling Technology, 40199), Goat-anti-Rabbit IRDye 800 (Licor, 926-32211), Goat-anti-mouse IRDye 680 (Licor, 926-68070).

To determine changes in protein expression, the integrated density was measured for each protein of interest band using Adobe Photoshop. Background signal was subtracted. For comparisons between Raw264.7 and iMEF, and when determining the KD efficiency, the integrated density of the protein of interest bands were normalized to the actin loading control and percentage compared to the Raw264.7 uninfected samples or NSC was calculated.

Immunoprecipitation-mass spectrometry

Cell lysates were generated from Raw264.7 cells by resuspending cells in 1X CHAPS lysis buffer (10mM HEPES, 200mM NaCl, 1% CHAPS, 10mM MgCl2, protease inhibitor (Thermo Scientific Pierce, PIA32955), 200U/ml murine RNase inhibitor (NEB, M0314)). Lysates were then passed through a 25G needle 4x and incubated on ice for 15min to ensure lysis. Thereafter, lysates were centrifuged at 16,000xg for 20 mins at 4°C and supernatants were transferred to a new tube. 50µl of Dynabeads protein G (Thermo, #10003D) were washed 2x in 500µl lysis buffer, after which they were incubated in 200µl lysis buffer along with 12µg of mouse J2 IgG2a Or mouse IgG2a isotype control (InVivoMAb, BE0085) for 30 mins at RT. Beads were then washed 3x in lysis buffer, incubated with 3mg of Raw264.7 lysate on the rotator for 2hrs at RT, washed again 3x in lysis buffer followed by 3x with freshly prepared 20mM ammonium bicarbonate. Samples were then trypsin digested in 20µl 20mM ammonium bicarbonate and incubated with 10µl of 10ng/µl sequencing grade trypsin (Promega, cat# V5111) at 37°C for 3hrs at 1500rpm. The supernatant was then carefully removed from the beads and the beads where washed 2x in 30µl 20mM ammonium bicarbonate, and all fractions were pooled. Samples were then reduced by adding tris(2-carboxyethyl)phosphine (TCEP) to a final concentration of 1mM and incubated at 37°C for 1h. Freshly prepared iodoacetamide (Thermo, cat# 90034) was then added to a final concentration of 10mM and incubated at RT for 30min in the dark, followed by quenching with final concentration 2mM N-AcetylCysteine. Samples were then cleaned-up and concentrated using C18 columns (Thermo-Pierce, cat# 89870) according to the manufacturers protocol. After clean-up, formic acid was added to the samples at a final concentration of 0.1%. Samples were analyzed by LC/MS at University of Washington's Proteomics Resource (UWPR).

SHAPE-MaP

VERO cells were seeded at 25E6 cells per 10cm dish. 24 hours post seeding, cells were infected with either TC83 or TC83/E1$_{ID\text{-}syn}$ at MOI 0.1. At 24hpi culture media was aspirated and cells were washed once with 1x PBS. In-cell SHAPE modifications were made by adding fresh 500µl of 100mM 1-Methyl-7-nitroisatoic anhydride (1M7) (Sigma-Aldrich, 908401) in DMSO to 4.5ml pre-warmed culture media to the dish and incubated for 3min at 37C. This was repeated 3x to increase modifications. Unmodified samples were similarly treated with DMSO. After treatment, whole-cell RNA was purified using TRIzol reagent (Fisher Scientific) according to the manufacturers protocol. Samples were treated with TURBO DNase (Thermo Fishter, AM2238) for 30min at 37C to remove any DNA. Polyadenylated RNA was then isolated from the whole-cell RNA using NEB Oligo d(T)25 Magnetic beads (NEB, S1419S) according to the manufacturers

protocol. To generate the denatured controls, 1µg of TC83 DMSO and TC83/E1$_{ID\text{-}syn}$ DMSO polyA purified RNA were heated to 95C for 2min in 1x DC buffer (50mM HEPES (pH 8.0), 4mM EDTA) with an equal volume of 100% formamide. Samples were then immediately transferred to a new tube containing fresh 1M7 to a final concentration of 10mM and heated at 95C for 2min, after which the samples were placed on ice. DC control RNA was then purified using G-50 columns (GE healthcare, 25-5330-01). All samples were then prepared for sequencing using the randomer library prep workflow protocol described in Smola et al. [227]. Samples were sequenced by Illumina NGS at the Fred Hutch Cancer Center genomics core. Sequencing data was analyzed using Shapemapper2 as previously described.

Translation reporter assays

VEEV translation reporters were constructed based on previously described constructs [140, 223]. The E1 gene from TC83 and TC83/E1$_{ID\text{-}syn}$ were cloned into the VRLF reporter plasmid using PacI and NotI (NEB). Plasmids were linearized overnight with NotI. Reporter RNAs were *in vitro* transcribed using HiScribe T7 High Yield RNA Synthesis kit (NEB, E2040) and capped using Vaccinia Capping System (NEB, M2080) according to the manufacturers protocol.

Reporter assays were performed by nucleofecting (Cell Line Nucleofector Kit V, Lonza VCA-1003) 1E6 Raw264.7 with 4µg of either reporter RNA and plated in 12 wells of a 96-well U-bottom plates. Cells were harvested at indicated time points, washed 1x in with PBS and lysed in 1x passive lysis buffer (Promega). Firefly luciferase assays were performed using Luciferase Assay System (Promega) according to the manufacturers protocol. Luciferase activity was measured using a BioTek Synergy luminometer. Experiments were performed 3 times independently in triplicate. The relative light units were normalized to total protein concentration using a BCA Protein assay (Pierce), and further normalized within each experiment to the 30min TC83 sample. Statistical analysis was performed using unpaired t-test. P values are reported in each figure.

For siRNA KD translation reporter assays, 10µl of a 10nM siRNA pool or NSC were mixed in 600µl neat DMEM with 10µl *Trans*IT-X2 Dynamic Delivery System (Mirus, 6003) and incubated at RT for 15mins. Transfection complexes were then added to 4E6 Raw264.7 macrophages in 6ml of growth media in a 10cm dish. Cells were transfected for 24h, after which translation reporter assays were performed as described above.

Replicon assays

To make the VEEV replicon nsp3-nanoluciferase and ORF2-fireflyluciferase reporters, we replaced the GFP in the previously described VEEV/nsp3-GFP reporter virus (a generous gift of

Dr. Ilya Frolov) [102]. This was done by PCR amplifying nano-luciferase with primers adding 5' ClaI and 3' NotI restriction sites using Q5 high fidelity polymerase (NEB, M0491): Fw primer: 5' CGACCCACCATCGATTAGGTTCCGGATCAatggtcttcacactcgaag 3', Rv primer: 5' attacgccagaatgcgttcgcTGGGCGGCCGCTGATCCGGAACC3'. VEEV/nsp3-GFP and the PCR amplified nano-luciferase were then digested with ClaI and NotI, and the VEEV/nsp3 backbone (13,341bp) and nano-luciferase fragments were gel purified. The nano-luciferase fragment was then ligated into the VEEV/nsp3 backbone using Instant Sticky-end Ligase Master Mix (NEB, M0370) followed by transformation into NEB Stable Competent *E. coli.* This cloning resulted in TC83/nsp3-nluc. Before introducing Firefly-luciferase into ORF2, the nano-luciferase from pVR21(F)-nluc [208] was first amplified using the following primers: Fw 5' TTGAGGGGCCCCTATAACTCTCTAC 3', Rv 5' GTCTCGGCCCGGGCATTACGCCAGAATGCGTTCG 3'. This fragment was then introduced into TC83/nsp3-nluc by digesting both the backbone and nano-luciferase fragments with ApaI and SrfI, gel purifying relevant fragments, and ligating using T4 DNA ligase (NEB, M0202) followed by transformation into NEB Stable Competent *E. coli*. This cloning resulted in TC83/nsp3-nluc_ORF2-nluc-SK-E1. To replace the ORF2 nano-luciferase with firefly-luciferase, firefly-luciferase was PCR amplified with primers adding 5'AscI and 3'SrfI restriction sites: Fw 5' gccaaggcgcgccATGGAAGACGCCAAAAACATAAAGAAAGG 3', Rv 5' gccaaggcgcgccATGGAAGACGCCAAAAACATAAAGAAAGG 3'. This fluc fragment was then introduced into TC83/nsp3-nluc_ORF2-nluc-SK-3'UTR by digesting with ApaI and SrfI, gel purifying and ligating using T4 DNA ligase followed by transformation into NEB Stable Competent *E. coli.* This cloning produced the replicon TC83/nsp3-nluc_ORF2-fluc_6K-E1. Lastly, the E1 sequence from TC83/$E1_{ID\text{-}syn}$ was introduced by digesting the TC83/$E1_{ID\text{-}syn}$ plasmid and the new replicon plasmid with SrfI and MluI. The relevant fragments were gel purified and transformed as described above.

Reporter plasmids were linearized overnight with MluI. Reporter RNAs were *in vitro* transcribed using HiScribe T7 High Yield RNA Synthesis kit (NEB, E2040) and capped using Vaccinia Capping System (NEB, M2080) according to the manufacturers protocol.

Reporter assays were performed by nucleofecting (Cell Line Nucleofector Kit V, Lonza VCA-1003) 1E6 Raw264.7 with 4µg of either reporter RNA and divided over 12 wells of a 96-well U-bottom plates. Cells were harvested at indicated time points, washed 1x in with PBS and lysed in 1x passive lysis buffer (Promega). Dual nano and firefly luciferase were measured using Nano-Glo Dual-luciferase reporter assay system (Promega, N1610) according to the manufacturers protocol. Luciferase activity was measured using a BioTek Synergy luminometer. Experiments

were performed 3 times independently in triplicate. The relative light units were normalized to total protein concentration using a BCA Protein assay (Pierce). Statistical analysis was performed using unpaired t-test. P values are reported in each figure.

RNA-aptamer affinity purification

RNA constructs encoding the core region of TC83 or TC83/E1$_{ID\text{-}syn}$ from nts 10,516 to 10,808 along with a 3' hepatitis delta virus ribozyme sequence (5'-gctagccatggtcccagcctcctcgctggcggctagtgggcaacatgcttcggcatggcgaatgggac-3) were cloned downstream of the S1m aptamer [252] using BamHI (5') and EcoRI (3') restriction sites. cDNA clones were linearized with either EcoRI (for TC83 and TC83/E1$_{ID\text{-}syn}$ RNAs) or with BamHI (for S1m aptamer only control RNA) and in vitro transcribed using the T7 HiScribe kit (NEB). Transcibed RNA was folded (65^{o}C for 5 min, cooled at room temperature for 5 min) and bound to MyOne Streptavidin C1 beads (Thermofisher) for 20 min at 4^{o}C. Beads were washed 4x with CHAPS lysis buffer (10mM HEPES, 200mM NaCl, 1% CHAPS, 10mM MgCl, 1mM DTT, 1x HALT protease and phosphatase inhibitor (Thermofisher), 200 U/mL murine RNase inhibitor (NEB) and pre-cleared Raw264.7 lysates in CHAPS buffer incubated with beads at 4^{o}C on a rotator for 2 hours. Beads were washed 6x in CHAPS lysis buffer and bound proteins eluted in 4x laemmeli buffer (Bio-rad). 1/5th of affinity purified eluate was analyzed by SDS-PAGE and western blot as described above.

Chapter V: References

1. Howley PM, Knipe DM. Fields virology. Seventh edition. ed. Philadelphia: Wolters Kluwer; 2021. volumes p.
2. Meyer KF, Haring CM, Howitt B. The Etiology of Epizootic Encephalomyelitis of Horses in the San Joaquin Valley, 1930. Science. 1931;74(1913):227-8. Epub 1931/08/28. doi: 10.1126/science.74.1913.227. PubMed PMID: 17834966.
3. Howitt B. Recovery of the Virus of Equine Encephalomyelitis from the Brain of a Child. Science. 1938;88(2289):455-6. Epub 1938/11/11. doi: 10.1126/science.88.2289.455. PubMed PMID: 17736946.
4. Gael Ten Broeck MHM. A Serological Difference Between Eastern and Western Equine Encephalomyelitis Virus. Experimental biology and medicine. 1933;31:217-20.
5. Giltner LT, Shahan MS. The Immunological Relationship of Eastern and Western Strains of Equine Encephalomyelitis Virus. Science. 1933;78(2034):587-8. Epub 1933/12/22. doi: 10.1126/science.78.2034.587-a. PubMed PMID: 17801697.
6. Hanson RP. An epizootic of equine encephalomyelitis that occurred in Massachusetts in 1831. Am J Trop Med Hyg. 1957;6(5):858-62. Epub 1957/09/01. doi: 10.4269/ajtmh.1957.6.858. PubMed PMID: 13470206.
7. Beck CE, Wyckoff RW. Venezuelan Equine Encephalomyelitis. Science. 1938;88(2292):530. Epub 1938/12/02. doi: 10.1126/science.88.2292.530. PubMed PMID: 17840536.
8. Kubes V, Rios FA. The Causative Agent of Infectious Equine Encephalomyelitis in Venezuela. Science. 1939;90(2323):20-1. Epub 1939/07/07. doi: 10.1126/science.90.2323.20. PubMed PMID: 17818578.
9. Sanmartin-Barberi C, Groot H, Osorno-Mesa E. Human epidemic in Colombia caused by the Venezuelan equine encephalomyelitis virus. Am J Trop Med Hyg. 1954;3(2):283-93. Epub 1954/03/01. doi: 10.4269/ajtmh.1954.3.283. PubMed PMID: 13138831.
10. Rossi AL. Rural epidemic encephalitis in Venezuela caused by a group A arbovirus (VEE). Prog Med Virol. 1967;9:176-203. Epub 1967/01/01. PubMed PMID: 4383416.
11. Weaver SC, Barrett AD. Transmission cycles, host range, evolution and emergence of arboviral disease. Nat Rev Microbiol. 2004;2(10):789-801. Epub 2004/09/21. doi: 10.1038/nrmicro1006. PubMed PMID: 15378043; PubMed Central PMCID: PMCPMC7097645.
12. Rico-Hesse R, Weaver SC, de Siger J, Medina G, Salas RA. Emergence of a new epidemic/epizootic Venezuelan equine encephalitis virus in South America. Proc Natl Acad Sci U

S A. 1995;92(12):5278-81. Epub 1995/06/06. doi: 10.1073/pnas.92.12.5278. PubMed PMID: 7777497; PubMed Central PMCID: PMCPMC41677.

13. Oberste MS, Fraire M, Navarro R, Zepeda C, Zarate ML, Ludwig GV, et al. Association of Venezuelan equine encephalitis virus subtype IE with two equine epizootics in Mexico. Am J Trop Med Hyg. 1998;59(1):100-7. Epub 1998/07/31. doi: 10.4269/ajtmh.1998.59.100. PubMed PMID: 9684636.

14. Weaver SC, Salas R, Rico-Hesse R, Ludwig GV, Oberste MS, Boshell J, et al. Re-emergence of epidemic Venezuelan equine encephalomyelitis in South America. VEE Study Group. Lancet. 1996;348(9025):436-40. Epub 1996/08/17. doi: 10.1016/s0140-6736(96)02275-1. PubMed PMID: 8709783.

15. Walton TE. Equine arboviral encephalomyelitides: A review. Journal of Equine Veterinary Science. 1988;8(1):49-54.

16. Dietz WH, Jr., Alvarez O, Jr., Martin DH, Walton TE, Ackerman LJ, Johnson KM. Enzootic and epizootic Venezuelan equine encephalomyelitis virus in horses infected by peripheral and intrathecal routes. J Infect Dis. 1978;137(3):227-37. Epub 1978/03/01. doi: 10.1093/infdis/137.3.227. PubMed PMID: 580289.

17. Groot H. Venezuelan Encephalitis. Pan American Health Organization; Washington, DC, USA. The health and economic impact of Venezuelan equine encephalitis. 1972:7-16.

18. Johnson KM, Martin DH. Venezuelan equine encephalitis. Adv Vet Sci Comp Med. 1974;18(0):79-116. Epub 1974/01/01. PubMed PMID: 4609399.

19. Charlier C, Beaudoin MC, Couderc T, Lortholary O, Lecuit M. Arboviruses and pregnancy: maternal, fetal, and neonatal effects. Lancet Child Adolesc Health. 2017;1(2):134-46. Epub 2018/09/01. doi: 10.1016/S2352-4642(17)30021-4. PubMed PMID: 30169203.

20. Forshey BM, Guevara C, Laguna-Torres VA, Cespedes M, Vargas J, Gianella A, et al. Arboviral etiologies of acute febrile illnesses in Western South America, 2000-2007. PLoS Negl Trop Dis. 2010;4(8):e787. Epub 2010/08/14. doi: 10.1371/journal.pntd.0000787. PubMed PMID: 20706628; PubMed Central PMCID: PMCPMC2919378.

21. Aguilar PV, Estrada-Franco JG, Navarro-Lopez R, Ferro C, Haddow AD, Weaver SC. Endemic Venezuelan equine encephalitis in the Americas: hidden under the dengue umbrella. Future Virol. 2011;6(6):721-40. Epub 2011/07/19. doi: 10.2217/FVL.11.5. PubMed PMID: 21765860; PubMed Central PMCID: PMCPMC3134406.

22. MacDonald GH, Johnston RE. Role of dendritic cell targeting in Venezuelan equine encephalitis virus pathogenesis. J Virol. 2000;74(2):914-22. Epub 2000/01/07. doi:

10.1128/jvi.74.2.914-922.2000. PubMed PMID: 10623754; PubMed Central PMCID: PMCPMC111612.

23. Charles PC, Trgovcich J, Davis NL, Johnston RE. Immunopathogenesis and immune modulation of Venezuelan equine encephalitis virus-induced disease in the mouse. Virology. 2001;284(2):190-202. Epub 2001/06/01. doi: 10.1006/viro.2001.0878. PubMed PMID: 11384219.

24. Grieder FB, Davis NL, Aronson JF, Charles PC, Sellon DC, Suzuki K, et al. Specific restrictions in the progression of Venezuelan equine encephalitis virus-induced disease resulting from single amino acid changes in the glycoproteins. Virology. 1995;206(2):994-1006. Epub 1995/02/01. doi: 10.1006/viro.1995.1022. PubMed PMID: 7856110.

25. Charles PC, Walters E, Margolis F, Johnston RE. Mechanism of neuroinvasion of Venezuelan equine encephalitis virus in the mouse. Virology. 1995;208(2):662-71. Epub 1995/04/20. doi: 10.1006/viro.1995.1197. PubMed PMID: 7747437.

26. Ryzhikov AB, Ryabchikova EI, Sergeev AN, Tkacheva NV. Spread of Venezuelan equine encephalitis virus in mice olfactory tract. Arch Virol. 1995;140(12):2243-54. Epub 1995/01/01. doi: 10.1007/BF01323243. PubMed PMID: 8572944.

27. Powers AM, Brault AC, Shirako Y, Strauss EG, Kang W, Strauss JH, et al. Evolutionary relationships and systematics of the alphaviruses. J Virol. 2001;75(21):10118-31. Epub 2001/10/03. doi: 10.1128/JVI.75.21.10118-10131.2001. PubMed PMID: 11581380; PubMed Central PMCID: PMCPMC114586.

28. Forrester NL, Wertheim JO, Dugan VG, Auguste AJ, Lin D, Adams AP, et al. Evolution and spread of Venezuelan equine encephalitis complex alphavirus in the Americas. PLoS Negl Trop Dis. 2017;11(8):e0005693. Epub 2017/08/05. doi: 10.1371/journal.pntd.0005693. PubMed PMID: 28771475; PubMed Central PMCID: PMCPMC5557581 following competing interests: David Lin, Kumar Hari and Ravi Jain work for cBio.

29. Weaver SC, Bellew LA, Rico-Hesse R. Phylogenetic analysis of alphaviruses in the Venezuelan equine encephalitis complex and identification of the source of epizootic viruses. Virology. 1992;191(1):282-90. Epub 1992/11/01. PubMed PMID: 1413507.

30. Brault AC, Powers AM, Ortiz D, Estrada-Franco JG, Navarro-Lopez R, Weaver SC. Venezuelan equine encephalitis emergence: enhanced vector infection from a single amino acid substitution in the envelope glycoprotein. Proc Natl Acad Sci U S A. 2004;101(31):11344-9. Epub 2004/07/28. doi: 10.1073/pnas.0402905101. PubMed PMID: 15277679; PubMed Central PMCID: PMCPMC509205.

31. Deardorff ER, Forrester NL, Travassos-da-Rosa AP, Estrada-Franco JG, Navarro-Lopez R, Tesh RB, et al. Experimental infection of potential reservoir hosts with Venezuelan equine

encephalitis virus, Mexico. Emerg Infect Dis. 2009;15(4):519-25. Epub 2009/04/01. doi: 10.3201/eid1504.081008. PubMed PMID: 19331726; PubMed Central PMCID: PMCPMC2671456.

32. Estrada-Franco JG, Navarro-Lopez R, Freier JE, Cordova D, Clements T, Moncayo A, et al. Venezuelan equine encephalitis virus, southern Mexico. Emerg Infect Dis. 2004;10(12):2113-21. Epub 2005/01/25. doi: 10.3201/eid1012.040393. PubMed PMID: 15663847; PubMed Central PMCID: PMCPMC3323369.

33. Grayson MA, Galindo P. Ecology of Venezuelan equine encephalitis virus in Panama. J Am Vet Med Assoc. 1969;155(12):2141-5. Epub 1969/12/15. PubMed PMID: 4904962.

34. Barrera R, Ferro C, Navarro JC, Freier J, Liria J, Salas R, et al. Contrasting sylvatic foci of Venezuelan equine encephalitis virus in northern South America. Am J Trop Med Hyg. 2002;67(3):324-34. Epub 2002/11/01. doi: 10.4269/ajtmh.2002.67.324. PubMed PMID: 12408676.

35. Ferro C, Boshell J, Moncayo AC, Gonzalez M, Ahumada ML, Kang W, et al. Natural enzootic vectors of Venezuelan equine encephalitis virus, Magdalena Valley, Colombia. Emerg Infect Dis. 2003;9(1):49-54. Epub 2003/01/21. doi: 10.3201/eid0901.020136. PubMed PMID: 12533281; PubMed Central PMCID: PMCPMC2873762.

36. Weaver SC, Ferro C, Barrera R, Boshell J, Navarro JC. Venezuelan equine encephalitis. Annu Rev Entomol. 2004;49:141-74. Epub 2003/12/04. doi: 10.1146/annurev.ento.49.061802.123422. PubMed PMID: 14651460.

37. Brault AC, Powers AM, Holmes EC, Woelk CH, Weaver SC. Positively charged amino acid substitutions in the e2 envelope glycoprotein are associated with the emergence of venezuelan equine encephalitis virus. J Virol. 2002;76(4):1718-30. Epub 2002/01/19. PubMed PMID: 11799167; PubMed Central PMCID: PMCPMC135911.

38. Powers AM, Oberste MS, Brault AC, Rico-Hesse R, Schmura SM, Smith JF, et al. Repeated emergence of epidemic/epizootic Venezuelan equine encephalitis from a single genotype of enzootic subtype ID virus. J Virol. 1997;71(9):6697-705. Epub 1997/09/01. PubMed PMID: 9261393; PubMed Central PMCID: PMCPMC191949.

39. Wang E, Bowen RA, Medina G, Powers AM, Kang W, Chandler LM, et al. Virulence and viremia characteristics of 1992 epizootic subtype IC Venezuelan equine encephalitis viruses and closely related enzootic subtype ID strains. Am J Trop Med Hyg. 2001;65(1):64-9. Epub 2001/08/16. doi: 10.4269/ajtmh.2001.65.64. PubMed PMID: 11504410.

40. Walton TE, Alvarez O, Jr., Buckwalter RM, Johnson KM. Experimental infection of horses with enzootic and epizootic strains of Venezuelan equine encephalomyelitis virus. J Infect Dis. 1973;128(3):271-82. Epub 1973/09/01. doi: 10.1093/infdis/128.3.271. PubMed PMID: 4728689.
41. Henderson BE, Chappell WA, Johnston JG, Jr., Sudia WD. Experimental infection of horses with three strains of Venezuelan equine encephalomyelitis virus. I. Clinical and virological studies. Am J Epidemiol. 1971;93(3):194-205. Epub 1971/03/01. doi: 10.1093/oxfordjournals.aje.a121246. PubMed PMID: 4397564.
42. Martin DH, Dietz WH, Alvaerez O, Jr., Johnson KM. Epidemiological significance of Venezuelan equine encephalomyelitis virus in vitro markers. Am J Trop Med Hyg. 1982;31(3 Pt 1):561-8. Epub 1982/05/01. doi: 10.4269/ajtmh.1982.31.561. PubMed PMID: 7200732.
43. Kissling RE, Chamberlain RW, Nelson DB, Stamm DD. Venezuelan equine encephalomyelitis in horses. Am J Hyg. 1956;63(3):274-87. Epub 1956/05/01. doi: 10.1093/oxfordjournals.aje.a119811. PubMed PMID: 13313529.
44. Mackenzie RM, de Siger J, Parra D. Venezuelan equine encephalitis virus: comparison of infectivity and virulence of strains V-38 and P676 in donkeys. Am J Trop Med Hyg. 1976;25(3):494-9. Epub 1976/05/01. doi: 10.4269/ajtmh.1976.25.494. PubMed PMID: 937636.
45. Ronca SE, Dineley KT, Paessler S. Neurological Sequelae Resulting from Encephalitic Alphavirus Infection. Front Microbiol. 2016;7:959. Epub 2016/07/06. doi: 10.3389/fmicb.2016.00959. PubMed PMID: 27379085; PubMed Central PMCID: PMCPMC4913092.
46. Kinney RM, Tsuchiya KR, Sneider JM, Trent DW. Genetic evidence that epizootic Venezuelan equine encephalitis (VEE) viruses may have evolved from enzootic VEE subtype I-D virus. Virology. 1992;191(2):569-80. Epub 1992/12/01. PubMed PMID: 1448915.
47. Anishchenko M, Bowen RA, Paessler S, Austgen L, Greene IP, Weaver SC. Venezuelan encephalitis emergence mediated by a phylogenetically predicted viral mutation. Proc Natl Acad Sci U S A. 2006;103(13):4994-9. Epub 2006/03/22. doi: 10.1073/pnas.0509961103. PubMed PMID: 16549790; PubMed Central PMCID: PMCPMC1458783.
48. Greene IP, Paessler S, Austgen L, Anishchenko M, Brault AC, Bowen RA, et al. Envelope glycoprotein mutations mediate equine amplification and virulence of epizootic venezuelan equine encephalitis virus. J Virol. 2005;79(14):9128-33. Epub 2005/07/05. doi: 10.1128/JVI.79.14.9128-9133.2005. PubMed PMID: 15994807; PubMed Central PMCID: PMCPMC1168750.
49. Bernard KA, Klimstra WB, Johnston RE. Mutations in the E2 glycoprotein of Venezuelan equine encephalitis virus confer heparan sulfate interaction, low morbidity, and rapid clearance

from blood of mice. Virology. 2000;276(1):93-103. Epub 2000/10/07. doi: 10.1006/viro.2000.0546. PubMed PMID: 11021998.

50. Kinney RM, Chang GJ, Tsuchiya KR, Sneider JM, Roehrig JT, Woodward TM, et al. Attenuation of Venezuelan equine encephalitis virus strain TC-83 is encoded by the 5'-noncoding region and the E2 envelope glycoprotein. J Virol. 1993;67(3):1269-77. Epub 1993/03/01. doi: 10.1128/JVI.67.3.1269-1277.1993. PubMed PMID: 7679745; PubMed Central PMCID: PMCPMC237493.

51. Kinney RM, Johnson BJ, Welch JB, Tsuchiya KR, Trent DW. The full-length nucleotide sequences of the virulent Trinidad donkey strain of Venezuelan equine encephalitis virus and its attenuated vaccine derivative, strain TC-83. Virology. 1989;170(1):19-30. Epub 1989/05/01. doi: 10.1016/0042-6822(89)90347-4. PubMed PMID: 2524126.

52. Brault AC, Powers AM, Weaver SC. Vector infection determinants of Venezuelan equine encephalitis virus reside within the E2 envelope glycoprotein. J Virol. 2002;76(12):6387-92. Epub 2002/05/22. doi: 10.1128/jvi.76.12.6387-6392.2002. PubMed PMID: 12021373; PubMed Central PMCID: PMCPMC136209.

53. Greene IP, Paessler S, Anishchenko M, Smith DR, Brault AC, Frolov I, et al. Venezuelan equine encephalitis virus in the guinea pig model: evidence for epizootic virulence determinants outside the E2 envelope glycoprotein gene. Am J Trop Med Hyg. 2005;72(3):330-8. Epub 2005/03/18. PubMed PMID: 15772331.

54. Spotts DR, Reich RM, Kalkhan MA, Kinney RM, Roehrig JT. Resistance to alpha/beta interferons correlates with the epizootic and virulence potential of Venezuelan equine encephalitis viruses and is determined by the 5' noncoding region and glycoproteins. J Virol. 1998;72(12):10286-91. Epub 1998/11/13. PubMed PMID: 9811777; PubMed Central PMCID: PMCPMC110615.

55. Jahrling PB, Navarro E, Scherer WF. Interferon induction and sensitivity as correlates to virulence of Venezuelan encephalitis viruses for hamsters. Arch Virol. 1976;51(1-2):23-35. Epub 1976/01/01. PubMed PMID: 962587.

56. Anishchenko M, Paessler S, Greene IP, Aguilar PV, Carrara AS, Weaver SC. Generation and characterization of closely related epizootic and enzootic infectious cDNA clones for studying interferon sensitivity and emergence mechanisms of Venezuelan equine encephalitis virus. J Virol. 2004;78(1):1-8. Epub 2003/12/13. doi: 10.1128/jvi.78.1.1-8.2004. PubMed PMID: 14671082; PubMed Central PMCID: PMCPMC303380.

57. Ortiz DI, Weaver SC. Susceptibility of Ochlerotatus taeniorhynchus (Diptera: Culicidae) to infection with epizootic (subtype IC) and enzootic (subtype ID) Venezuelan equine encephalitis

viruses: evidence for epizootic strain adaptation. J Med Entomol. 2004;41(5):987-93. Epub 2004/11/13. doi: 10.1603/0022-2585-41.5.987. PubMed PMID: 15535633.

58. Moncayo AC, Lanzaro G, Kang W, Orozco A, Ulloa A, Arredondo-Jimenez J, et al. Vector competence of eastern and western forms of Psorophora columbiae (Diptera: Culicidae) mosquitoes for enzootic and epizootic Venezuelan equine encephalitis virus. Am J Trop Med Hyg. 2008;78(3):413-21. Epub 2008/03/14. PubMed PMID: 18337337.

59. Kramer LD, Scherer WF. Vector competence of mosquitoes as a marker to distinguish Central American and Mexican epizootic from enzootic strains of Venezuelan encephalitis virus. Am J Trop Med Hyg. 1976;25(2):336-46. Epub 1976/03/01. doi: 10.4269/ajtmh.1976.25.336. PubMed PMID: 1259093.

60. Deardorff ER, Weaver SC. Vector competence of Culex (Melanoconion) taeniopus for equine-virulent subtype IE strains of Venezuelan equine encephalitis virus. Am J Trop Med Hyg. 2010;82(6):1047-52. Epub 2010/06/04. doi: 10.4269/ajtmh.2010.09-0556. PubMed PMID: 20519599; PubMed Central PMCID: PMCPMC2877410.

61. Oberste MS, Schmura SM, Weaver SC, Smith JF. Geographic distribution of Venezuelan equine encephalitis virus subtype IE genotypes in Central America and Mexico. Am J Trop Med Hyg. 1999;60(4):630-4. Epub 1999/05/29. doi: 10.4269/ajtmh.1999.60.630. PubMed PMID: 10348239.

62. Weaver SC, Pfeffer M, Marriott K, Kang W, Kinney RM. Genetic evidence for the origins of Venezuelan equine encephalitis virus subtype IAB outbreaks. Am J Trop Med Hyg. 1999;60(3):441-8. Epub 1999/08/31. doi: 10.4269/ajtmh.1999.60.441. PubMed PMID: 10466974.

63. Fuller SD. The T=4 envelope of Sindbis virus is organized by interactions with a complementary T=3 capsid. Cell. 1987;48(6):923-34. Epub 1987/03/27. doi: 10.1016/0092-8674(87)90701-x. PubMed PMID: 3829124.

64. Paredes A, Alwell-Warda K, Weaver SC, Chiu W, Watowich SJ. Venezuelan equine encephalomyelitis virus structure and its divergence from old world alphaviruses. J Virol. 2001;75(19):9532-7. Epub 2001/09/05. doi: 10.1128/JVI.75.19.9532-9537.2001. PubMed PMID: 11533216; PubMed Central PMCID: PMCPMC114521.

65. Hefti E, Bishop DH, Dubin DT, Stollar V. 5' nucleotide sequence of sindbis viral RNA. J Virol. 1975;17(1):149-59. Epub 1975/01/01. doi: 10.1128/JVI.17.1.149-159.1976. PubMed PMID: 173879; PubMed Central PMCID: PMCPMC515398.

66. Rozanov MN, Koonin EV, Gorbalenya AE. Conservation of the putative methyltransferase domain: a hallmark of the 'Sindbis-like' supergroup of positive-strand RNA viruses. J Gen Virol.

1992;73 (Pt 8):2129-34. Epub 1992/08/01. doi: 10.1099/0022-1317-73-8-2129. PubMed PMID: 1645151.

67. Rupp JC, Jundt N, Hardy RW. Requirement for the amino-terminal domain of sindbis virus nsP4 during virus infection. J Virol. 2011;85(7):3449-60. Epub 2011/01/21. doi: 10.1128/JVI.02058-10. PubMed PMID: 21248049; PubMed Central PMCID: PMCPMC3067876.

68. Fata CL, Sawicki SG, Sawicki DL. Modification of Asn374 of nsP1 suppresses a Sindbis virus nsP4 minus-strand polymerase mutant. J Virol. 2002;76(17):8641-9. Epub 2002/08/07. doi: 10.1128/jvi.76.17.8641-8649.2002. PubMed PMID: 12163583; PubMed Central PMCID: PMCPMC136982.

69. Hahn YS, Strauss EG, Strauss JH. Mapping of RNA- temperature-sensitive mutants of Sindbis virus: assignment of complementation groups A, B, and G to nonstructural proteins. J Virol. 1989;63(7):3142-50. Epub 1989/07/01. doi: 10.1128/JVI.63.7.3142-3150.1989. PubMed PMID: 2724421; PubMed Central PMCID: PMCPMC250872.

70. Shirako Y, Strauss EG, Strauss JH. Modification of the 5' terminus of Sindbis virus genomic RNA allows nsP4 RNA polymerases with nonaromatic amino acids at the N terminus to function in RNA replication. J Virol. 2003;77(4):2301-9. Epub 2003/01/29. doi: 10.1128/jvi.77.4.2301-2309.2003. PubMed PMID: 12551967; PubMed Central PMCID: PMCPMC141077.

71. Kim DY, Firth AE, Atasheva S, Frolova EI, Frolov I. Conservation of a packaging signal and the viral genome RNA packaging mechanism in alphavirus evolution. J Virol. 2011;85(16):8022-36. Epub 2011/06/18. doi: 10.1128/JVI.00644-11. PubMed PMID: 21680508; PubMed Central PMCID: PMCPMC3147971.

72. Gomez de Cedron M, Ehsani N, Mikkola ML, Garcia JA, Kaariainen L. RNA helicase activity of Semliki Forest virus replicase protein NSP2. FEBS Lett. 1999;448(1):19-22. Epub 1999/04/27. doi: 10.1016/s0014-5793(99)00321-x. PubMed PMID: 10217401.

73. Rikkonen M, Peranen J, Kaariainen L. ATPase and GTPase activities associated with Semliki Forest virus nonstructural protein nsP2. J Virol. 1994;68(9):5804-10. Epub 1994/09/01. doi: 10.1128/JVI.68.9.5804-5810.1994. PubMed PMID: 8057461; PubMed Central PMCID: PMCPMC236984.

74. Vasiljeva L, Merits A, Auvinen P, Kaariainen L. Identification of a novel function of the alphavirus capping apparatus. RNA 5'-triphosphatase activity of Nsp2. J Biol Chem. 2000;275(23):17281-7. Epub 2000/04/05. doi: 10.1074/jbc.M910340199. PubMed PMID: 10748213.

75. Hardy WR, Strauss JH. Processing the nonstructural polyproteins of sindbis virus: nonstructural proteinase is in the C-terminal half of nsP2 and functions both in cis and in trans. J Virol. 1989;63(11):4653-64. Epub 1989/11/01. doi: 10.1128/JVI.63.11.4653-4664.1989. PubMed PMID: 2529379; PubMed Central PMCID: PMCPMC251099.

76. Lulla A, Lulla V, Tints K, Ahola T, Merits A. Molecular determinants of substrate specificity for Semliki Forest virus nonstructural protease. J Virol. 2006;80(11):5413-22. Epub 2006/05/16. doi: 10.1128/JVI.00229-06. PubMed PMID: 16699022; PubMed Central PMCID: PMCPMC1472149.

77. Russo AT, White MA, Watowich SJ. The crystal structure of the Venezuelan equine encephalitis alphavirus nsP2 protease. Structure. 2006;14(9):1449-58. Epub 2006/09/12. doi: 10.1016/j.str.2006.07.010. PubMed PMID: 16962975.

78. Hu X, Compton JR, Leary DH, Olson MA, Lee MS, Cheung J, et al. Kinetic, Mutational, and Structural Studies of the Venezuelan Equine Encephalitis Virus Nonstructural Protein 2 Cysteine Protease. Biochemistry. 2016;55(21):3007-19. Epub 2016/04/01. doi: 10.1021/acs.biochem.5b00992. PubMed PMID: 27030368; PubMed Central PMCID: PMCPMC5290728.

79. Atasheva S, Gorchakov R, English R, Frolov I, Frolova E. Development of Sindbis viruses encoding nsP2/GFP chimeric proteins and their application for studying nsP2 functioning. J Virol. 2007;81(10):5046-57. Epub 2007/03/03. doi: 10.1128/JVI.02746-06. PubMed PMID: 17329335; PubMed Central PMCID: PMCPMC1900196.

80. Frolov I, Agapov E, Hoffman TA, Jr., Pragai BM, Lippa M, Schlesinger S, et al. Selection of RNA replicons capable of persistent noncytopathic replication in mammalian cells. J Virol. 1999;73(5):3854-65. Epub 1999/04/10. doi: 10.1128/JVI.73.5.3854-3865.1999. PubMed PMID: 10196280; PubMed Central PMCID: PMCPMC104163.

81. Gorchakov R, Frolova E, Frolov I. Inhibition of transcription and translation in Sindbis virus-infected cells. J Virol. 2005;79(15):9397-409. Epub 2005/07/15. doi: 10.1128/JVI.79.15.9397-9409.2005. PubMed PMID: 16014903; PubMed Central PMCID: PMCPMC1181568.

82. Breakwell L, Dosenovic P, Karlsson Hedestam GB, D'Amato M, Liljestrom P, Fazakerley J, et al. Semliki Forest virus nonstructural protein 2 is involved in suppression of the type I interferon response. J Virol. 2007;81(16):8677-84. Epub 2007/06/08. doi: 10.1128/JVI.02411-06. PubMed PMID: 17553895; PubMed Central PMCID: PMCPMC1951358.

83. Frolov I, Garmashova N, Atasheva S, Frolova EI. Random insertion mutagenesis of sindbis virus nonstructural protein 2 and selection of variants incapable of downregulating cellular

transcription. J Virol. 2009;83(18):9031-44. Epub 2009/07/03. doi: 10.1128/JVI.00850-09. PubMed PMID: 19570872; PubMed Central PMCID: PMCPMC2738241.

84. Bhalla N, Sun C, Metthew Lam LK, Gardner CL, Ryman KD, Klimstra WB. Host translation shutoff mediated by non-structural protein 2 is a critical factor in the antiviral state resistance of Venezuelan equine encephalitis virus. Virology. 2016;496:147-65. Epub 2016/06/19. doi: 10.1016/j.virol.2016.06.005. PubMed PMID: 27318152; PubMed Central PMCID: PMCPMC5821108.

85. Garmashova N, Gorchakov R, Volkova E, Paessler S, Frolova E, Frolov I. The Old World and New World alphaviruses use different virus-specific proteins for induction of transcriptional shutoff. J Virol. 2007;81(5):2472-84. Epub 2006/11/17. doi: 10.1128/JVI.02073-06. PubMed PMID: 17108023; PubMed Central PMCID: PMCPMC1865960.

86. LaStarza MW, Lemm JA, Rice CM. Genetic analysis of the nsP3 region of Sindbis virus: evidence for roles in minus-strand and subgenomic RNA synthesis. J Virol. 1994;68(9):5781-91. Epub 1994/09/01. doi: 10.1128/JVI.68.9.5781-5791.1994. PubMed PMID: 8057460; PubMed Central PMCID: PMCPMC236982.

87. Wang YF, Sawicki SG, Sawicki DL. Alphavirus nsP3 functions to form replication complexes transcribing negative-strand RNA. J Virol. 1994;68(10):6466-75. Epub 1994/10/01. doi: 10.1128/JVI.68.10.6466-6475.1994. PubMed PMID: 8083984; PubMed Central PMCID: PMCPMC237067.

88. Park E, Griffin DE. The nsP3 macro domain is important for Sindbis virus replication in neurons and neurovirulence in mice. Virology. 2009;388(2):305-14. Epub 2009/04/28. doi: 10.1016/j.virol.2009.03.031. PubMed PMID: 19395054; PubMed Central PMCID: PMCPMC2683903.

89. Malet H, Coutard B, Jamal S, Dutartre H, Papageorgiou N, Neuvonen M, et al. The crystal structures of Chikungunya and Venezuelan equine encephalitis virus nsP3 macro domains define a conserved adenosine binding pocket. J Virol. 2009;83(13):6534-45. Epub 2009/04/24. doi: 10.1128/JVI.00189-09. PubMed PMID: 19386706; PubMed Central PMCID: PMCPMC2698539.

90. Cristea IM, Carroll JW, Rout MP, Rice CM, Chait BT, MacDonald MR. Tracking and elucidating alphavirus-host protein interactions. J Biol Chem. 2006;281(40):30269-78. Epub 2006/08/10. doi: 10.1074/jbc.M603980200. PubMed PMID: 16895903.

91. Frolova E, Gorchakov R, Garmashova N, Atasheva S, Vergara LA, Frolov I. Formation of nsP3-specific protein complexes during Sindbis virus replication. J Virol. 2006;80(8):4122-34. Epub 2006/03/31. doi: 10.1128/JVI.80.8.4122-4134.2006. PubMed PMID: 16571828; PubMed Central PMCID: PMCPMC1440443.

92. Gorchakov R, Garmashova N, Frolova E, Frolov I. Different types of nsP3-containing protein complexes in Sindbis virus-infected cells. J Virol. 2008;82(20):10088-101. Epub 2008/08/08. doi: 10.1128/JVI.01011-08. PubMed PMID: 18684830; PubMed Central PMCID: PMCPMC2566286.

93. Shin G, Yost SA, Miller MT, Elrod EJ, Grakoui A, Marcotrigiano J. Structural and functional insights into alphavirus polyprotein processing and pathogenesis. Proc Natl Acad Sci U S A. 2012;109(41):16534-9. Epub 2012/09/27. doi: 10.1073/pnas.1210418109. PubMed PMID: 23010928; PubMed Central PMCID: PMCPMC3478664.

94. Lastarza MW, Grakoui A, Rice CM. Deletion and duplication mutations in the C-terminal nonconserved region of Sindbis virus nsP3: effects on phosphorylation and on virus replication in vertebrate and invertebrate cells. Virology. 1994;202(1):224-32. Epub 1994/07/01. doi: 10.1006/viro.1994.1338. PubMed PMID: 7912020.

95. De I, Fata-Hartley C, Sawicki SG, Sawicki DL. Functional analysis of nsP3 phosphoprotein mutants of Sindbis virus. J Virol. 2003;77(24):13106-16. Epub 2003/12/03. doi: 10.1128/jvi.77.24.13106-13116.2003. PubMed PMID: 14645567; PubMed Central PMCID: PMCPMC296081.

96. Tuittila M, Hinkkanen AE. Amino acid mutations in the replicase protein nsP3 of Semliki Forest virus cumulatively affect neurovirulence. J Gen Virol. 2003;84(Pt 6):1525-33. Epub 2003/05/29. doi: 10.1099/vir.0.18936-0. PubMed PMID: 12771422.

97. Davis NL, Willis LV, Smith JF, Johnston RE. In vitro synthesis of infectious venezuelan equine encephalitis virus RNA from a cDNA clone: analysis of a viable deletion mutant. Virology. 1989;171(1):189-204. Epub 1989/07/01. doi: 10.1016/0042-6822(89)90526-6. PubMed PMID: 2525837.

98. Galbraith SE, Sheahan BJ, Atkins GJ. Deletions in the hypervariable domain of the nsP3 gene attenuate Semliki Forest virus virulence. J Gen Virol. 2006;87(Pt 4):937-47. Epub 2006/03/11. doi: 10.1099/vir.0.81406-0. PubMed PMID: 16528043.

99. Li GP, La Starza MW, Hardy WR, Strauss JH, Rice CM. Phosphorylation of Sindbis virus nsP3 in vivo and in vitro. Virology. 1990;179(1):416-27. Epub 1990/11/01. doi: 10.1016/0042-6822(90)90310-n. PubMed PMID: 2145690.

100. Peranen J, Takkinen K, Kalkkinen N, Kaariainen L. Semliki Forest virus-specific non-structural protein nsP3 is a phosphoprotein. J Gen Virol. 1988;69 (Pt 9):2165-78. Epub 1988/09/01. doi: 10.1099/0022-1317-69-9-2165. PubMed PMID: 2970523.

101. Vihinen H, Ahola T, Tuittila M, Merits A, Kaariainen L. Elimination of phosphorylation sites of Semliki Forest virus replicase protein nsP3. J Biol Chem. 2001;276(8):5745-52. Epub 2000/12/06. doi: 10.1074/jbc.M006077200. PubMed PMID: 11104756.

102. Foy NJ, Akhrymuk M, Shustov AV, Frolova EI, Frolov I. Hypervariable domain of nonstructural protein nsP3 of Venezuelan equine encephalitis virus determines cell-specific mode of virus replication. J Virol. 2013;87(13):7569-84. Epub 2013/05/03. doi: 10.1128/JVI.00720-13. PubMed PMID: 23637407; PubMed Central PMCID: PMCPMC3700263.

103. Forrester NL, Guerbois M, Seymour RL, Spratt H, Weaver SC. Vector-borne transmission imposes a severe bottleneck on an RNA virus population. PLoS Pathog. 2012;8(9):e1002897. Epub 2012/10/03. doi: 10.1371/journal.ppat.1002897. PubMed PMID: 23028310; PubMed Central PMCID: PMCPMC3441635.

104. Khan AH, Morita K, Parquet MDC, Hasebe F, Mathenge EGM, Igarashi A. Complete nucleotide sequence of chikungunya virus and evidence for an internal polyadenylation site. J Gen Virol. 2002;83(Pt 12):3075-84. Epub 2002/12/06. doi: 10.1099/0022-1317-83-12-3075. PubMed PMID: 12466484.

105. O'Reilly EK, Kao CC. Analysis of RNA-dependent RNA polymerase structure and function as guided by known polymerase structures and computer predictions of secondary structure. Virology. 1998;252(2):287-303. Epub 1999/01/08. doi: 10.1006/viro.1998.9463. PubMed PMID: 9878607.

106. Rubach JK, Wasik BR, Rupp JC, Kuhn RJ, Hardy RW, Smith JL. Characterization of purified Sindbis virus nsP4 RNA-dependent RNA polymerase activity in vitro. Virology. 2009;384(1):201-8. Epub 2008/11/28. doi: 10.1016/j.virol.2008.10.030. PubMed PMID: 19036396; PubMed Central PMCID: PMCPMC3107704.

107. Tomar S, Hardy RW, Smith JL, Kuhn RJ. Catalytic core of alphavirus nonstructural protein nsP4 possesses terminal adenylyltransferase activity. J Virol. 2006;80(20):9962-9. Epub 2006/09/29. doi: 10.1128/JVI.01067-06. PubMed PMID: 17005674; PubMed Central PMCID: PMCPMC1617302.

108. Shirako Y, Strauss EG, Strauss JH. Suppressor mutations that allow sindbis virus RNA polymerase to function with nonaromatic amino acids at the N-terminus: evidence for interaction between nsP1 and nsP4 in minus-strand RNA synthesis. Virology. 2000;276(1):148-60. Epub 2000/10/07. doi: 10.1006/viro.2000.0544. PubMed PMID: 11022003.

109. Garmashova N, Atasheva S, Kang W, Weaver SC, Frolova E, Frolov I. Analysis of Venezuelan equine encephalitis virus capsid protein function in the inhibition of cellular

transcription. J Virol. 2007;81(24):13552-65. Epub 2007/10/05. doi: 10.1128/JVI.01576-07. PubMed PMID: 17913819; PubMed Central PMCID: PMCPMC2168819.

110. Atasheva S, Fish A, Fornerod M, Frolova EI. Venezuelan equine Encephalitis virus capsid protein forms a tetrameric complex with CRM1 and importin alpha/beta that obstructs nuclear pore complex function. J Virol. 2010;84(9):4158-71. Epub 2010/02/12. doi: 10.1128/JVI.02554-09. PubMed PMID: 20147401; PubMed Central PMCID: PMCPMC2863722.

111. Helenius A, Kartenbeck J, Simons K, Fries E. On the entry of Semliki forest virus into BHK-21 cells. J Cell Biol. 1980;84(2):404-20. Epub 1980/02/01. doi: 10.1083/jcb.84.2.404. PubMed PMID: 6991511; PubMed Central PMCID: PMCPMC2110562.

112. DeTulleo L, Kirchhausen T. The clathrin endocytic pathway in viral infection. EMBO J. 1998;17(16):4585-93. Epub 1998/08/26. doi: 10.1093/emboj/17.16.4585. PubMed PMID: 9707418; PubMed Central PMCID: PMCPMC1170788.

113. Ghietto LM, Gil PI, Olmos Quinteros P, Gomez E, Piris FM, Kunda P, et al. Members of Venezuelan Equine Encephalitis complex entry into host cells by clathrin-mediated endocytosis in a pH-dependent manner. Sci Rep. 2022;12(1):14556. Epub 2022/08/26. doi: 10.1038/s41598-022-18846-w. PubMed PMID: 36008558; PubMed Central PMCID: PMCPMC9411563.

114. Wahlberg JM, Bron R, Wilschut J, Garoff H. Membrane fusion of Semliki Forest virus involves homotrimers of the fusion protein. J Virol. 1992;66(12):7309-18. Epub 1992/12/01. doi: 10.1128/JVI.66.12.7309-7318.1992. PubMed PMID: 1433520; PubMed Central PMCID: PMCPMC240435.

115. Kielian M, Chanel-Vos C, Liao M. Alphavirus Entry and Membrane Fusion. Viruses. 2010;2(4):796-825. Epub 2010/03/26. doi: 10.3390/v2040796. PubMed PMID: 21546978; PubMed Central PMCID: PMCPMC3086016.

116. Lobigs M, Zhao HX, Garoff H. Function of Semliki Forest virus E3 peptide in virus assembly: replacement of E3 with an artificial signal peptide abolishes spike heterodimerization and surface expression of E1. J Virol. 1990;64(9):4346-55. Epub 1990/09/01. doi: 10.1128/JVI.64.9.4346-4355.1990. PubMed PMID: 2200886; PubMed Central PMCID: PMCPMC247902.

117. Lobigs M, Garoff H. Fusion function of the Semliki Forest virus spike is activated by proteolytic cleavage of the envelope glycoprotein precursor p62. J Virol. 1990;64(3):1233-40. Epub 1990/03/01. doi: 10.1128/JVI.64.3.1233-1240.1990. PubMed PMID: 2304141; PubMed Central PMCID: PMCPMC249238.

118. Wahlberg JM, Boere WA, Garoff H. The heterodimeric association between the membrane proteins of Semliki Forest virus changes its sensitivity to low pH during virus maturation. J Virol.

1989;63(12):4991-7. Epub 1989/12/01. doi: 10.1128/JVI.63.12.4991-4997.1989. PubMed PMID: 2479769; PubMed Central PMCID: PMCPMC251158.

119. Ryman KD, Klimstra WB, Johnston RE. Attenuation of Sindbis virus variants incorporating uncleaved PE2 glycoprotein is correlated with attachment to cell-surface heparan sulfate. Virology. 2004;322(1):1-12. Epub 2004/04/06. doi: 10.1016/j.virol.2004.01.003. PubMed PMID: 15063111.

120. Zhang R, Hryc CF, Cong Y, Liu X, Jakana J, Gorchakov R, et al. 4.4 A cryo-EM structure of an enveloped alphavirus Venezuelan equine encephalitis virus. EMBO J. 2011;30(18):3854-63. Epub 2011/08/11. doi: 10.1038/emboj.2011.261. PubMed PMID: 21829169; PubMed Central PMCID: PMCPMC3173789.

121. Wu SR, Haag L, Sjoberg M, Garoff H, Hammar L. The dynamic envelope of a fusion class II virus. E3 domain of glycoprotein E2 precursor in Semliki Forest virus provides a unique contact with the fusion protein E1. J Biol Chem. 2008;283(39):26452-60. Epub 2008/07/04. doi: 10.1074/jbc.M801470200. PubMed PMID: 18596032; PubMed Central PMCID: PMCPMC3258923.

122. Firth AE, Chung BY, Fleeton MN, Atkins JF. Discovery of frameshifting in Alphavirus 6K resolves a 20-year enigma. Virol J. 2008;5:108. Epub 2008/09/30. doi: 10.1186/1743-422X-5-108. PubMed PMID: 18822126; PubMed Central PMCID: PMCPMC2569925.

123. Snyder JE, Kulcsar KA, Schultz KL, Riley CP, Neary JT, Marr S, et al. Functional characterization of the alphavirus TF protein. J Virol. 2013;87(15):8511-23. Epub 2013/05/31. doi: 10.1128/JVI.00449-13. PubMed PMID: 23720714; PubMed Central PMCID: PMCPMC3719798.

124. Liljestrom P, Lusa S, Huylebroeck D, Garoff H. In vitro mutagenesis of a full-length cDNA clone of Semliki Forest virus: the small 6,000-molecular-weight membrane protein modulates virus release. J Virol. 1991;65(8):4107-13. Epub 1991/08/01. doi: 10.1128/JVI.65.8.4107-4113.1991. PubMed PMID: 2072446; PubMed Central PMCID: PMCPMC248843.

125. Loewy A, Smyth J, von Bonsdorff CH, Liljestrom P, Schlesinger MJ. The 6-kilodalton membrane protein of Semliki Forest virus is involved in the budding process. J Virol. 1995;69(1):469-75. Epub 1995/01/01. doi: 10.1128/JVI.69.1.469-475.1995. PubMed PMID: 7983743; PubMed Central PMCID: PMCPMC188595.

126. Hyde JL, Chen R, Trobaugh DW, Diamond MS, Weaver SC, Klimstra WB, et al. The 5' and 3' ends of alphavirus RNAs--Non-coding is not non-functional. Virus Res. 2015;206:99-107. Epub 2015/01/30. doi: 10.1016/j.virusres.2015.01.016. PubMed PMID: 25630058; PubMed Central PMCID: PMCPMC4654126.

127. Ahola T, Kaariainen L. Reaction in alphavirus mRNA capping: formation of a covalent complex of nonstructural protein nsP1 with 7-methyl-GMP. Proc Natl Acad Sci U S A. 1995;92(2):507-11. Epub 1995/01/17. doi: 10.1073/pnas.92.2.507. PubMed PMID: 7831320; PubMed Central PMCID: PMCPMC42770.

128. Mi S, Durbin R, Huang HV, Rice CM, Stollar V. Association of the Sindbis virus RNA methyltransferase activity with the nonstructural protein nsP1. Virology. 1989;170(2):385-91. Epub 1989/06/01. doi: 10.1016/0042-6822(89)90429-7. PubMed PMID: 2728344.

129. Dong H, Ray D, Ren S, Zhang B, Puig-Basagoiti F, Takagi Y, et al. Distinct RNA elements confer specificity to flavivirus RNA cap methylation events. J Virol. 2007;81(9):4412-21. Epub 2007/02/16. doi: 10.1128/JVI.02455-06. PubMed PMID: 17301144; PubMed Central PMCID: PMCPMC1900168.

130. Berben-Bloemheuvel G, Kasperaitis MA, van Heugten H, Thomas AA, van Steeg H, Voorma HO. Interaction of initiation factors with the cap structure of chimaeric mRNA containing the 5'-untranslated regions of Semliki Forest virus RNA is related to translational efficiency. Eur J Biochem. 1992;208(3):581-7. Epub 1992/09/15. doi: 10.1111/j.1432-1033.1992.tb17222.x. PubMed PMID: 1396664.

131. Castello A, Sanz MA, Molina S, Carrasco L. Translation of Sindbis virus 26S mRNA does not require intact eukariotic initiation factor 4G. J Mol Biol. 2006;355(5):942-56. Epub 2005/12/14. doi: 10.1016/j.jmb.2005.11.024. PubMed PMID: 16343528.

132. Kulasegaran-Shylini R, Atasheva S, Gorenstein DG, Frolov I. Structural and functional elements of the promoter encoded by the 5' untranslated region of the Venezuelan equine encephalitis virus genome. J Virol. 2009;83(17):8327-39. Epub 2009/06/12. doi: 10.1128/JVI.00586-09. PubMed PMID: 19515761; PubMed Central PMCID: PMCPMC2738147.

133. Frolov I, Hardy R, Rice CM. Cis-acting RNA elements at the 5' end of Sindbis virus genome RNA regulate minus- and plus-strand RNA synthesis. RNA. 2001;7(11):1638-51. Epub 2001/11/27. doi: 10.1017/s135583820101010x. PubMed PMID: 11720292; PubMed Central PMCID: PMCPMC1370205.

134. Gorchakov R, Hardy R, Rice CM, Frolov I. Selection of functional 5' cis-acting elements promoting efficient sindbis virus genome replication. J Virol. 2004;78(1):61-75. Epub 2003/12/13. doi: 10.1128/jvi.78.1.61-75.2004. PubMed PMID: 14671088; PubMed Central PMCID: PMCPMC303405.

135. White LJ, Wang JG, Davis NL, Johnston RE. Role of alpha/beta interferon in Venezuelan equine encephalitis virus pathogenesis: effect of an attenuating mutation in the 5' untranslated

region. J Virol. 2001;75(8):3706-18. Epub 2001/03/27. doi: 10.1128/JVI.75.8.3706-3718.2001. PubMed PMID: 11264360; PubMed Central PMCID: PMCPMC114862.

136. Klimstra WB, Ryman KD, Bernard KA, Nguyen KB, Biron CA, Johnston RE. Infection of neonatal mice with sindbis virus results in a systemic inflammatory response syndrome. J Virol. 1999;73(12):10387-98. Epub 1999/11/13. doi: 10.1128/JVI.73.12.10387-10398.1999. PubMed PMID: 10559357; PubMed Central PMCID: PMCPMC113094.

137. Kobiler D, Rice CM, Brodie C, Shahar A, Dubuisson J, Halevy M, et al. A single nucleotide change in the 5' noncoding region of Sindbis virus confers neurovirulence in rats. J Virol. 1999;73(12):10440-6. Epub 1999/11/13. doi: 10.1128/JVI.73.12.10440-10446.1999. PubMed PMID: 10559362; PubMed Central PMCID: PMCPMC113099.

138. Logue CH, Sheahan BJ, Atkins GJ. The 5' untranslated region as a pathogenicity determinant of Semliki Forest virus in mice. Virus Genes. 2008;36(2):313-21. Epub 2008/02/12. doi: 10.1007/s11262-008-0209-1. PubMed PMID: 18264748.

139. Kuhn RJ, Griffin DE, Zhang H, Niesters HG, Strauss JH. Attenuation of Sindbis virus neurovirulence by using defined mutations in nontranslated regions of the genome RNA. J Virol. 1992;66(12):7121-7. Epub 1992/12/01. doi: 10.1128/JVI.66.12.7121-7127.1992. PubMed PMID: 1433509; PubMed Central PMCID: PMCPMC240395.

140. Hyde JL, Gardner CL, Kimura T, White JP, Liu G, Trobaugh DW, et al. A viral RNA structural element alters host recognition of nonself RNA. Science. 2014;343(6172):783-7. Epub 2014/02/01. doi: 10.1126/science.1248465. PubMed PMID: 24482115; PubMed Central PMCID: PMCPMC4209899.

141. Diamond MS, Farzan M. The broad-spectrum antiviral functions of IFIT and IFITM proteins. Nat Rev Immunol. 2013;13(1):46-57. Epub 2012/12/15. doi: 10.1038/nri3344. PubMed PMID: 23237964; PubMed Central PMCID: PMCPMC3773942.

142. Kuhn RJ, Hong Z, Strauss JH. Mutagenesis of the 3' nontranslated region of Sindbis virus RNA. J Virol. 1990;64(4):1465-76. Epub 1990/04/01. doi: 10.1128/JVI.64.4.1465-1476.1990. PubMed PMID: 2319643; PubMed Central PMCID: PMCPMC249280.

143. Strauss JH, Strauss EG. The alphaviruses: gene expression, replication, and evolution. Microbiol Rev. 1994;58(3):491-562. Epub 1994/09/01. doi: 10.1128/mr.58.3.491-562.1994. PubMed PMID: 7968923; PubMed Central PMCID: PMCPMC372977.

144. Pfeffer M, Kinney RM, Kaaden OR. The alphavirus 3'-nontranslated region: size heterogeneity and arrangement of repeated sequence elements. Virology. 1998;240(1):100-8. Epub 1998/02/04. doi: 10.1006/viro.1997.8907. PubMed PMID: 9448694.

145. Chen R, Wang E, Tsetsarkin KA, Weaver SC. Chikungunya virus 3' untranslated region: adaptation to mosquitoes and a population bottleneck as major evolutionary forces. PLoS Pathog. 2013;9(8):e1003591. Epub 2013/09/07. doi: 10.1371/journal.ppat.1003591. PubMed PMID: 24009512; PubMed Central PMCID: PMCPMC3757053.
146. Weaver SC, Brault AC, Kang W, Holland JJ. Genetic and fitness changes accompanying adaptation of an arbovirus to vertebrate and invertebrate cells. J Virol. 1999;73(5):4316-26. Epub 1999/04/10. doi: 10.1128/JVI.73.5.4316-4326.1999. PubMed PMID: 10196330; PubMed Central PMCID: PMCPMC104213.
147. Villordo SM, Filomatori CV, Sanchez-Vargas I, Blair CD, Gamarnik AV. Dengue virus RNA structure specialization facilitates host adaptation. PLoS Pathog. 2015;11(1):e1004604. Epub 2015/01/31. doi: 10.1371/journal.ppat.1004604. PubMed PMID: 25635835; PubMed Central PMCID: PMCPMC4311971.
148. George J, Raju R. Alphavirus RNA genome repair and evolution: molecular characterization of infectious sindbis virus isolates lacking a known conserved motif at the 3' end of the genome. J Virol. 2000;74(20):9776-85. Epub 2000/09/23. doi: 10.1128/jvi.74.20.9776-9785.2000. PubMed PMID: 11000254; PubMed Central PMCID: PMCPMC112414.
149. Hardy RW, Rice CM. Requirements at the 3' end of the sindbis virus genome for efficient synthesis of minus-strand RNA. J Virol. 2005;79(8):4630-9. Epub 2005/03/30. doi: 10.1128/JVI.79.8.4630-4639.2005. PubMed PMID: 15795249; PubMed Central PMCID: PMCPMC1069581.
150. Hardy RW. The role of the 3' terminus of the Sindbis virus genome in minus-strand initiation site selection. Virology. 2006;345(2):520-31. Epub 2005/11/22. doi: 10.1016/j.virol.2005.10.018. PubMed PMID: 16297426.
151. Trobaugh DW, Gardner CL, Sun C, Haddow AD, Wang E, Chapnik E, et al. RNA viruses can hijack vertebrate microRNAs to suppress innate immunity. Nature. 2014;506(7487):245-8. Epub 2013/12/20. doi: 10.1038/nature12869. PubMed PMID: 24352241; PubMed Central PMCID: PMCPMC4349380.
152. Trobaugh DW, Sun C, Bhalla N, Gardner CL, Dunn MD, Klimstra WB. Cooperativity between the 3' untranslated region microRNA binding sites is critical for the virulence of eastern equine encephalitis virus. PLoS Pathog. 2019;15(10):e1007867. Epub 2019/10/29. doi: 10.1371/journal.ppat.1007867. PubMed PMID: 31658290.
153. Sokoloski KJ, Dickson AM, Chaskey EL, Garneau NL, Wilusz CJ, Wilusz J. Sindbis virus usurps the cellular HuR protein to stabilize its transcripts and promote productive infections in mammalian and mosquito cells. Cell Host Microbe. 2010;8(2):196-207. Epub 2010/08/17. doi:

10.1016/j.chom.2010.07.003. PubMed PMID: 20709296; PubMed Central PMCID: PMCPMC2929003.

154. Silverman MA, Misasi J, Smole S, Feldman HA, Cohen AB, Santagata S, et al. Eastern equine encephalitis in children, Massachusetts and New Hampshire,USA, 1970-2010. Emerg Infect Dis. 2013;19(2):194-201; quiz 352. Epub 2013/01/25. doi: 10.3201/eid1902.120039. PubMed PMID: 23343480; PubMed Central PMCID: PMCPMC3559032.

155. Dickson AM, Anderson JR, Barnhart MD, Sokoloski KJ, Oko L, Opyrchal M, et al. Dephosphorylation of HuR protein during alphavirus infection is associated with HuR relocalization to the cytoplasm. J Biol Chem. 2012;287(43):36229-38. Epub 2012/08/24. doi: 10.1074/jbc.M112.371203. PubMed PMID: 22915590; PubMed Central PMCID: PMCPMC3476290.

156. De Caluwe L, Coppens S, Vereecken K, Daled S, Dhaenens M, Van Ostade X, et al. The CD147 Protein Complex Is Involved in Entry of Chikungunya Virus and Related Alphaviruses in Human Cells. Front Microbiol. 2021;12:615165. Epub 2021/03/16. doi: 10.3389/fmicb.2021.615165. PubMed PMID: 33717005; PubMed Central PMCID: PMCPMC7946996.

157. Ma H, Kim AS, Kafai NM, Earnest JT, Shah AP, Case JB, et al. LDLRAD3 is a receptor for Venezuelan equine encephalitis virus. Nature. 2020;588(7837):308-14. Epub 2020/11/20. doi: 10.1038/s41586-020-2915-3. PubMed PMID: 33208938; PubMed Central PMCID: PMCPMC7769003.

158. Klimstra WB, Ryman KD, Johnston RE. Adaptation of Sindbis virus to BHK cells selects for use of heparan sulfate as an attachment receptor. J Virol. 1998;72(9):7357-66. Epub 1998/08/08. doi: 10.1128/JVI.72.9.7357-7366.1998. PubMed PMID: 9696832; PubMed Central PMCID: PMCPMC109960.

159. Smit JM, Waarts BL, Kimata K, Klimstra WB, Bittman R, Wilschut J. Adaptation of alphaviruses to heparan sulfate: interaction of Sindbis and Semliki forest viruses with liposomes containing lipid-conjugated heparin. J Virol. 2002;76(20):10128-37. Epub 2002/09/20. doi: 10.1128/jvi.76.20.10128-10137.2002. PubMed PMID: 12239287; PubMed Central PMCID: PMCPMC136541.

160. Byrnes AP, Griffin DE. Large-plaque mutants of Sindbis virus show reduced binding to heparan sulfate, heightened viremia, and slower clearance from the circulation. J Virol. 2000;74(2):644-51. Epub 2000/01/07. doi: 10.1128/jvi.74.2.644-651.2000. PubMed PMID: 10623725; PubMed Central PMCID: PMCPMC111583.

161. Pretorius D, Richter RP, Anand T, Cardenas JC, Richter JR. Alterations in heparan sulfate proteoglycan synthesis and sulfation and the impact on vascular endothelial function. Matrix Biol Plus. 2022;16:100121. Epub 2022/09/27. doi: 10.1016/j.mbplus.2022.100121. PubMed PMID: 36160687; PubMed Central PMCID: PMCPMC9494232.
162. Klimstra WB, Nangle EM, Smith MS, Yurochko AD, Ryman KD. DC-SIGN and L-SIGN can act as attachment receptors for alphaviruses and distinguish between mosquito cell- and mammalian cell-derived viruses. J Virol. 2003;77(22):12022-32. Epub 2003/10/29. doi: 10.1128/jvi.77.22.12022-12032.2003. PubMed PMID: 14581539; PubMed Central PMCID: PMCPMC254289.
163. Lozach PY, Burleigh L, Staropoli I, Amara A. The C type lectins DC-SIGN and L-SIGN: receptors for viral glycoproteins. Methods Mol Biol. 2007;379:51-68. Epub 2007/05/16. doi: 10.1007/978-1-59745-393-6_4. PubMed PMID: 17502670; PubMed Central PMCID: PMCPMC7122727.
164. Moller-Tank S, Kondratowicz AS, Davey RA, Rennert PD, Maury W. Role of the phosphatidylserine receptor TIM-1 in enveloped-virus entry. J Virol. 2013;87(15):8327-41. Epub 2013/05/24. doi: 10.1128/JVI.01025-13. PubMed PMID: 23698310; PubMed Central PMCID: PMCPMC3719829.
165. Kolokoltsov AA, Fleming EH, Davey RA. Venezuelan equine encephalitis virus entry mechanism requires late endosome formation and resists cell membrane cholesterol depletion. Virology. 2006;347(2):333-42. Epub 2006/01/24. doi: 10.1016/j.virol.2005.11.051. PubMed PMID: 16427678.
166. Wengler G, Wengler G. In vitro analysis of factors involved in the disassembly of Sindbis virus cores by 60S ribosomal subunits identifies a possible role of low pH. J Gen Virol. 2002;83(Pt 10):2417-26. Epub 2002/09/19. doi: 10.1099/0022-1317-83-10-2417. PubMed PMID: 12237423.
167. Strauss EG, Rice CM, Strauss JH. Sequence coding for the alphavirus nonstructural proteins is interrupted by an opal termination codon. Proc Natl Acad Sci U S A. 1983;80(17):5271-5. Epub 1983/09/01. doi: 10.1073/pnas.80.17.5271. PubMed PMID: 6577423; PubMed Central PMCID: PMCPMC384235.
168. Li G, Rice CM. The signal for translational readthrough of a UGA codon in Sindbis virus RNA involves a single cytidine residue immediately downstream of the termination codon. J Virol. 1993;67(8):5062-7. Epub 1993/08/01. doi: 10.1128/JVI.67.8.5062-5067.1993. PubMed PMID: 8331741; PubMed Central PMCID: PMCPMC237898.
169. Shirako Y, Strauss JH. Regulation of Sindbis virus RNA replication: uncleaved P123 and nsP4 function in minus-strand RNA synthesis, whereas cleaved products from P123 are required

for efficient plus-strand RNA synthesis. J Virol. 1994;68(3):1874-85. Epub 1994/03/01. doi: 10.1128/JVI.68.3.1874-1885.1994. PubMed PMID: 8107248; PubMed Central PMCID: PMCPMC236650.

170. Lemm JA, Rice CM. Assembly of functional Sindbis virus RNA replication complexes: requirement for coexpression of P123 and P34. J Virol. 1993;67(4):1905-15. Epub 1993/04/01. doi: 10.1128/JVI.67.4.1905-1915.1993. PubMed PMID: 8445716; PubMed Central PMCID: PMCPMC240258.

171. Sawicki DL, Sawicki SG. Alphavirus positive and negative strand RNA synthesis and the role of polyproteins in formation of viral replication complexes. Arch Virol Suppl. 1994;9:393-405. Epub 1994/01/01. doi: 10.1007/978-3-7091-9326-6_39. PubMed PMID: 8032270.

172. Lemm JA, Rumenapf T, Strauss EG, Strauss JH, Rice CM. Polypeptide requirements for assembly of functional Sindbis virus replication complexes: a model for the temporal regulation of minus- and plus-strand RNA synthesis. EMBO J. 1994;13(12):2925-34. Epub 1994/06/15. doi: 10.1002/j.1460-2075.1994.tb06587.x. PubMed PMID: 7517863; PubMed Central PMCID: PMCPMC395174.

173. Spuul P, Balistreri G, Kaariainen L, Ahola T. Phosphatidylinositol 3-kinase-, actin-, and microtubule-dependent transport of Semliki Forest Virus replication complexes from the plasma membrane to modified lysosomes. J Virol. 2010;84(15):7543-57. Epub 2010/05/21. doi: 10.1128/JVI.00477-10. PubMed PMID: 20484502; PubMed Central PMCID: PMCPMC2897599.

174. Frolova EI, Gorchakov R, Pereboeva L, Atasheva S, Frolov I. Functional Sindbis virus replicative complexes are formed at the plasma membrane. J Virol. 2010;84(22):11679-95. Epub 2010/09/10. doi: 10.1128/JVI.01441-10. PubMed PMID: 20826696; PubMed Central PMCID: PMCPMC2977861.

175. Ahola T, Lampio A, Auvinen P, Kaariainen L. Semliki Forest virus mRNA capping enzyme requires association with anionic membrane phospholipids for activity. EMBO J. 1999;18(11):3164-72. Epub 1999/06/05. doi: 10.1093/emboj/18.11.3164. PubMed PMID: 10357827; PubMed Central PMCID: PMCPMC1171397.

176. Kujala P, Ikaheimonen A, Ehsani N, Vihinen H, Auvinen P, Kaariainen L. Biogenesis of the Semliki Forest virus RNA replication complex. J Virol. 2001;75(8):3873-84. Epub 2001/03/27. doi: 10.1128/JVI.75.8.3873-3884.2001. PubMed PMID: 11264376; PubMed Central PMCID: PMCPMC114878.

177. Aliperti G, Schlesinger MJ. Evidence for an autoprotease activity of sindbis virus capsid protein. Virology. 1978;90(2):366-9. Epub 1978/10/15. doi: 10.1016/0042-6822(78)90321-5. PubMed PMID: 726255.

178. Hahn CS, Strauss JH. Site-directed mutagenesis of the proposed catalytic amino acids of the Sindbis virus capsid protein autoprotease. J Virol. 1990;64(6):3069-73. Epub 1990/06/01. doi: 10.1128/JVI.64.6.3069-3073.1990. PubMed PMID: 2335827; PubMed Central PMCID: PMCPMC249494.
179. Frolova E, Frolov I, Schlesinger S. Packaging signals in alphaviruses. J Virol. 1997;71(1):248-58. Epub 1997/01/01. PubMed PMID: 8985344; PubMed Central PMCID: PMCPMC191045.
180. Weiss B, Nitschko H, Ghattas I, Wright R, Schlesinger S. Evidence for specificity in the encapsidation of Sindbis virus RNAs. J Virol. 1989;63(12):5310-8. Epub 1989/12/01. doi: 10.1128/JVI.63.12.5310-5318.1989. PubMed PMID: 2585607; PubMed Central PMCID: PMCPMC251197.
181. Garoff H, Huylebroeck D, Robinson A, Tillman U, Liljestrom P. The signal sequence of the p62 protein of Semliki Forest virus is involved in initiation but not in completing chain translocation. J Cell Biol. 1990;111(3):867-76. Epub 1990/09/01. doi: 10.1083/jcb.111.3.867. PubMed PMID: 2391367; PubMed Central PMCID: PMCPMC2116283.
182. Schlee M, Hartmann G. Discriminating self from non-self in nucleic acid sensing. Nat Rev Immunol. 2016;16(9):566-80. Epub 2016/07/28. doi: 10.1038/nri.2016.78. PubMed PMID: 27455396; PubMed Central PMCID: PMCPMC7097691 SFB670 to M.S. and G.H.; DFG SCHL1930/1-1 to M.S.; SFB704 to G.H.; SFB832 and KFO177 to G.H. G.H. and M.S. are supported by the DFG Excellence Cluster ImmunoSensation. G.H. is supported by the German Center of Infectious Disease (DZIF). G.H. is a co-founder and shareholder of Rigontec GmbH; M.S. and G.H. are inventors on a patent covering structures described in a manuscript that is cited in this Review.
183. Akhrymuk I, Frolov I, Frolova EI. Both RIG-I and MDA5 detect alphavirus replication in concentration-dependent mode. Virology. 2016;487:230-41. Epub 2015/11/10. doi: 10.1016/j.virol.2015.09.023. PubMed PMID: 26550947; PubMed Central PMCID: PMCPMC4721224.
184. McDougal MB, De Maria AM, Ohlson MB, Kumar A, Xing C, Schoggins JW. Interferon inhibits a model RNA virus via a limited set of inducible effector genes. EMBO Rep. 2023;24(9):e56901. Epub 2023/07/27. doi: 10.15252/embr.202356901. PubMed PMID: 37497756; PubMed Central PMCID: PMCPMC10481653.
185. Reynaud JM, Kim DY, Atasheva S, Rasalouskaya A, White JP, Diamond MS, et al. IFIT1 Differentially Interferes with Translation and Replication of Alphavirus Genomes and Promotes Induction of Type I Interferon. PLoS Pathog. 2015;11(4):e1004863. Epub 2015/05/01. doi:

10.1371/journal.ppat.1004863. PubMed PMID: 25927359; PubMed Central PMCID: PMCPMC4415776.

186. Sarah E. Hickson EB, Johannes Schwerk, Indraneel Saluhke, Shivam Zaver, Joshua Woodward, Ram Savan, Jennifer L. Hyde. Sequence diversity in the 3' untranslated region of alphavirus modulates IFIT2-dependent restriction in a cell type-dependent manner. bioRxiv. 2021. Epub 11 December 2021. doi: https://doi.org/10.1101/2021.12.10.472177.

187. Berchtold S, Manncke B, Klenk J, Geisel J, Autenrieth IB, Bohn E. Forced IFIT-2 expression represses LPS induced TNF-alpha expression at posttranscriptional levels. BMC Immunol. 2008;9:75. Epub 2008/12/26. doi: 10.1186/1471-2172-9-75. PubMed PMID: 19108715; PubMed Central PMCID: PMCPMC2632614.

188. Yin J, Gardner CL, Burke CW, Ryman KD, Klimstra WB. Similarities and differences in antagonism of neuron alpha/beta interferon responses by Venezuelan equine encephalitis and Sindbis alphaviruses. J Virol. 2009;83(19):10036-47. Epub 2009/07/31. doi: 10.1128/JVI.01209-09. PubMed PMID: 19641001; PubMed Central PMCID: PMCPMC2748036.

189. Burke CW, Gardner CL, Steffan JJ, Ryman KD, Klimstra WB. Characteristics of alpha/beta interferon induction after infection of murine fibroblasts with wild-type and mutant alphaviruses. Virology. 2009;395(1):121-32. Epub 2009/09/29. doi: 10.1016/j.virol.2009.08.039. PubMed PMID: 19782381; PubMed Central PMCID: PMCPMC4381786.

190. Bhalla N, Gardner CL, Downs SN, Dunn M, Sun C, Klimstra WB. Macromolecular Synthesis Shutoff Resistance by Myeloid Cells Is Critical to IRF7-Dependent Systemic Interferon Alpha/Beta Induction after Alphavirus Infection. J Virol. 2019;93(24). Epub 2019/10/04. doi: 10.1128/JVI.00872-19. PubMed PMID: 31578290; PubMed Central PMCID: PMCPMC6880179.

191. Fayzulin R, Frolov I. Changes of the secondary structure of the 5' end of the Sindbis virus genome inhibit virus growth in mosquito cells and lead to accumulation of adaptive mutations. J Virol. 2004;78(10):4953-64. Epub 2004/04/29. PubMed PMID: 15113874; PubMed Central PMCID: PMCPMC400360.

192. Niesters HG, Strauss JH. Mutagenesis of the conserved 51-nucleotide region of Sindbis virus. J Virol. 1990;64(4):1639-47. Epub 1990/04/01. doi: 10.1128/JVI.64.4.1639-1647.1990. PubMed PMID: 2319648; PubMed Central PMCID: PMCPMC249300.

193. Michel G, Petrakova O, Atasheva S, Frolov I. Adaptation of Venezuelan equine encephalitis virus lacking 51-nt conserved sequence element to replication in mammalian and mosquito cells. Virology. 2007;362(2):475-87. Epub 2007/02/13. doi: 10.1016/j.virol.2007.01.009. PubMed PMID: 17292936; PubMed Central PMCID: PMCPMC2810489.

194. Kutchko KM, Madden EA, Morrison C, Plante KS, Sanders W, Vincent HA, et al. Structural divergence creates new functional features in alphavirus genomes. Nucleic Acids Res. 2018;46(7):3657-70. Epub 2018/01/24. doi: 10.1093/nar/gky012. PubMed PMID: 29361131; PubMed Central PMCID: PMCPMC6283419.

195. Madden EA, Plante KS, Morrison CR, Kutchko KM, Sanders W, Long KM, et al. Using SHAPE-MaP To Model RNA Secondary Structure and Identify 3'UTR Variation in Chikungunya Virus. J Virol. 2020;94(24). Epub 2020/10/02. doi: 10.1128/JVI.00701-20. PubMed PMID: 32999019; PubMed Central PMCID: PMCPMC7925192.

196. Frolov I, Schlesinger S. Translation of Sindbis virus mRNA: analysis of sequences downstream of the initiating AUG codon that enhance translation. J Virol. 1996;70(2):1182-90. Epub 1996/02/01. doi: 10.1128/JVI.70.2.1182-1190.1996. PubMed PMID: 8551579; PubMed Central PMCID: PMCPMC189927.

197. Ventoso I, Sanz MA, Molina S, Berlanga JJ, Carrasco L, Esteban M. Translational resistance of late alphavirus mRNA to eIF2alpha phosphorylation: a strategy to overcome the antiviral effect of protein kinase PKR. Genes Dev. 2006;20(1):87-100. Epub 2006/01/05. doi: 10.1101/gad.357006. PubMed PMID: 16391235; PubMed Central PMCID: PMCPMC1356103.

198. Garcia MA, Gil J, Ventoso I, Guerra S, Domingo E, Rivas C, et al. Impact of protein kinase PKR in cell biology: from antiviral to antiproliferative action. Microbiol Mol Biol Rev. 2006;70(4):1032-60. Epub 2006/12/13. doi: 10.1128/MMBR.00027-06. PubMed PMID: 17158706; PubMed Central PMCID: PMCPMC1698511.

199. Gorchakov R, Frolova E, Williams BR, Rice CM, Frolov I. PKR-dependent and -independent mechanisms are involved in translational shutoff during Sindbis virus infection. J Virol. 2004;78(16):8455-67. Epub 2004/07/29. doi: 10.1128/JVI.78.16.8455-8467.2004. PubMed PMID: 15280454; PubMed Central PMCID: PMCPMC479073.

200. Toribio R, Ventoso I. Inhibition of host translation by virus infection in vivo. Proc Natl Acad Sci U S A. 2010;107(21):9837-42. Epub 2010/05/12. doi: 10.1073/pnas.1004110107. PubMed PMID: 20457920; PubMed Central PMCID: PMCPMC2906859.

201. Chung BY, Firth AE, Atkins JF. Frameshifting in alphaviruses: a diversity of 3' stimulatory structures. J Mol Biol. 2010;397(2):448-56. Epub 2010/02/02. doi: 10.1016/j.jmb.2010.01.044. PubMed PMID: 20114053.

202. Gruber AR, Lorenz R, Bernhart SH, Neubock R, Hofacker IL. The Vienna RNA websuite. Nucleic Acids Res. 2008;36(Web Server issue):W70-4. Epub 2008/04/22. doi: 10.1093/nar/gkn188. PubMed PMID: 18424795; PubMed Central PMCID: PMCPMC2447809.

203. Zuker M, Stiegler P. Optimal computer folding of large RNA sequences using thermodynamics and auxiliary information. Nucleic Acids Res. 1981;9(1):133-48. Epub 1981/01/10. doi: 10.1093/nar/9.1.133. PubMed PMID: 6163133; PubMed Central PMCID: PMCPMC326673.

204. Wuchty S, Fontana W, Hofacker IL, Schuster P. Complete suboptimal folding of RNA and the stability of secondary structures. Biopolymers. 1999;49(2):145-65. Epub 1999/03/10. doi: 10.1002/(SICI)1097-0282(199902)49:2<145::AID-BIP4>3.0.CO;2-G. PubMed PMID: 10070264.

205. McCaskill JS. The equilibrium partition function and base pair binding probabilities for RNA secondary structure. Biopolymers. 1990;29(6-7):1105-19. Epub 1990/05/01. doi: 10.1002/bip.360290621. PubMed PMID: 1695107.

206. Kendra JA, de la Fuente C, Brahms A, Woodson C, Bell TM, Chen B, et al. Ablation of Programmed -1 Ribosomal Frameshifting in Venezuelan Equine Encephalitis Virus Results in Attenuated Neuropathogenicity. J Virol. 2017;91(3). Epub 2016/11/18. doi: 10.1128/JVI.01766-16. PubMed PMID: 27852852; PubMed Central PMCID: PMCPMC5244343.

207. Saitou N, Nei M. The neighbor-joining method: a new method for reconstructing phylogenetic trees. Mol Biol Evol. 1987;4(4):406-25. Epub 1987/07/01. doi: 10.1093/oxfordjournals.molbev.a040454. PubMed PMID: 3447015.

208. Gardner CL, Burke CW, Tesfay MZ, Glass PJ, Klimstra WB, Ryman KD. Eastern and Venezuelan equine encephalitis viruses differ in their ability to infect dendritic cells and macrophages: impact of altered cell tropism on pathogenesis. J Virol. 2008;82(21):10634-46. Epub 2008/09/05. doi: 10.1128/JVI.01323-08. PubMed PMID: 18768986; PubMed Central PMCID: PMCPMC2573165.

209. Frolova EI, Fayzulin RZ, Cook SH, Griffin DE, Rice CM, Frolov I. Roles of nonstructural protein nsP2 and Alpha/Beta interferons in determining the outcome of Sindbis virus infection. J Virol. 2002;76(22):11254-64. Epub 2002/10/22. doi: 10.1128/jvi.76.22.11254-11264.2002. PubMed PMID: 12388685; PubMed Central PMCID: PMCPMC136776.

210. Fragkoudis R, Breakwell L, McKimmie C, Boyd A, Barry G, Kohl A, et al. The type I interferon system protects mice from Semliki Forest virus by preventing widespread virus dissemination in extraneural tissues, but does not mediate the restricted replication of avirulent virus in central nervous system neurons. J Gen Virol. 2007;88(Pt 12):3373-84. Epub 2007/11/21. doi: 10.1099/vir.0.83191-0. PubMed PMID: 18024907.

211. Ryman KD, Meier KC, Gardner CL, Adegboyega PA, Klimstra WB. Non-pathogenic Sindbis virus causes hemorrhagic fever in the absence of alpha/beta and gamma interferons.

Virology. 2007;368(2):273-85. Epub 2007/08/08. doi: 10.1016/j.virol.2007.06.039. PubMed PMID: 17681583.

212. Sanchez David RY, Combredet C, Sismeiro O, Dillies MA, Jagla B, Coppee JY, et al. Comparative analysis of viral RNA signatures on different RIG-I-like receptors. Elife. 2016;5:e11275. Epub 2016/03/25. doi: 10.7554/eLife.11275. PubMed PMID: 27011352; PubMed Central PMCID: PMCPMC4841775.

213. Schonborn J, Oberstrass J, Breyel E, Tittgen J, Schumacher J, Lukacs N. Monoclonal antibodies to double-stranded RNA as probes of RNA structure in crude nucleic acid extracts. Nucleic Acids Res. 1991;19(11):2993-3000. Epub 1991/06/11. doi: 10.1093/nar/19.11.2993. PubMed PMID: 2057357; PubMed Central PMCID: PMCPMC328262.

214. Paranjape SM, Harris E. Y box-binding protein-1 binds to the dengue virus 3'-untranslated region and mediates antiviral effects. J Biol Chem. 2007;282(42):30497-508. Epub 2007/08/30. doi: 10.1074/jbc.M705755200. PubMed PMID: 17726010.

215. Varjak M, Saul S, Arike L, Lulla A, Peil L, Merits A. Magnetic fractionation and proteomic dissection of cellular organelles occupied by the late replication complexes of Semliki Forest virus. J Virol. 2013;87(18):10295-312. Epub 2013/07/19. doi: 10.1128/JVI.01105-13. PubMed PMID: 23864636; PubMed Central PMCID: PMCPMC3754020.

216. LaPointe AT, Gebhart NN, Meller ME, Hardy RW, Sokoloski KJ. Identification and Characterization of Sindbis Virus RNA-Host Protein Interactions. J Virol. 2018;92(7). Epub 2018/01/13. doi: 10.1128/JVI.02171-17. PubMed PMID: 29321325; PubMed Central PMCID: PMCPMC5972874.

217. Garcia-Moreno M, Sanz MA, Carrasco L. A Viral mRNA Motif at the 3'-Untranslated Region that Confers Translatability in a Cell-Specific Manner. Implications for Virus Evolution. Sci Rep. 2016;6:19217. Epub 2016/01/13. doi: 10.1038/srep19217. PubMed PMID: 26755446; PubMed Central PMCID: PMCPMC4709744.

218. Carrasco L, Sanz MA, Gonzalez-Almela E. The Regulation of Translation in Alphavirus-Infected Cells. Viruses. 2018;10(2). Epub 2018/02/09. doi: 10.3390/v10020070. PubMed PMID: 29419763; PubMed Central PMCID: PMCPMC5850377.

219. Weingarten-Gabbay S, Elias-Kirma S, Nir R, Gritsenko AA, Stern-Ginossar N, Yakhini Z, et al. Comparative genetics. Systematic discovery of cap-independent translation sequences in human and viral genomes. Science. 2016;351(6270). Epub 2016/01/28. doi: 10.1126/science.aad4939. PubMed PMID: 26816383.

220. Decle-Carrasco S, Rodriguez-Pina AL, Rodriguez-Zapata LC, Castano E. Current research on viral proteins that interact with fibrillarin. Mol Biol Rep. 2023;50(5):4631-43. Epub

2023/03/18. doi: 10.1007/s11033-023-08343-2. PubMed PMID: 36928641; PubMed Central PMCID: PMCPMC10018631.

221. Lu JC, Lu CY, Wu YY. THRAP3 depletion reduces PPARgamma mRNA and anti-inflammatory action in 3T3-L1 adipocytes. J Mol Endocrinol. 2021;67(3):149-59. Epub 2021/08/10. doi: 10.1530/JME-20-0334. PubMed PMID: 34370683.

222. Luo EC, Nathanson JL, Tan FE, Schwartz JL, Schmok JC, Shankar A, et al. Large-scale tethered function assays identify factors that regulate mRNA stability and translation. Nat Struct Mol Biol. 2020;27(10):989-1000. Epub 2020/08/19. doi: 10.1038/s41594-020-0477-6. PubMed PMID: 32807991; PubMed Central PMCID: PMCPMC8221285.

223. Tesfay MZ, Yin J, Gardner CL, Khoretonenko MV, Korneeva NL, Rhoads RE, et al. Alpha/beta interferon inhibits cap-dependent translation of viral but not cellular mRNA by a PKR-independent mechanism. J Virol. 2008;82(6):2620-30. Epub 2007/12/28. doi: 10.1128/JVI.01784-07. PubMed PMID: 18160435; PubMed Central PMCID: PMCPMC2259014.

224. Iadevaia V, Burke JM, Eke L, Moller-Levet C, Parker R, Locker N. Novel stress granule-like structures are induced via a paracrine mechanism during viral infection. J Cell Sci. 2022;135(4). Epub 2022/02/01. doi: 10.1242/jcs.259194. PubMed PMID: 35098996; PubMed Central PMCID: PMCPMC8976915.

225. Bish R, Cuevas-Polo N, Cheng Z, Hambardzumyan D, Munschauer M, Landthaler M, et al. Comprehensive Protein Interactome Analysis of a Key RNA Helicase: Detection of Novel Stress Granule Proteins. Biomolecules. 2015;5(3):1441-66. Epub 2015/07/18. doi: 10.3390/biom5031441. PubMed PMID: 26184334; PubMed Central PMCID: PMCPMC4598758.

226. Smola MJ, Weeks KM. In-cell RNA structure probing with SHAPE-MaP. Nat Protoc. 2018;13(6):1181-95. Epub 2018/05/05. doi: 10.1038/nprot.2018.010. PubMed PMID: 29725122; PubMed Central PMCID: PMCPMC6402486.

227. Smola MJ, Rice GM, Busan S, Siegfried NA, Weeks KM. Selective 2'-hydroxyl acylation analyzed by primer extension and mutational profiling (SHAPE-MaP) for direct, versatile and accurate RNA structure analysis. Nat Protoc. 2015;10(11):1643-69. Epub 2015/10/02. doi: 10.1038/nprot.2015.103. PubMed PMID: 26426499; PubMed Central PMCID: PMCPMC4900152.

228. Medina G, Garzaro DJ, Barrios M, Auguste AJ, Weaver SC, Pujol FH. Genetic diversity of Venezuelan alphaviruses and circulation of a Venezuelan equine encephalitis virus subtype IAB strain during an interepizootic period. Am J Trop Med Hyg. 2015;93(1):7-10. Epub 2015/05/06. doi: 10.4269/ajtmh.14-0543. PubMed PMID: 25940191; PubMed Central PMCID: PMCPMC4497907.

229. Gardner SN, McLoughlin K, Be NA, Allen J, Weaver SC, Forrester N, et al. Characterization of Genetic Variability of Venezuelan Equine Encephalitis Viruses. PLoS One. 2016;11(4):e0152604. Epub 2016/04/08. doi: 10.1371/journal.pone.0152604. PubMed PMID: 27054586; PubMed Central PMCID: PMCPMC4824352.
230. Bernhart SH, Hofacker IL, Will S, Gruber AR, Stadler PF. RNAalifold: improved consensus structure prediction for RNA alignments. BMC Bioinformatics. 2008;9:474. Epub 2008/11/19. doi: 10.1186/1471-2105-9-474. PubMed PMID: 19014431; PubMed Central PMCID: PMCPMC2621365.
231. Powers AM, Williamson LE, Carnahan RH, Crowe JE, Jr., Hyde JL, Jonsson CB, et al. Developing a Prototype Pathogen Plan and Research Priorities for the Alphaviruses. J Infect Dis. 2023;228(Suppl 6):S414-S26. Epub 2023/10/18. doi: 10.1093/infdis/jiac326. PubMed PMID: 37849399.
232. Wang E, Barrera R, Boshell J, Ferro C, Freier JE, Navarro JC, et al. Genetic and phenotypic changes accompanying the emergence of epizootic subtype IC Venezuelan equine encephalitis viruses from an enzootic subtype ID progenitor. J Virol. 1999;73(5):4266-71. Epub 1999/04/10. doi: 10.1128/JVI.73.5.4266-4271.1999. PubMed PMID: 10196323; PubMed Central PMCID: PMCPMC104206.
233. Vohhodina J, Barros EM, Savage AL, Liberante FG, Manti L, Bankhead P, et al. The RNA processing factors THRAP3 and BCLAF1 promote the DNA damage response through selective mRNA splicing and nuclear export. Nucleic Acids Res. 2017;45(22):12816-33. Epub 2017/11/08. doi: 10.1093/nar/gkx1046. PubMed PMID: 29112714; PubMed Central PMCID: PMCPMC5728405.
234. Marcheva B, Perelis M, Weidemann BJ, Taguchi A, Lin H, Omura C, et al. Erratum: A role for alternative splicing in circadian control of exocytosis and glucose homeostasis. Genes Dev. 2021;35(5-6):425. Epub 2021/03/03. doi: 10.1101/gad.348303.121. PubMed PMID: 33649163; PubMed Central PMCID: PMCPMC7919415.
235. Varia S, Potabathula D, Deng Z, Bubulya A, Bubulya PA. Btf and TRAP150 have distinct roles in regulating subcellular mRNA distribution. Nucleus. 2013;4(3):229-40. Epub 2013/06/20. doi: 10.4161/nucl.25187. PubMed PMID: 23778535; PubMed Central PMCID: PMCPMC3720753.
236. Jonsson J, Wang L, Kajitani N, Schwartz S. A novel HPV16 splicing enhancer critical for viral oncogene expression and cell immortalization. Nucleic Acids Res. 2024;52(1):316-36. Epub 2023/11/23. doi: 10.1093/nar/gkad1099. PubMed PMID: 37994701; PubMed Central PMCID: PMCPMC10783526.

237. Choi JH, Choi SS, Kim ES, Jedrychowski MP, Yang YR, Jang HJ, et al. Thrap3 docks on phosphoserine 273 of PPARgamma and controls diabetic gene programming. Genes Dev. 2014;28(21):2361-9. Epub 2014/10/16. doi: 10.1101/gad.249367.114. PubMed PMID: 25316675; PubMed Central PMCID: PMCPMC4215181.

238. Ino Y, Arakawa N, Ishiguro H, Uemura H, Kubota Y, Hirano H, et al. Phosphoproteome analysis demonstrates the potential role of THRAP3 phosphorylation in androgen-independent prostate cancer cell growth. Proteomics. 2016;16(7):1069-78. Epub 2016/02/04. doi: 10.1002/pmic.201500365. PubMed PMID: 26841317.

239. Bracken CP, Wall SJ, Barre B, Panov KI, Ajuh PM, Perkins ND. Regulation of cyclin D1 RNA stability by SNIP1. Cancer Res. 2008;68(18):7621-8. Epub 2008/09/17. doi: 10.1158/0008-5472.CAN-08-1217. PubMed PMID: 18794151; PubMed Central PMCID: PMCPMC2546513.

240. Riggs CL, Kedersha N, Amarsanaa M, Zubair SN, Ivanov P, Anderson P. UBAP2L contributes to formation of P-bodies and modulates their association with stress granules. J Cell Biol. 2024;223(10). Epub 2024/07/15. doi: 10.1083/jcb.202307146. PubMed PMID: 39007803; PubMed Central PMCID: PMCPMC11248227 submitted work. No other disclosures were reported.

241. Cirillo L, Cieren A, Barbieri S, Khong A, Schwager F, Parker R, et al. UBAP2L Forms Distinct Cores that Act in Nucleating Stress Granules Upstream of G3BP1. Curr Biol. 2020;30(4):698-707 e6. Epub 2020/01/21. doi: 10.1016/j.cub.2019.12.020. PubMed PMID: 31956030.

242. Paget M, Cadena C, Ahmad S, Wang HT, Jordan TX, Kim E, et al. Stress granules are shock absorbers that prevent excessive innate immune responses to dsRNA. Mol Cell. 2023;83(7):1180-96 e8. Epub 2023/04/08. doi: 10.1016/j.molcel.2023.03.010. PubMed PMID: 37028415; PubMed Central PMCID: PMCPMC10170497.

243. An H, Tan JT, Shelkovnikova TA. Stress granules regulate stress-induced paraspeckle assembly. J Cell Biol. 2019;218(12):4127-40. Epub 2019/10/23. doi: 10.1083/jcb.201904098. PubMed PMID: 31636118; PubMed Central PMCID: PMCPMC6891081.

244. Youn JY, Dunham WH, Hong SJ, Knight JDR, Bashkurov M, Chen GI, et al. High-Density Proximity Mapping Reveals the Subcellular Organization of mRNA-Associated Granules and Bodies. Mol Cell. 2018;69(3):517-32 e11. Epub 2018/02/06. doi: 10.1016/j.molcel.2017.12.020. PubMed PMID: 29395067.

245. Otsuka H, Fukao A, Funakami Y, Duncan KE, Fujiwara T. Emerging Evidence of Translational Control by AU-Rich Element-Binding Proteins. Front Genet. 2019;10:332. Epub

2019/05/24. doi: 10.3389/fgene.2019.00332. PubMed PMID: 31118942; PubMed Central PMCID: PMCPMC6507484.

246. Hake LE, Mendez R, Richter JD. Specificity of RNA binding by CPEB: requirement for RNA recognition motifs and a novel zinc finger. Mol Cell Biol. 1998;18(2):685-93. Epub 1998/02/03. doi: 10.1128/MCB.18.2.685. PubMed PMID: 9447964; PubMed Central PMCID: PMCPMC108779.

247. Cruz-Gallardo I, Aroca A, Gunzburg MJ, Sivakumaran A, Yoon JH, Angulo J, et al. The binding of TIA-1 to RNA C-rich sequences is driven by its C-terminal RRM domain. RNA Biol. 2014;11(6):766-76. Epub 2014/05/16. doi: 10.4161/rna.28801. PubMed PMID: 24824036; PubMed Central PMCID: PMCPMC4156507.

248. Stickeler E, Fraser SD, Honig A, Chen AL, Berget SM, Cooper TA. The RNA binding protein YB-1 binds A/C-rich exon enhancers and stimulates splicing of the CD44 alternative exon v4. EMBO J. 2001;20(14):3821-30. Epub 2001/07/12. doi: 10.1093/emboj/20.14.3821. PubMed PMID: 11447123; PubMed Central PMCID: PMCPMC125550.

249. Weaver SC, Reisen WK. Present and future arboviral threats. Antiviral Res. 2010;85(2):328-45. Epub 2009/10/28. doi: 10.1016/j.antiviral.2009.10.008. PubMed PMID: 19857523; PubMed Central PMCID: PMCPMC2815176.

250. Ran FA, Hsu PD, Wright J, Agarwala V, Scott DA, Zhang F. Genome engineering using the CRISPR-Cas9 system. Nat Protoc. 2013;8(11):2281-308. Epub 2013/10/26. doi: 10.1038/nprot.2013.143. PubMed PMID: 24157548; PubMed Central PMCID: PMCPMC3969860.

251. Kowarz E, Loscher D, Marschalek R. Optimized Sleeping Beauty transposons rapidly generate stable transgenic cell lines. Biotechnol J. 2015;10(4):647-53. Epub 2015/02/05. doi: 10.1002/biot.201400821. PubMed PMID: 25650551.

252. Leppek K, Stoecklin G. An optimized streptavidin-binding RNA aptamer for purification of ribonucleoprotein complexes identifies novel ARE-binding proteins. Nucleic Acids Res. 2014;42(2):e13. Epub 2013/10/26. doi: 10.1093/nar/gkt956. PubMed PMID: 24157833; PubMed Central PMCID: PMCPMC3902943.